Wind Mapping of Sweden

Summary of results and methods used

Elforsk rapport 09:04

Hans Bergström & Stefan Söderberg

January 2008

Vindforsk Energimyndigheten ELFORSK

Wind Mapping of Sweden

Summary of results and methods used

Elforsk rapport 09:04

Hans Bergström & Stefan Söderberg

January 2008

Preface

Previous projects as 'Mapping the Wind Potential in Sweden' has produced a large database of meteorological parameters at different heights over the whole of Sweden with 1 km horizontal resolution. In the current project the database has been further analysed to obtain additional data such as e.g. extreme wind speeds, turbulence intensities etc.

The work was carried out by Hans Bergström and Stefan Söderberg at Uppsala University as a project within the Swedish wind energy research programme "Vindforsk – II". The report is the final report for project V-115 "Statistical analysis of results from the Swedish wind resource mapping and downscaling of the results".

The report contains a general description of the wind mapping model and wind mapping results reported in 2007. Current work in project V-115 contains development which has resulted in additional data such as wind distributions, extreme wind speeds, turbulence intensities, wind gradient, and matched wind turbine classes. The report also show results from downscaling the calculations locally to a 100x100 meter grid resolution.

The results and work of older projects are included in order to get all results complete in one report.

Vindforsk – II is funded by ABB, the Norwegian based EBL-Kompetanse, E.ON Sverige AB, Falkenberg Energi AB, Göteborg Energi, Jämtkraft AB, Karlstad Energi AB, Luleå Energi AB, Lunds Energi AB, Skellefteå Kraft AB, Svenska Kraftnät, Swedish Energy Agency, Tekniska Verken i Linköping AB, Umeå Energi AB, Varberg Energi, Vattenfall AB and Öresundskraft AB.

Comments on the work and the final report have been given by a reference group with the following members: Sven-Erik Thor Vattenfall, Staffan Niklasson Vindkompaniet, Staffan Engström Ägir konsult and Sara Hallert Elforsk.

Stockholm January 2009

Anders Björck

Elforsk, Electricity and Power Production

Vindforsk Programme manager

Summary

A three-dimensional meso-scale numerical higher-order closure model, the MIUU-model developed at Uppsala University, has been used to investigate the wind climate in Sweden. This type of model takes special notice of the conditions in the atmospheric boundary layer. Results from a wind resource mapping of Sweden with 1 km^2 horizontal resolution is presented here.

A technique to just model some samples of the meteorological conditions governing the wind climate at heights of interest to wind energy has been used. This was shown to give accurate results in good agreement with observations, making it unnecessary to model a long period of 'true weather' cases. By choosing the 'relevant' samples, the number of model runs could be limited to 192, which correspond to 4608 simulated hours (representing 4 months x 3 speeds x 16 directions x 24 hours each).

Statistics on the horizontal air pressure gradient (geostrophic wind), the major force driving the actual wind, were used to weight the model output together into the final wind climate estimates. Surface pressure data from 3 pressure observing sites in Southern Sweden and 3 sites in Northern Scandinavia were then primarily used. As the geostrophic mean wind varies quite a lot over an area as large as Sweden, it was also needed to take this into account. For this purpose the NCEP/NCAR reanalysis data were used to calculate the geostrophic wind. These results were then used to weight the influence of the geographical variation in geostrophic wind into the results regarding the modelled wind climate.

Comparisons with wind observations at 84 sites showed that the modelled annual average wind speed is in good agreement with measured values. The average difference between model results and observations were found to be -0.03 m/s, and for 87 % of the comparisons the differences were within ±0.4 m/s.

Additional wind statistics, besides the annual average wind speed, have also been determined using the database of modelled atmospheric conditions. These results include:

- Distributions of wind speed and wind directions, giving the sector wise Weibull parameters for 12 wind direction sectors.
- Extreme wind speed for 10 min average wind speed and 3 s gust wind speed with an expected 50-year return period.
- The wind gradient presented as the exponent of the exponential wind profile.
- Turbulence intensity determined from the modelled turbulent kinetic energy.
- Wind turbine classes estimated from the modelled average wind speed and turbulence intensity being translated to reference wind speed and reference turbulence intensity at 15 m/s.

All wind statistics is available through Internet at:

http://www.geo.uu.se/luva/default.aspx?pageid=13152&lan=0.

It is, however, important to remember that the model does not adequately resolve influence from terrain features smaller than a few times the model grid spacing. With 1 km^2 resolution the main characteristics of the geographical variability of the wind climate is captured, but this resolution is often too coarse when planning the details of a wind farm and the exact wind turbine locations within the farm. For that case higher resolution wind resource mapping is needed. This has previously often been done using a model such as WA^{S}P, either directly or as a tool within WindPro. This type of model has a simplified physical description of the atmosphere why the results may sometimes be questioned.

Using a higher-order closure meteorological CFD-model such as the MIUU-model has previously in practice been unrealistic for downscaling to the high resolutions needed for local micro scale planning. Due to the hydrostatic approximation in the MIUU-model it was decided also to test another meteorological CDF-model of the same type, but with a non-hydrostatic closure. The decision fell on COAMPS®, Coupled Ocean/Atmosphere Mesoscale Prediction System (COAMPS®, a registered trademark of the Naval Research Laboratory).

A comparison between modelled annual average wind speeds in the Fjällberget/Saxberget area in Sweden showed that both CFD-models give realistic results. Some differences are found, however, and comparisons with observations at the site showed that the MIUU-model seems to perform better in spite of its hydrostatic approximations. The reasons for this may have to do with differences regarding the turbulence closure and also regarding the surface energy balance routine which may in turn result in differences in thermal stratification.

The conclusion of the comparisons is that downscaling using higher-order meteorological CFD-models is realistic and gives results in agreement with observations. However, observations with much higher horizontal resolution are needed to fully evaluate the differences found between the two models. We may also assume that the results are probably more realistic than results using models with more simplified physics, especially when input data to the simplified models are not available from the site or even only at a specific location with an altitude not representative for the whole area of interest. This is so because the differences between high and low altitude terrain were found to be much smaller using a simplified model than using a CFD-model.

Note that no local wind observations are included or needed when calculating the wind resources using the MIUU-technique together with the results from a higher-order model. Hence, the model output is totally independent of the observations with which comparisons may be made.

Sammanfattning

En tre-dimensionell numerisk mesoskalemodell av högre ordningen, MIUU-modellen utvecklad vid Uppsala universitet, har använts för att undersöka vindklimatet i Sverige. Denna modelltyp tar speciell hänsyn till förhållandena i det atmosfäriska gränsskiktet. Resultaten från en kartering av vindresursen i Sverige med 1 km^2 horisontell upplösning presenteras här.

En teknik har använts där man enbart modellerar ett urval av de meteorologiska förhållanden som styr vindklimatet på de höjder som är av intresse för vindenergin. Detta kunde visas ge resultat i god överensstämmelse med observationer, varför det inte var nödvändigt att modellera en lång period av `riktigt väder'. Genom att välja ett `relevant' urval, kunde antalet modellberäkningar begränsas till 192 st, vilket svarar mot 4608 modellsimulerade timmar (representerande 4 månader x 3 styrkor x 16 riktningar x 24 timmar vardera).

Statistik för den horisontella lufttrycksgradienten (geostrofiska vinden), den huvudsakliga kraft som driver den faktiska vinden, användes för att vikta samman modellresultaten till det slutliga klimatologiska resultatet. Lufttrycksdata från 3 observationsplatser i södra Sverige och 3 platser i norra Skandinavien utnyttjades då primärt. Då den geostrofiska medelvinden varierar en hel del över ett så pass stort område som Sverige behövde hänsyn tas till detta. För detta ändamål användes återanalysdata från NCEP/NCAR för att beräkna den geostrofiska vindens geografiska variationer vilket utnyttjades vid beräkningen av vindklimatet.

Jämförelser med vindobservationer på 84 platser visade att den modellberäknade årsmedelvinden är i god överensstämmelse med uppmätta värden. Medeldifferensen mellan modellresultaten och observationerna visade sig vara -0.03 m/s och för 87 % av jämförelsepunkterna låg differenserna inom ±0.4 m/s.

Ytterligare vindstatistik, förutom årsmedelvärdena, har beräknats utgående från databasen av modellerade atmosfärsparametrar. Den innehåller:

- Fördelningarna av vindhastighet och vindriktning, tillsammans med de sektorsvisa Weibullparametrarna i 12 riktningssektorer.
- Extremvindar av 10 min medelvind och 3 s byvinden som förväntas för en 50 årsperiod.
- Vindgradienten given som exponenten i den exponentiella vindprofilen.
- Turbulensintensiteten beräknad utgående från den turbulenta kinetiska energin.
- Vindturbinklasser beräknade utgående från den modellerade medelvinden och turbulensintensiteten vilka översatts till referensvindhastigheten och referensvärdet av turbulensintensiteten vid 15 m/s.

All vindstatistik finns tillgänglig via Internet på:

http://www.geo.uu.se/luva/default.aspx?pageid=13152&lan=0.

Det är emellertid viktigt att komma ihåg att modellen inte med exakthet löser upp inflytandet av terrängvariationer på skalor mindre än några gånger avståndet mellan modellens beräkningspunkter. Med 1 km^2 upplösning fångas huvuddragen hos de geografiska variationerna i vindklimatet, med upplösningen är ofta för grov för detaljerad planläggning av en vindpark och för bestämning av de exakta positionerna av vindturbinerna i en vindpark. För detta ändamål krävs en vindkartering med högre upplösning. Detta har tidigare oftast gjorts med hjälp av en modell som WA^{S}P, antingen direkt eller som ett verktyg i WindPro. En sådan modell har en förenklad fysikalisk beskrivning av atmosfären varför resultaten i vissa fall kan ifrågasättas.

Att används en högre ordningens meteorologisk CFD-modell såsom MIUU-modellen har tidigare i praktiken varit orealistiskt för en nedskalning till den höga upplösning som behövs för lokal mikroskaleplanering. Som en följd av den hydrostatiska approximationen i MIUU-modellen beslöts att testa ytterligare en meteorologisk CFD-modell av samma typ, men av icke-hydrostatisk typ. Valet av denna andra modell blev COAMPS®, Coupled Ocean/Atmosphere Mesoscale Prediction System (COAMPS®, ett av Naval Research Laboratory registrerat varumärke).

En jämförelse mellan modellerade årsmedelvindar i området vid Fjällberget/Saxberget i Dalarna, Sverige, visade att båda CFD-modellerna ger realistiska resultat. Vissa skillnader finns emellertid, och jämförelser med observationer i området visade att MIUU-modellen verkar ge bäst överensstämmelse med mätningarna trots antagandet om hydrostatik. Orsaken till detta kan höra samman med skillnader avseende beräkningen av turbulensen och även avseende den rutin som beräknar energibalansen vid ytan vilket i sin tur kan resultera i skillnader i den termiska skiktningen.

Slutsatsen av jämförelsen blir att nedskalning med hjälp av en högre ordningens CFD-modell är realistisk och ger resultat i överensstämmelse med observationer. Observationer med mycket högre horisontell upplösning krävs dock för att fullt ut utvärdera skillnaderna mellan de två modellerna. Det är även sannolikt att resultaten är mer realistiska jämfört med resultaten från modeller med en mer förenklad fysik, speciellt när de indata som behövs till de förenklade modellerna inte finns tillgängliga på platsen eller endast från en plats i området på en höjd som inte är representativ för hela området av intresse. Detta som en följd av att skillnaderna mellan den högre och den lägre terrängen befanns vara mycket mindre för den enklare modellen än för CFD-modellen.

Det bör noteras att inga lokala vindobservationer inkluderas eller behövs för beräkning av vindresursen med användande av MIUU-tekniken tillsammans med resultaten från en högre ordningens modell. Således är modellresultaten helt oberoende av observationerna med vilka en jämförelse kan göras.

Innehåll

1 Introduction

The use of meso-scale models for wind resource assessments has increased during resent years. Especially in complex terrain, the need for more advanced models than has earlier been used is often obvious. Also observations of offshore winds over the Baltic Sea show complexity and inhomogeneity to a much larger extent than are often expected regarding offshore winds (Källstrand et al., 2000). This may also affect winds in coastal areas.

Spatial variations of wind speed over large offshore areas, such as the Baltic Sea, are difficult to measure directly, although radar observations from satellites look promising at least for estimating the 10 m winds (Hasager et al., 2004). Instead models still have to be used. Often these models include just a simplified description of the physics determining the boundary layer wind profiles and the horizontal variation of the wind at a particular site, as e.g. in the WA^{S}P-model. For instance, simplified models will not be able to account for the effects of large-scale thermally drive flows, since the physics needed for this is not included in the models (Bergström, 2002).

Existing measurements over the Baltic Sea area have shown that the atmospheric boundary layer often departs from the simplified relations. Even during the thermally most stable conditions, when the adapting process is very slow, the wind in the layer of interest for wind energy should, according to the simplified models, soon be in equilibrium with the new surface. This is at least true for distances from the coast of the order 20 km. Several factors, however, make this assumption about equilibrium conditions at large distances from the coast invalid, (Källstrand et al., 2000). One factor is the low-level jets often observed in the Baltic Sea area, whose origins may be an inertial oscillation initiated with air flowing from land (Källstrand, 1998). Coastal convergence, thermally driven flows as the sea breeze circulations, and thermal winds are other phenomena, which may give rise to low-level jets and heterogeneous offshore wind fields. Although the thermally driven flows may not always give rise to a sea breeze, the temperature differences between land and sea often affect the wind field far out at sea; such influences change both wind speed and direction from what would otherwise occur.

Non-homogeneous offshore conditions may also be due to the growth of the internal boundary layer differing from the expected. Offshore internal boundary layers may develop much more slowly than predicted by the simplified models. Moreover, observations show that, with stable conditions over the sea, the wind speed may even, contrary to what is normally assumed, decrease with distance offshore up to at least 100 km from the coast (Källstrand et al.; 2000, Törnblom et al, 2007). Due to the complex interaction between land and sea, the offshore wind is often not only a function of distance from the coast but also of the curvature of the shoreline. Such influences may be complex and can even be found upstream the coast (Källstrand and Smedman, 1997).

Results with a higher-order closure meso-scale models show that with this type of model the observed complex and inhomogeneous wind fields also turn up in the model results (Källstrand et al., 2000; Bergström, 2002). A higher-order closure model is, however, computer-time consuming to run, why care has to be taken to limit the number of model runs needed as much as possible.

A method to simulate the climatological wind field using the MIUU-model (Meteorological Institute Uppsala University model) has been developed at Uppsala University, reducing the total number of simulations needed. With this method a limited number of climatologically relevant simulations are performed, with different wind and temperature conditions, and a weighting based on climatological data for the geostrophic wind (horizontal pressure gradient) is made in order to finally estimate the wind climate. The method is applicable for mapping the wind resources with a resolution of 0.5-10 km. To use this method geostrophic wind (strength and direction), sea and land temperatures, topography, roughness, and land use are needed. No observed boundary-layer winds are needed other than for verification. Comparisons between model results and measurements show good agreement.

2 The MIUU-model

The MIUU-model is a three-dimensional hydrostatic, non-linear meso-scale model with terrain following coordinates. The model has been developed at the Department of Meteorology, Uppsala University, Sweden, (Enger, 1990). It uses a higher order turbulence closure scheme of level 2.5 following Mellor and Yamada, (1974). This means that the model has prognostic equations for the mean variables U = wind component in east-west direction, V = wind component in north-south direction, θ = the potential temperature, and r = specific humidity, as well as for q^2 = twice the turbulent kinetic energy (TKE), while the other parameters are treated diagnostically in every time step. The model includes a radiation scheme that calculates the surface temperature and humidity from an energy balance equation at the surface. The energy balance equation includes a vegetation layer.

2.1 Basic equations

A terrain following coordinate system is used (Pielke, 2002). The vertical coordinate is then defined as

$$\eta = s\frac{z - z_g}{s - z_g} \tag{2.1}$$

where s is the height of the model top, z the height above ground and z_g is expressed as:

$$z_g = h + d + z_0 \tag{2.2}$$

where h is the terrain height, d is the zero displacement and z_0 is the surface roughness length. Thus the coordinate system is roughly following the terrain close to the surface and gradually transforming into horizontal at the model top.

The basic equations of motions for the mean horizontal wind components U and V are transformed into the new co-ordinate system using tensor analysis (see Pielke, 2002) and take on the following form:

$$\frac{dU}{dt} = \left(\frac{s}{s - z_g}\right)^2 \frac{\partial}{\partial \eta}\left(K_m \frac{\partial U}{\partial \eta}\right) - fV_g - \Theta\left(\frac{\partial \pi}{\partial x}\right)_{\eta=c} + g\frac{\eta - s}{s}\frac{\partial z_g}{\partial x} + fV \tag{2.3}$$

$$\frac{dV}{dt} = \left(\frac{s}{s - z_g}\right)^2 \frac{\partial}{\partial \eta}\left(K_m \frac{\partial V}{\partial \eta}\right) + fU_g - \Theta\left(\frac{\partial \pi}{\partial y}\right)_{\eta=c} + g\frac{\eta - s}{s}\frac{\partial z_g}{\partial y} - fU \tag{2.4}$$

where f is the Coriolis parameter, U_g and V_g are the geostrophic wind components, θ is the potential temperature, and K_m is the turbulent exchange coefficient for momentum.

The prognostic equations for potential temperature and humidity are given by:

$$\frac{d\theta}{dt} = \left(\frac{s}{s - z_g}\right)^2 \frac{\partial}{\partial \eta}\left(K_H \frac{\partial \theta}{\partial \eta}\right) + \sigma_r \tag{2.5}$$

$$\frac{dr}{dt} = \left(\frac{s}{s - z_g}\right)^2 \frac{\partial}{\partial \eta}\left(K_H \frac{\partial r}{\partial \eta}\right) \tag{2.6}$$

Where K_H is the turbulent exchange coefficient for heat and σ_r is the radiative heating/cooling rate.

The total derivative is given by:

$$\frac{d}{dt} = \frac{\partial}{\partial t} + U\frac{\partial}{\partial x} + V\frac{\partial}{\partial y} + W^*\frac{\partial}{\partial \eta} \tag{2.7}$$

U and V are the new quasi-horizontal wind components, W^* is the vertical component in the terrain following co-ordinate system

The vertical velocity is calculated from the continuity equation, which for the hydrostatic conditions becomes:

$$\frac{\partial U}{\partial x} + \frac{\partial U}{\partial y} + \frac{\partial W^*}{\partial \eta} = \frac{1}{s - z_g}\left(U\frac{\partial z_g}{\partial x} + \frac{V\partial z_g}{\partial y}\right) \tag{2.8}$$

The Cartesian vertical velocity can then be calculated as:

$$W = \left(\frac{\partial \eta}{\partial z}\right)^{-1}\left(W^* - U\frac{\partial \eta}{\partial x} - V\frac{\partial \eta}{\partial y}\right) \tag{2.9}$$

$$\pi = c_p\left(\frac{p}{p_{00}}\right)^{\left(\frac{R_d}{c_p}\right)} \tag{2.10}$$

is the Exner function (also named scaling pressure), where p is the pressure, p_{00} a reference pressure (usually p_{00}=1000 hPa), c_p the specific heat for air at constant pressure and R_d the gas constant for dry air.

By using the hydrostatic assumption the third equation of motion, for the vertical velocity W, takes the form of the hydrostatic equation in terrain-following co-ordinates that is:

$$\frac{\partial \pi}{\partial \eta} = -\frac{g}{\theta}\frac{s - z_g}{s} \qquad (2.11)$$

This equation is only valid if the terrain slope in the model always is less then 45°, i.e. if $\frac{\partial z_g}{\partial x} << 1$ and $\frac{\partial z_g}{\partial y} << 1$ which has to be fulfilled in the whole model domain.

The present version of the MIUU-model contains a higher order turbulence closure scheme of the level 2.5. This scheme is basically a so called "Yamada-Mellor level 2.5" scheme

The turbulent kinetic energy $\frac{q^2}{2}$ is calculated from, based on a higher order closure scheme (Andrén, 1990):

$$\frac{dq^2}{dt} = \left(\frac{s}{s - z_g}\right)^2 \frac{\partial}{\partial \eta}\left(Eq\lambda \frac{\partial q^2}{\partial \eta}\right) + 2\frac{s}{s - z_g}\left(-\overline{uw}\frac{\partial U}{\partial \eta} - \overline{vw}\frac{\partial V}{\partial \eta}\right) + 2\beta g \overline{w\theta} - \frac{2q^3}{B\lambda} \qquad (2.12)$$

where β is the coefficient of thermal expansion, λ a turbulent length scale (=mixing length) which is diagnostically calculated every time step. E and B are empirical closure constants and

$$\left(-\overline{uw}, -\overline{vw}\right) = \frac{s}{s - z_g} K_M \left(\frac{\partial U}{\partial \eta}, \frac{\partial V}{\partial \eta}\right) \qquad (2.13)$$

and

$$-\overline{w\theta} = \frac{s}{s - z_g} K_H \frac{\partial \theta}{\partial \eta} \qquad (2.14)$$

The first term on the right hand side of equation (2.12) is the turbulent transport forces (Andrén 1990), the second term is the shear production, the third is buoyancy production and the fourth term is the dissipation.

Dissipation is parameterised in terms of the turbulent kinetic energy q^2 and the length scale λ:

$$\varepsilon = \frac{q^3}{B\lambda} \qquad (2.15)$$

In the model, the problem of expressing the unknown terms as a function of the second order moments and mean quantities reduces to formulating a dependence on the length scale λ. An accurate formulation of the length scale is the main problem of second-order schemes. For formulations of the length scale, see Enger, 1990 and Andrén, 1990.

The turbulent exchange coefficients for momentum and heat, K_M and K_H, are finally calculated as functions of q^2, λ, $\partial U/\partial \eta$, $\partial V/\partial \eta$ and $\partial \theta/\partial \eta$.

To reduce influences from the model boundaries, the modelled area is chosen to be much larger than the area of interest. This also makes it possible to account for effects of, for instance, mountains and enclosed water areas which are outside the investigated area, but which may anyhow be of importance to the wind field within the area of interest. To limit the number of horizontal grid points, a telescopic grid may be used, with the highest resolution only in the area of interest. The distance between adjacent grid points is then not allowed to increase by more than 6 %.

In the vertical, the lower levels are log spaced while the higher levels are linearly spaced. The lowest grid point is at height z_0, where z_0 is the roughness length, and the model top is typically at 10000 m. Commonly 8 levels are used in the model up to 100 m height. These 8 levels are 2.0, 6.4, 12.4, 20.9, 32.6, 48.9, 71.3 and 103.0 m.

At the lower boundary, roughness length and altitude (of land) have to be specified at each grid point. Topography and land use are taken from digitised maps, with a resolution of 1 km (the U.S. Geological Survey, the University of Nebraska-Lincoln, and the European Commission's Joint Research Centre 1-km resolution global land cover characteristics database, 1999, version 2.0). The roughness, z_0, over land has been divided into classes according to land use, see Table 1. During winter, the roughness length is set to 0.001 m over open terrain to represent snow-covered land areas.

Also temperature has to be given or estimated at the lower boundary for each grid point. The land surface temperature, and its daily and monthly variation, is estimated with a surface energy balance routine using as input deep (~2 m) soil temperature, solar radiation and land use with the assumption that the soil consist mainly of clay loam. The deep soil temperature is approximated with the seasonal average screen height temperature, whereby the model reproduces the observed temperatures. Over sea the observed monthly average sea-surface temperatures have been used at the lower boundary, as the daily variation is small at least over the deep sea not close to the coasts.

The MIUU model has been used earlier in many case studies in different types of terrains, showing good agreement with observations. In Källstrand et al. (2000) the Baltic Sea offshore wind field is investigated. Simulations with the MIUU model in mountainous terrain have been done, for example around Lake Mohave in the Colorado River Valley (Enger and Grisogono 1998, Enger et al. 1993, Koracin and Enger, 1994). In Brooks et al. (2003), the turbulence structure in a coastal environment was studied with the MIUU-model and compared to aircraft observations. Wind climate investigations have been made for a mountain area in northern Sweden (Bergström and Källstrand, 2000 and 2001). In Bergström (1996) and Sandström (1997) the MIUU-model has been used to simulate the climatological wind field over the Baltic Sea. Bergström (2002) gives a general description on modelling the wind climate using a higher-order closure model like the MIUU-model, and in Bergström and Lindholm (2003) some tests are presented regarding the sensitivity of the resulting wind climate on the choice of model runs used for the final

climatological weighting. More details about the wind mapping over Sweden and wind climate modelling in general are given in Bergström (2004).

Table 1: IGBP Land Cover (International Geosphere Biosphere Programme Land Cover Classification, Belward et al., 1999) and the accompanying roughness lengths used.

Value	Description	roughness length (m)
1	Evergreen Needle-leaf Forest	0.6
2	Evergreen Broadleaf Forest	0.6
3	Deciduous Needle-leaf Forest	0.6
4	Deciduous Broadleaf Forest	0.6
5	Mixed Forest	0.6
6	Closed Shrub lands	0.2
7	Open Shrub lands	0.06
8	Woody Savannas	0.2
9	Savannas	0.08
10	Grasslands	0.07
11	Permanent Wetlands	0.07
12	Croplands	0.07
13	Urban and Built-Up	0.7
14	Cropland/Natural Vegetation Mosaic	0.07
15	Snow and Ice	0.001
16	Barren or Sparsely Vegetated	0.01
17	Water Bodies	0.00025

3 Wind climate modelling

In an ideal climate study, model runs should be made representing all weather conditions. But this would require an unrealistic large number of simulations. Since the MIUU-model is rather computer-time consuming to run, some compromises have to be made. The parameters of greatest importance to the flow have to be identified and varied in order to cover an as wide range of atmospheric conditions as needed in order to get an accurate description of the wind climatology. The parameters judged to be of most importance to the wind field are (based on comparisons between modelled and observed average winds): The horizontal air pressure gradient (i.e. geostrophic wind, strength and direction), thermal stratification (through the daily temperature variation), surface roughness, topography, and land-sea/lake temperature differences (Bergström, 2002).

The primary force driving the wind is the horizontal air pressure gradient, which could be translated into the geostrophic wind speed U_g,

$$U_g = \sqrt{u_g{}^2 + v_g{}^2} \tag{3.1}$$

where

$$u_g = -\frac{1}{\rho f}\cdot\frac{\partial p}{\partial y}; \qquad v_g = \frac{1}{\rho f}\cdot\frac{\partial p}{\partial x} \tag{3.2}$$

are the west-east and south-north geostrophic wind components respectively, ρ = air density, p = air pressure, x and y are the west-east and south-north coordinates respectively. The Coriolis parameter $f = 2\Omega\sin\phi$, where Ω = the rotational speed of the Earth and ϕ = latitude.

The simplest approach would be to use only the mean geostrophic wind speed in the simulations. But this would reduce the effect of thermal stability, i.e. of how the temperature varies with height in the atmospheric boundary layer. This is so because the daily stability variations are much larger with a low geostrophic wind speed compared to a high one. The effect of thermal stability is sometimes very large, and this is why it is important to include simulations with different geostrophic wind speeds. Therefore model runs with three values of the geostrophic wind speed (5, 10, and 15 m/s) for 8 wind directions have been used in earlier investigations of the wind climate made with the MIUU-model (Bergström, 1996, Sandström, 1997).

Here 4, 9, and 14 m/s were used instead, as this was judged to be somewhat more representative for the actual geostrophic wind distribution in the Scandinavian area, and also 16 wind directions were used instead of 8 in order to better resolve topographical and coastline flow modifications.

The air temperature shows both clear annual and daily variations, which also must be included in the simulations. To limit the number of model runs, but still include the annual variations, four months (January, April, July and

October) have in earlier investigations been selected to represent the four seasons, which is sufficiently accurate for the purpose of modelling the wind climate. This will also make it possible to take into account seasonal variations in the difference in temperature between land and sea, which affects the wind climate.

A monthly average soil temperature has been used as input to the surface energy balance routine, which estimates the surface temperatures over land. To include the spatial differences, observed screen height (1.5 m) temperatures from a number of weather stations have been used to estimate the average soil temperature, and the observed data have been interpolated within the model domain. The mean temperature is also allowed to vary with wind direction. Typically winds from the northern sector are colder than winds from the south in Northern Europe. Thus the mean temperature for different directions was also estimated. The daily variation of sea surface temperature is small compared with the variations of the air temperature. Therefore, model runs were made with the seasonal mean sea surface temperature at each grid point, with no daily variation but including a spatial variation. Although it is important to keep the daily variation in air temperature, it is accurate enough to use the average sea surface temperature at the lower model boundary.

Summing up, for each season, runs were made with three values of the geostrophic wind speed, and with 16 wind direction sectors, summing up to 192 model runs to cover the most important parameters determining the boundary layer wind climate. Each simulation was made for a 30-hour time period, of which only the last 24 hours were used, allowing for 6 hours initialisation of the model. The background flow for each model run is specified as a geostrophic wind constant in time but with a variation with height (thermal wind) following climatological averages estimated from radio-soundings in the area. Also the initial potential temperature and humidity profiles were taken from climatologically averaged radiosonde data for the different seasons.

All simulations are finally weighted together using climatological statistics of the geostrophic wind. The statistics used for southern Sweden was estimated from sea-level pressure data measured at Visby, Göteborg, and Lund 1900-2000. The corresponding statistics used for northern Sweden was estimated from pressure data measured at Bodö, Härnösand, and Haparanda. Monthly distributions of the geostrophic wind speed were determined for the 16 directions of the geostrophic wind using 1 m/s bins. The annual distributions of geostrophic wind speed and direction are shown in

Figure **1** and Figure 2 for northern and southern Sweden respectively.

The climatological averages for each month, grid point, and height are then given by

$$U_{CLIM}(month) = \sum_{j=1}^{16}\left[\sum_{i=1}^{7} U_4 \cdot W_4(i)\cdot f_u(i) + \sum_{i=8}^{13} U_9 \cdot W_9(i)\cdot f_u(i) + \sum_{i=14}^{50} U_{14} \cdot W_{14}(i)\cdot f_u(i)\right]\cdot f_{wd}(j) \quad (3.3)$$

U_k (k=4,9,14) are the modelled daily average wind speeds at each location, based on 24 hourly values representing the daily variation as given by the model for simulations with the surface geostrophic wind speeds 4, 9 and 14 m/s. $W_k(i)$ are weighting functions by which the wind speed for all geostrophic wind speeds in bins of 1 m/s may be evaluated from the simulations made for 4, 9, and 14 m/s of the geostrophic wind. Linear weighting has been used where the model results for runs with 4 m/s of the geostrophic wind speed are used to represent geostrophic winds between 1 m/s and 7 m/s, summing for i=1-7. Runs with 9 m/s geostrophic wind speed are taken to represent the interval 8 m/s to 13 m/s summing for i=8-13, and runs made with the geostrophic wind speed 14 m/s are used for geostrophic winds between 14 m/s and 50 m/s, summing for i=14-50. The seldom-occurring higher geostrophic winds are not taken into account. The probabilities for different geostrophic wind speeds, estimated from observed surface pressure statistics translated to geostrophic wind speeds according to Eq. (3.1) and (3.2), are given by $f_u(i)$. Finally a summation over $j=1-16$ is made over the 16 geostrophic wind directions for which model runs have been made and $f_{wd}(j)$ gives the observed probabilities of the 16 geostrophic wind directions.

The annual mean wind speed may then be calculated by weighting the four individual months together. Thus, the result from a study of the climatological wind field may be presented as the mean wind speed (annual or seasonal), or wind energy potential, at different heights. The wind speed distribution and the corresponding Weibull parameters may also be determined. It should be pointed out that the MIUU model uses no local wind measurements as input, but it is of course important to validate the results against observations.

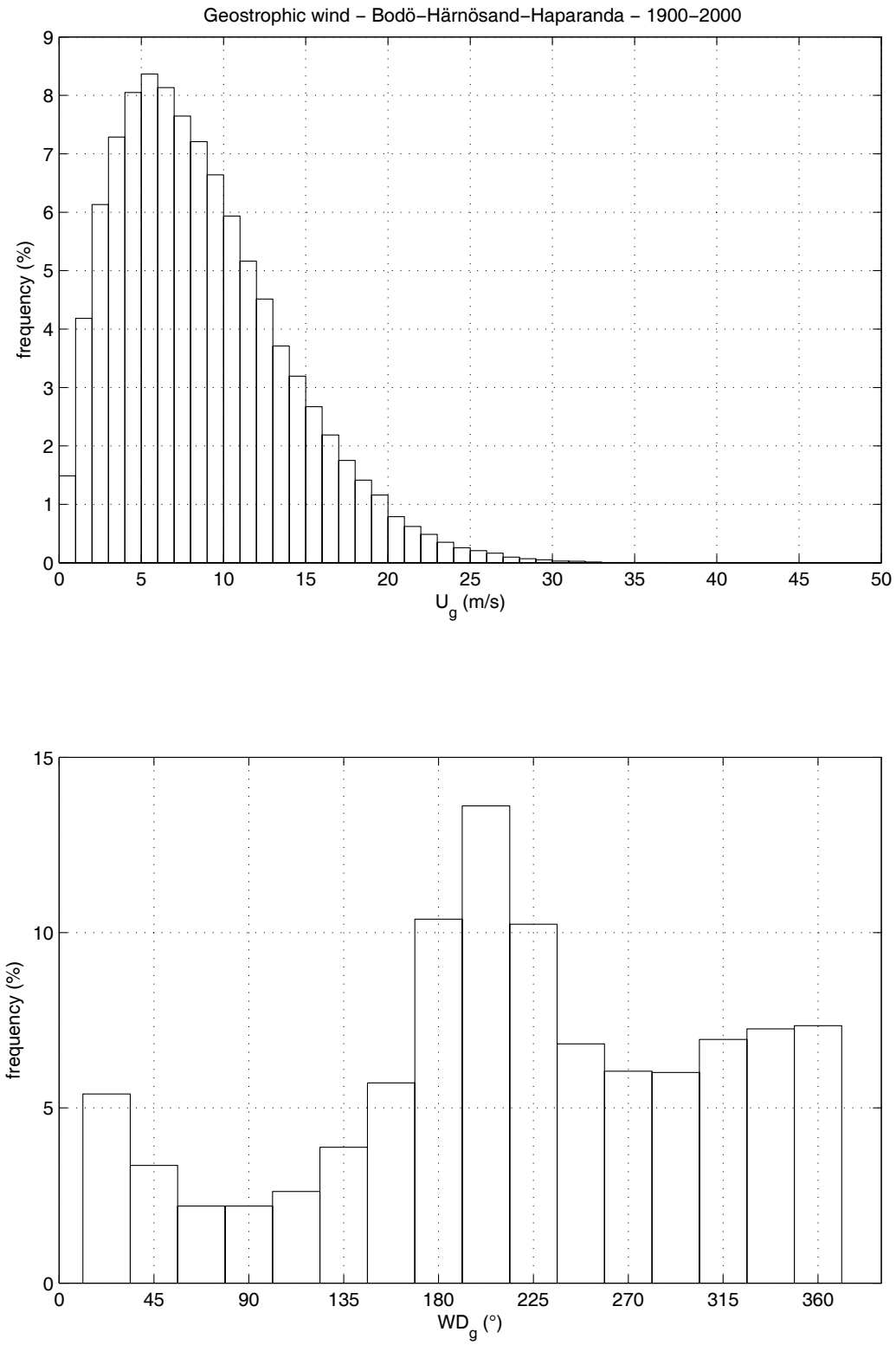

Figure 1: Distribution of geostrophic wind speed (top) and direction (bottom) calculated from sea-level pressure data taken at Bodö, Härnösand, and Haparanda 1900-2000.

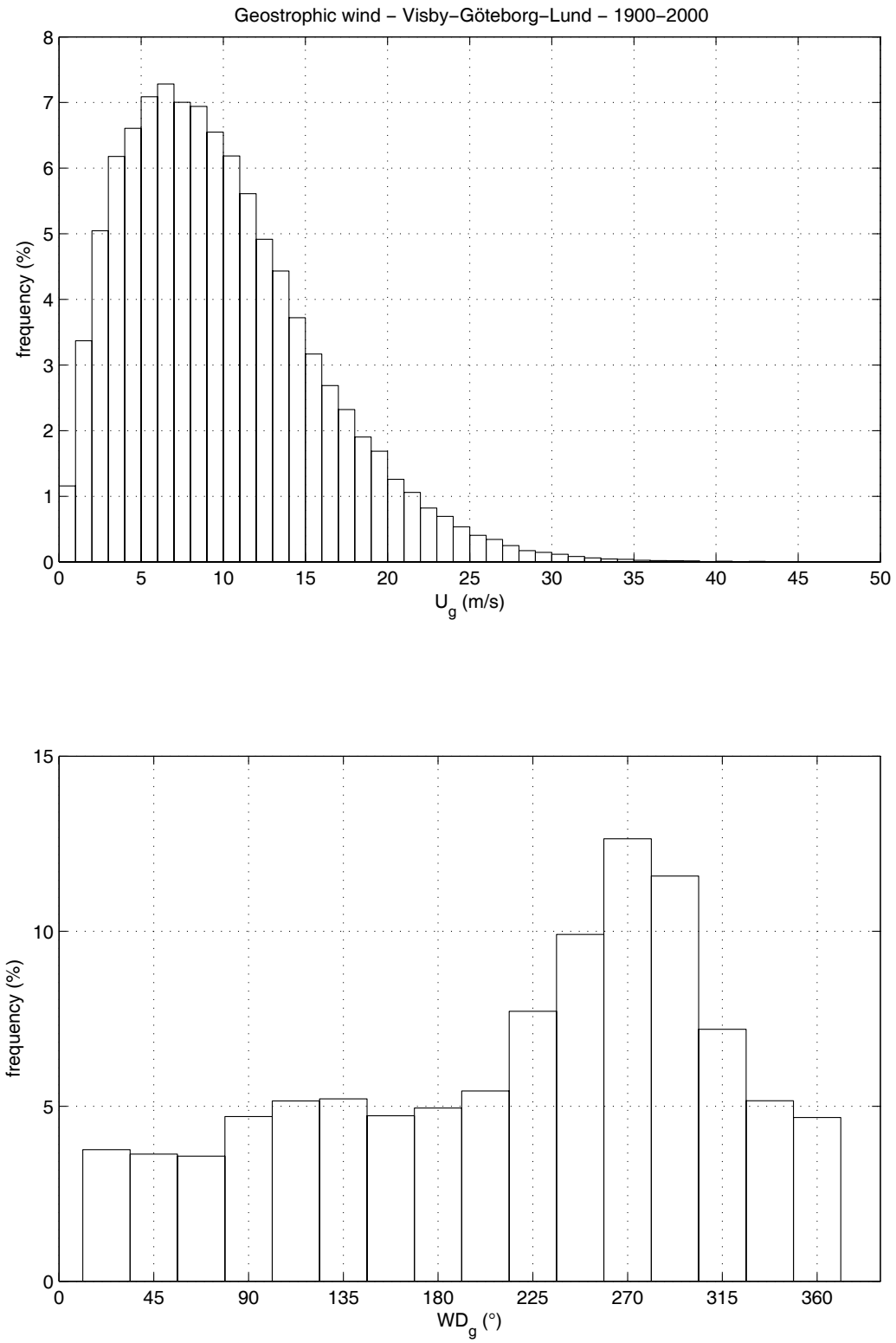

Figure 2: Distribution of geostrophic wind speed (top) and direction (bottom) calculated from sea-level pressure data taken at Visby, Göreborg, and Lund 1900-2000.

4 Model domain

When mapping the wind resources of a limited area, like Sweden, earlier investigations have shown the importance of including surrounding sea and mountain areas in order to get accurate results, see e.g. Källstrand et al. (2000). Therefore it is not sufficient to just include Sweden in the modelled area. The Baltic Sea and the surrounding land areas must be included for example to adequately take into account the influence from marine low-level jets and thermally driven flows evolving due to temperature differences between land and sea (Bergström, 2002). Also the Scandinavian mountain range has a great impact in the wind pattern over Sweden, and must consequently be included into the model domain.

Due to these effects upon the wind climate over Sweden from features outside Sweden itself, it was judged necessary to include the whole of Scandinavia, together with the Baltic Sea and the Bothnian Sea, including surrounding land areas, into the model domain. The goal of the wind mapping was to get the wind resource over the whole of Sweden on a 1 km resolution. But as the area, which has to be included in order to take the necessary surroundings into account, is rather large, almost 3000000 km^2, it was not possible to run the MIUU-model for the whole area on a 1 km horizontal resolution in one step. Instead the work was done in two phases.

Therefore phase one of the wind-mapping project was to make a first set of runs using 5 km horizontal resolution. For practical reasons these 5 km model runs were made for two separate areas, one covering Southern Scandinavia and one over Northern Scandinavia, as can be seen in Figure 3. Not only Scandinavia, but also surrounding areas, was included into the model domains. Outside the 5 km grid spacing areas, shown in Figure 3, a region with gradually expanding grid distances was used to increase the modelled area even further but at the same time limiting the number of grid points. Typically this boundary region was chosen to be about 200 km wide, but to the north of the Southern Scandinavia grid about 1200 km wide and to the south of the Northern Scandinavia grid about 800 km wide. This was done so in order to include the whole Scandinavian Peninsula in the Southern Scandinavia model runs, and to include the whole Baltic Sea area in the Northern Scandinavia runs.

The two model domains overlap in an area, about 400 km wide, over the central part of Scandinavia. This allowed a comparison between the results from the northern and the southern domains. Generally good agreement was found between the two (not shown), justifying the choice to make the 5 km model runs in two steps.

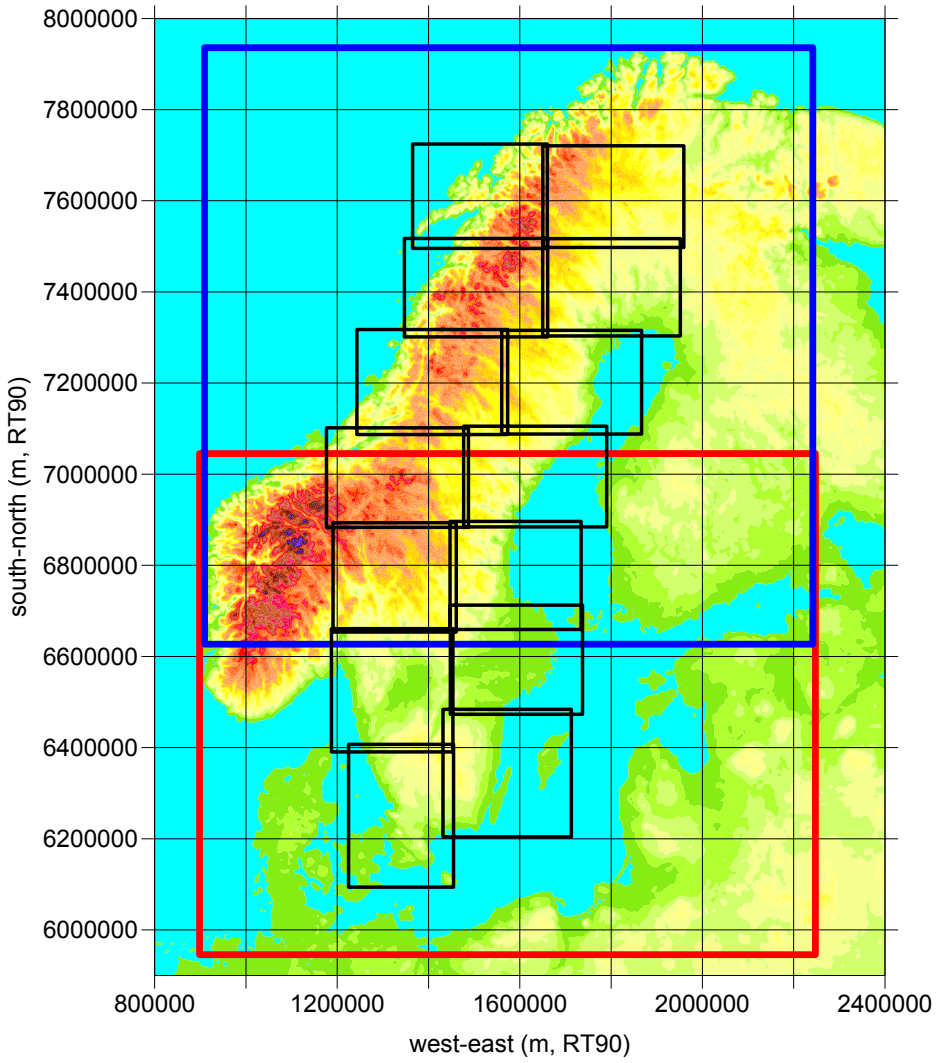

Figure 3: Map over Scandinavia and the Baltic Sea area showing the two 5 km model domains: 'Southern Scandinavia' (red square) and 'Northern Scandinavia' (blue square). Also shown are the 14 areas for which the 1 km model runs were made. Coordinates are given in the Swedish RT90-system in metres.

In phase two of the wind mapping project, as the aim is to model the wind climate on a 1 km horizontal resolution, smaller model domains with 1 km grid spacing were nested into the 5 km model runs. This means that the results from the 5 km runs were used to give the boundary conditions of 14 smaller model domains with a 1 km horizontal grid resolution; see Figure 3. For each of these 14 smaller 1 km domains, all 192 model runs was made to get the final estimates of the wind resource on the 1 km scale over the whole of Sweden. Also as regards the 1 km model domains, they overlap somewhat, as can be seen in Figure 3. Typically this overlapping region is here about 20 km wide, but outside this boundary region with a 1 km grid spacing, an area with expanding grid was used, typically about 50 km wide with a grid distance of about 5 km between the outermost grid points.

5 Geographical variation of geostrophic winds

In order to be able to weight the results from the different model runs together into the final wind climate estimate for the whole of Sweden, statistics of the horizontal air pressure gradient, i.e. the geostrophic wind, is needed. The geostrophic wind components are then given by Eq. (3.1) and (3.2). As discussed above surface air pressure observations, reduced to mean sea level, have been used for this purpose. To calculate the geostrophic wind from the air pressure data, simultaneous observations at three sites are needed. For Southern Sweden observations taken at Visby, Göteborg, and Lund have been used, while for Northern Sweden geostrophic winds were determined from observations at Bodö, Härnösand, and Haparanda. Pressure data from the weather stations at these sites have been thoroughly checked and homogenized; see Schmith at el. (1997). The location of these pressure observations sites are shown in Figure 4.

The geostrophic winds vary, however, with geographical locations, and also with time, see Johansson and Bergström (2004). Thus e.g. the annual average estimated from Bodö, Härnösand, and Haparanda is 8.7 m/s, while the annual average calculated from the pressure observations at Visby, Göteborg, and Lund is 9.7 m/s. This geographical variation should be taken into account when weighting together the model results. As the number of weather stations with reliable and homogenized surface pressure data is limited, and not evenly geographically distributed, the use of global atmospheric reanalysis data would be an interesting alternative. Two such datasets have been tested, the ERA40 reanalysis data from ECMWF using the European global circulation model, and the reanalysis data from NCEP/NCAR using the American global circulation model.

NCEP/NCAR data (Kalnay et al., 1996) for the years 1948-2006 was used here having data four times per day with a longitudinal and latitudinal resolution of 2.5°. Coordinates approximately corresponding to the pressure observation sites were chosen from the reanalysis data sets, and the mean sea level pressure reanalysis data was used to determine the geostrophic wind every six hours. These results were then compared to the geostrophic winds estimated from surface pressure data. The two estimates compare well both for Southern and Northern Scandinavia. The averages agree to within 0.1 m/s from each other, although the individual observations are somewhat scattered. In Bergström (2004) it was shown that the distribution of the differences in geostrophic wind for the Southern Scandinavian sites as estimated using sea level pressure observations or NCEP/NCAR data to more than 70% agree within ±2 m/s and almost 90% differ by less than ±3 m/s. Also the distributions of geostrophic wind speed itself agree well comparing results using the two methods to calculate the geostrophic wind, as was also shown in Bergström (2004). We may thus conclude that geostrophic winds calculated from NCEP/NCAR data agree well with results using weather station data, both for the northern and for the southern area.

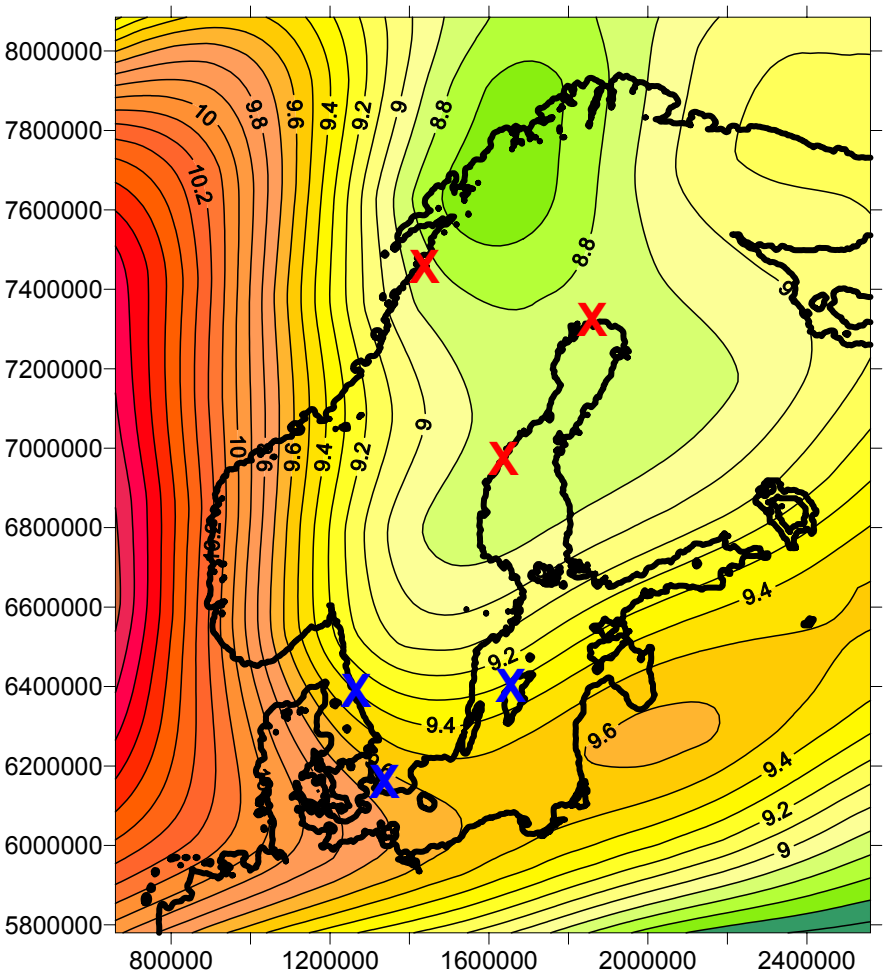

Figure 4: Annual average geostrophic wind speed over the Scandinavian area as estimated from NCEP/NCAR 850 hPa geopotential height data four times per day 1948 to 2006. The crosses mark the location of the sites from which surface pressure data were used to estimate geostrophic winds; blue crosses mark Visby, Göteborg and Lund; red crosses mark Bodö, Härnösand and Haparanda.

The variation in annual average geostrophic wind speed over Scandinavia and the Baltic Sea area as estimated using heights to the 850 hPa pressure surface (about 1000-1500 m above ground) from the NCEP/NCAR reanalysis data and the result is shown in Figure 4. The geostrophic wind was estimated using data from three points at a time, forming triangles from which the north-south and west-east gradients of the air pressure was determined, where after the geostrophic wind components were calculated using Eq. (3.2) and. These three points were separated by 2.5° in latitude and 5° in longitude.

The results show an area with higher values of the geostrophic wind speed over Southern Scandinavia and in over the southern parts of the Baltic Sea, where the averages reach 9.5 to 10 m/s. From this maximum the geostrophic wind decreases northwards to an area with a minimum below 9 m/s over

Northern Scandinavia and the northern parts of the Bothnian Sea. Further to the west over the North Sea and the Atlantic Ocean the numbers increase to between 10.5 and 11 m/s. It is obvious that the Scandinavian mountain range has a great influence upon the geostrophic wind field on the average. The minimum over central and northern Scandinavia is located in lee of the mountains and in the north centred above the mountains. The general patterns in the average field are probably related to the typical cyclone paths in the area. We conclude that the agreement with the results from the NCEP/NCAR data and the two sets of geostrophic winds calculated from surface pressure observation data are good.

To estimate the wind climate from the MIUU-model runs detailed geostrophic wind speed statistics (dependent on month and wind direction) are needed. Instead of determining all these detailed statistics for each model grid points using NCEP/NCAR data, geostrophic winds from Visby-Göteborg-Lund were used for the Southern Scandinavia runs, and data from Bodö-Härnösand-Haparanda were used for the Northern Scandinavia runs. Thus the first wind climate estimates from the climatological weighting of the MIUU-model results are arrived at assuming the same average geostrophic wind speed over either Southern Scandinavia or over Northern Scandinavia, cf. Eq. (3.3).

As this is obviously not true (cf. Figure 4), we need to account for the geographical variations after the first climatological weighting. This is done by making a second weighting. The resulting average winds are simply, at each grid point, multiplied with a factor estimated as the ratio between the average geostrophic wind at the individual grid points and the average geostrophic wind speed as given by the geostrophic wind data calculated using observations from Visby-Göteborg-Lund or Bodö-Härnösand-Haparanda, as these latter were originally used to weight the model output together to get the wind climate.

6 Wind climate over Sweden

The model runs using a 1 km horizontal grid spacing (cf. Section 4) have been used to estimate the wind resources over Sweden according to the procedures outlined in Section 3 and Section 4. The resulting annual average wind speed is presented in Figure 5, Figure 6, and Figure 7 at the heights 49 m, 72 m, and 103 m above the zero-plane displacement respectively. It is important to remember, however, that the results are based on model estimates with a 1 km grid spacing in the horizontal, why smaller terrain features, which may locally influence the wind climate, are absent in the results.

At 49 m the average wind speed is modelled to be 8.0-8.5 m/s offshore over the Baltic Sea, while over Southern Sweden typical average wind speeds are 5.5-6.5 m/s. In Northern Sweden the average wind speed is typically lower, 4.5-5.5 m/s, but the topographical influences are large and areas with annual average wind speeds up to 6-7 m/s are found over higher elevation terrain also in the forested parts. In the mountain areas average wind speeds up to 8-9 m/s are found. The offshore average wind speed in Northern Sweden, over the Bothnian Sea, is 7.0-7.5 m/s at 49 m height.

At 72 m height, see Figure 6, the model results show offshore average wind speed over the Baltic Sea which is 8-9 m/s, about 0.5 m/s higher than at 49 m. Over land in Southern Sweden, the 72 m average wind speed is typically 6.0-7.5 m/s, while in Northern Sweden the inland average wind speed is 5.0-6.5 m/s. Over some higher elevation terrain in Northern Sweden the average wind speed increases to 6.5-7.5 m/s, and in the mountain areas average winds around 9 m/s and more are common at 100 m height, while the offshore average wind speed over the Bothnian Sea is 7.5-8.5 m/s.

At 103 m height, see Figure 7, the model results show offshore average wind speed over the Baltic Sea which is 9.0-9.5 m/s, about 1 m/s higher than at 49 m. Over land in Southern Sweden, the 100 m average wind speed is typically 6.5-8.0 m/s, while in Northern Sweden the inland average wind speed is 5.5-7.5 m/s. Over some higher elevation terrain in Northern Sweden the average wind speed increases to 7.5-8.5 m/s, and in the mountain areas average winds around 10 m/s and more are common at 100 m height, while the offshore average wind speed over the Bothnian Sea is 8-9 m/s.

More detailed wind maps can be found at:
http://www.geo.uu.se/luva/default.aspx?pageid=13152&lan=1

The maps may be downloaded and show the annual average wind speed at 49 m, 72 m, and 103 m above the zero-plane displacement. All results are given for heights above the zero-plane displacement, which is commonly estimated to be about 3/4 of the height of the vegetation. That is having a 20 m high forest 15 m should be added to get height above ground. For the case with a 20 m high forest we get that the results at for example the height 72 m is valid at 72+15=87 m above ground.

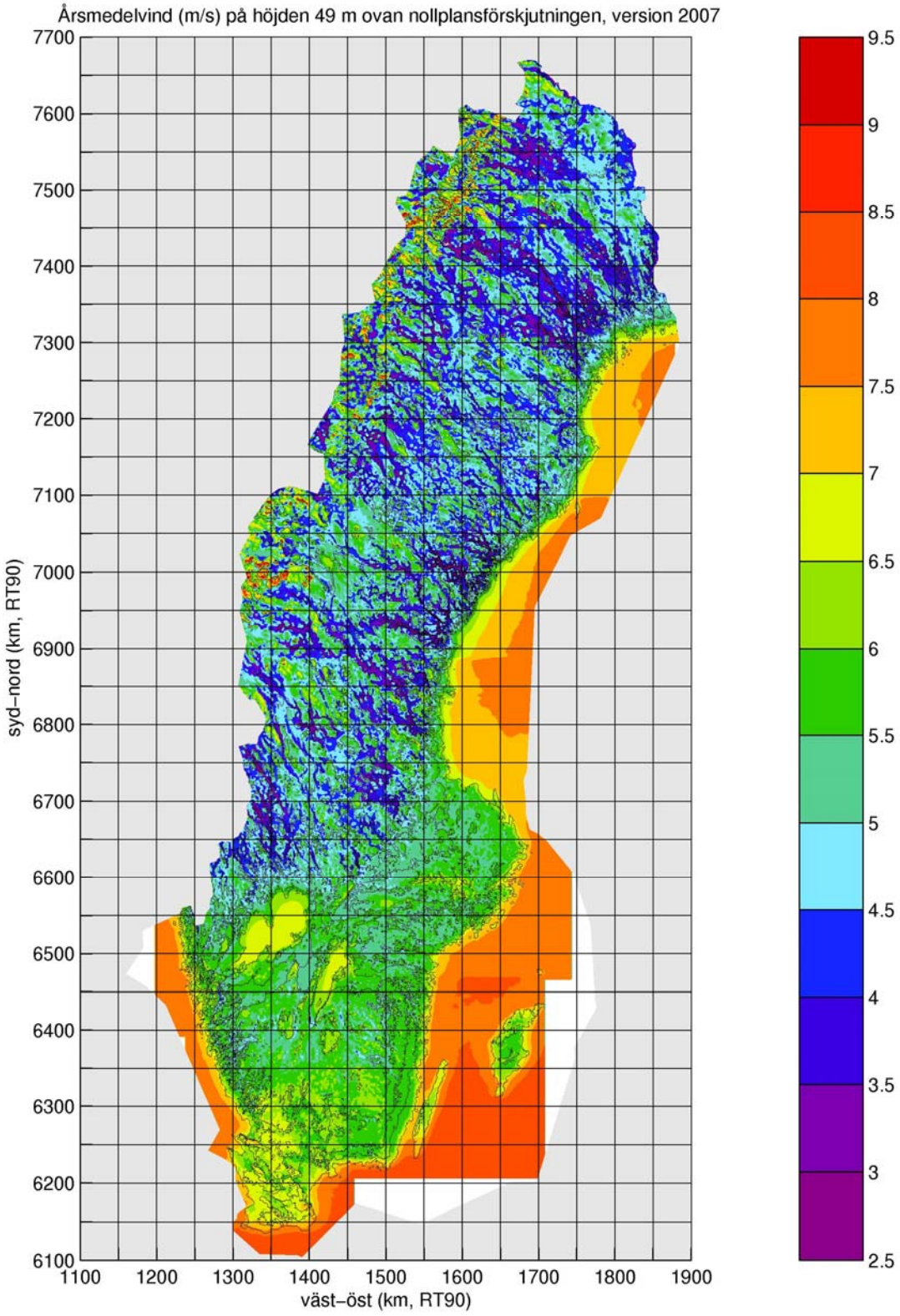

Figure 5: Annual average wind speed at 49 m height above zero-plane displacement as estimated from MIUU-model results.

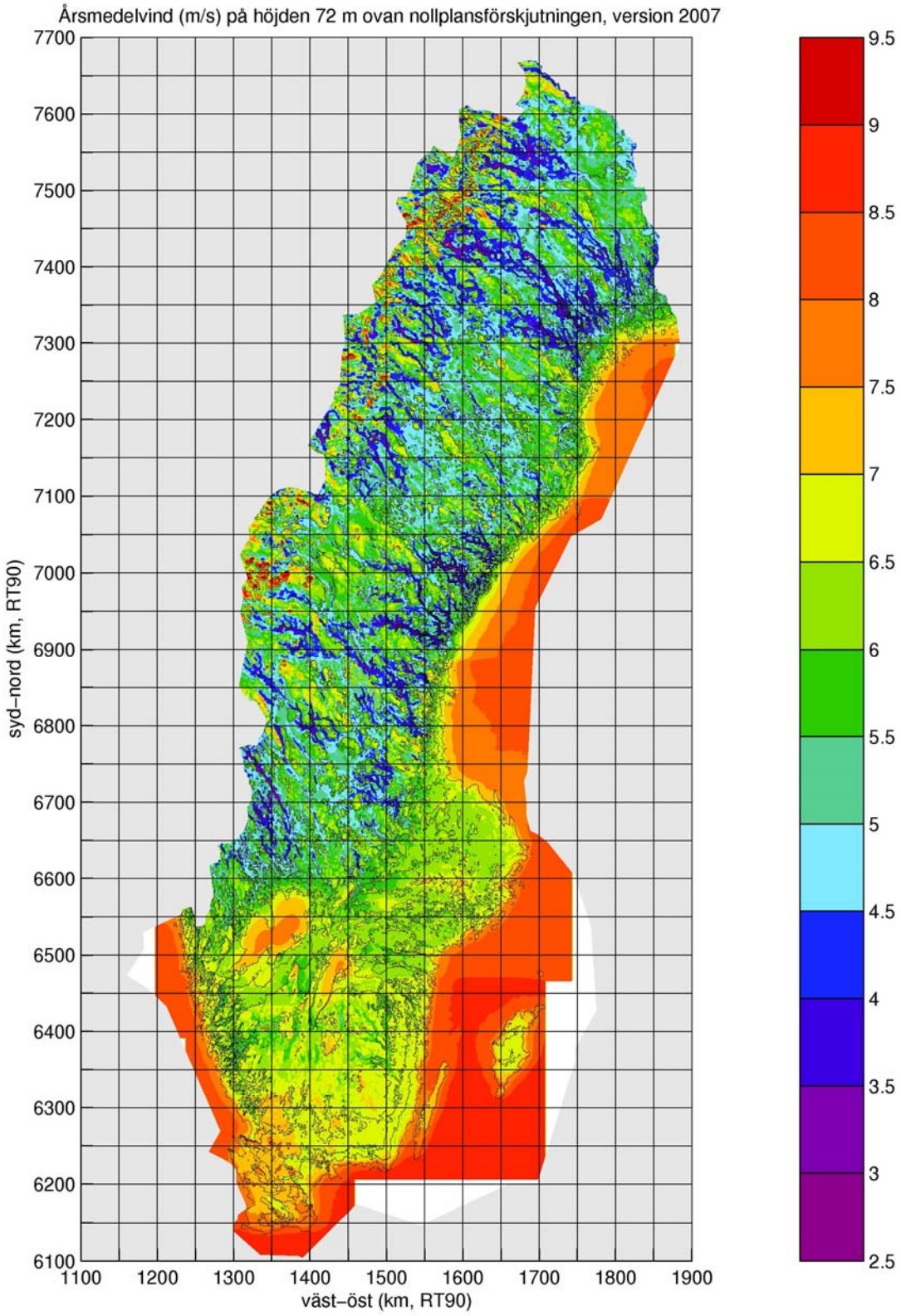

Figure 6: Annual average wind speed at 72 m height above zero-plane displacement as estimated from MIUU-model results.

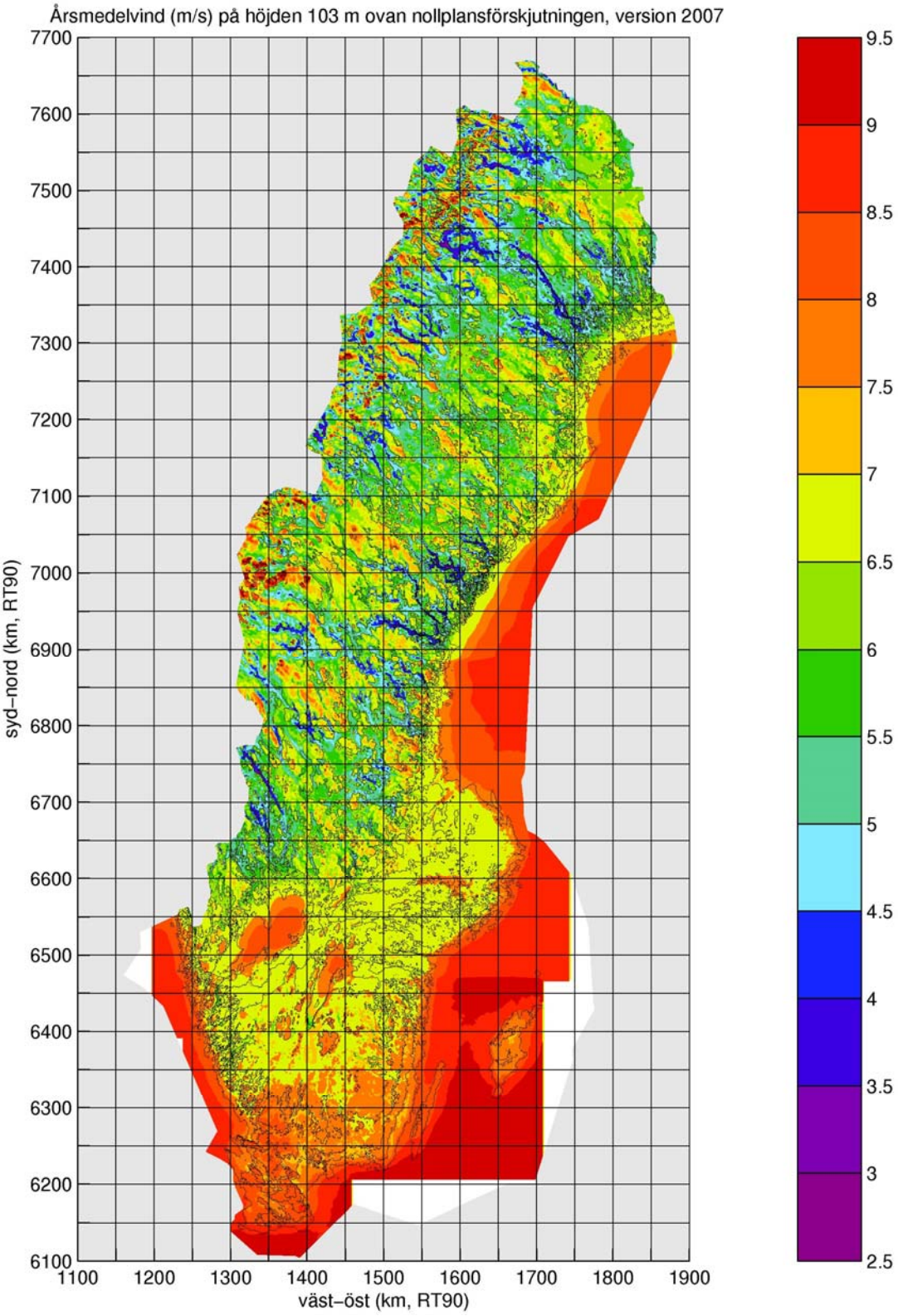

Figure 7: Annual average wind speed at 103 m height above zero-plane displacement as estimated from MIUU-model results.

7 Verification of modelled wind climate

In earlier investigations, where the MIUU-model was used with a 9 km horizontal resolution over the Baltic Sea area, the results have shown good agreement with observations; cf. Bergström (1996), Sandström (1997), and Bergström (2002). The new results with the 1 km resolution have also been verified against wind measurements. Altogether 84 sites have been used. Their locations are given in Figure 8, and Figure 9 show the distribution of the measurement heights. At some of the sites wind measurements were taken at more than one height, so that altogether 116 wind observations were compared to the model result. Some of the measurements were taken already during the 1980s, and the statistics concerning those have been taken from Krieg et al. (1987). Some wind measurements were initiated as part of the wind mapping project. Several of these newer measurements, and also some of the earlier, were taken as part of wind power projects and in cooperation with Bohus Energi AB, Orsa Besparingsskog, Suorvavind AB, Svevind AB, Vindkompaniet AB, Norra Smålands Energi AB, and HS Kraft AB.

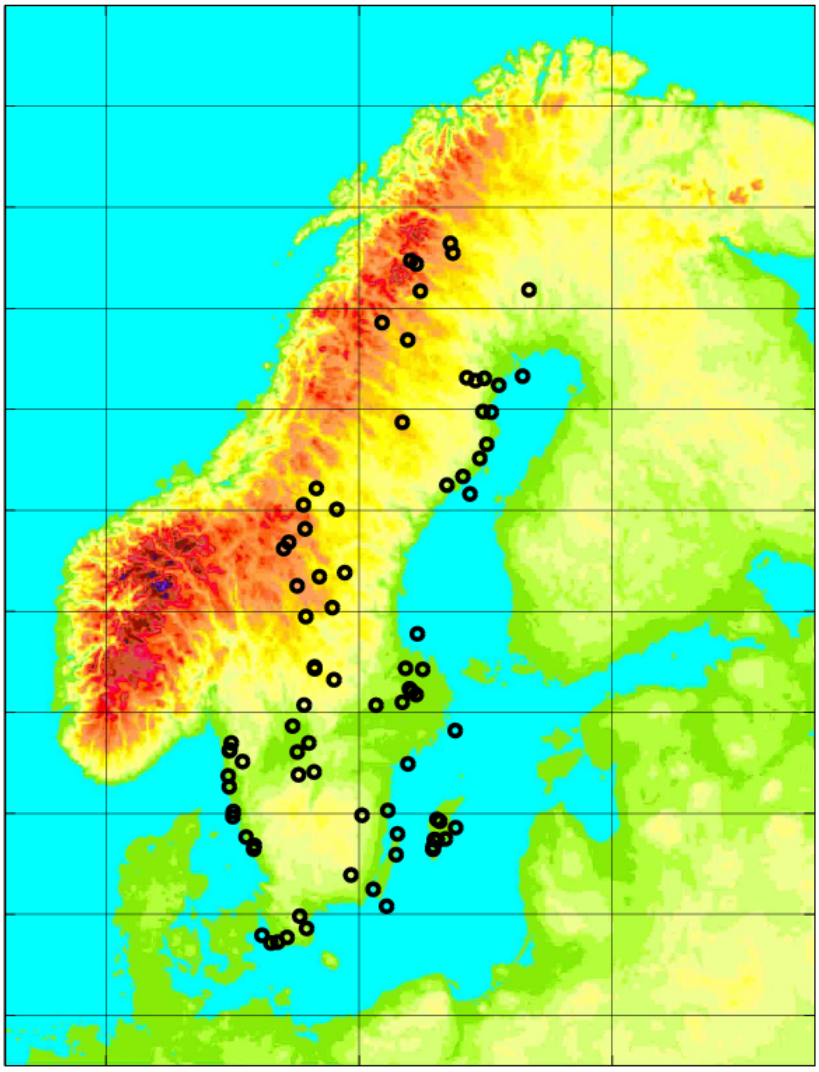

Figure 8: Map showing locations of 84 wind measurement sites used for model verification.

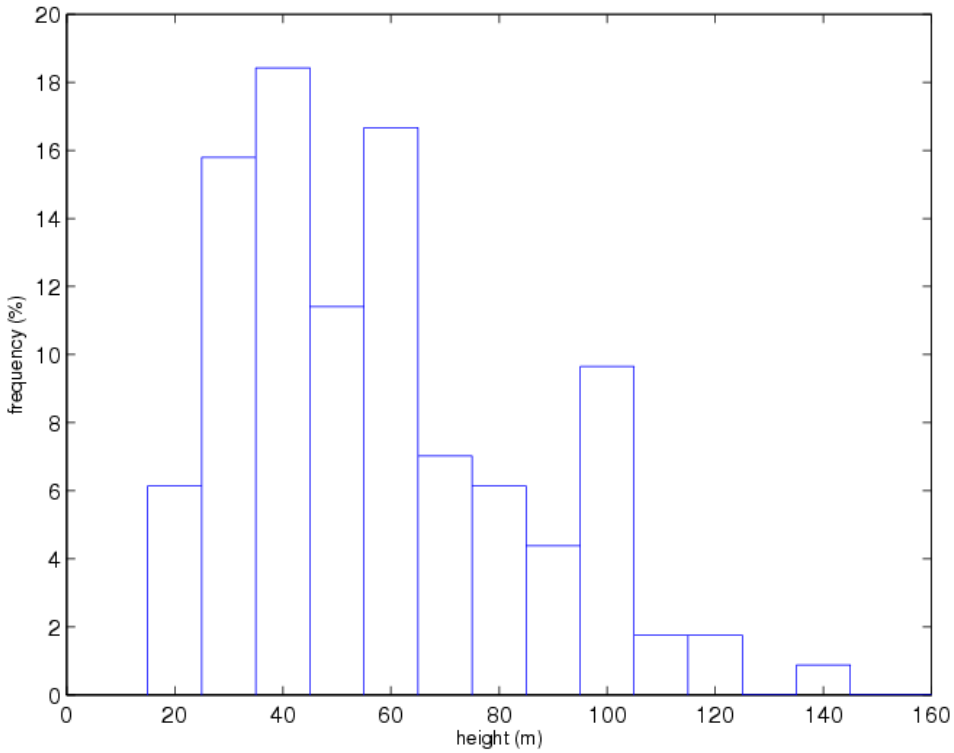

Figure 9: Distribution of measurement heights at the 84 sites used for model verifications.

A comparison between modelled and observed annual average wind speed is shown in Figure 10. The agreement is good between the two, deviations typically being of the order of just a few tenths of a m/s, although quite large deviations are occasionally found. Especially this is so for 11 sites, indicated by the red crosses in Figure 10. These sites were, however, located in terrain with small-scale variability, which clearly could not be resolved by the model with a grid resolution of 1 km. Also for several others of the observational sites the model could be expected not to completely resolve the terrain, giving additional uncertainty in the modelled average wind speed and consequently increasing the scatter seen in Figure 10. It is, however, difficult to quantify this effect. Excluding the 11 sites which clearly have small scale terrain variations, the average difference between observed and modelled mean wind speed is just –0.03 m/s at the remaining 105 measurement points, i.e. less than 0.5 %, indicating that there are no systematic differences between the two. The correlation coefficient between modelled and observed average wind speed is 0.975.

The distribution of the differences between observed and modelled annual average wind speeds is shown in Figure 11. Differences between observations and modelled wind speed less than 0.2 m/s are found for 48 % of the data, while differences less than 0.4 m/s are found for 87 % of the data. Only 5 % of the comparisons have differences larger than 0.6 m/s.
The distribution of the ratio between observed and modelled annual average wind speed is shown in Figure 12. The average ratio is 0.999 and 46 % of the

data are within ±3 % (0.97 – 1.03), while 77 % are within ±6% and 94 % of the comparisons are within ±9 % from each other.

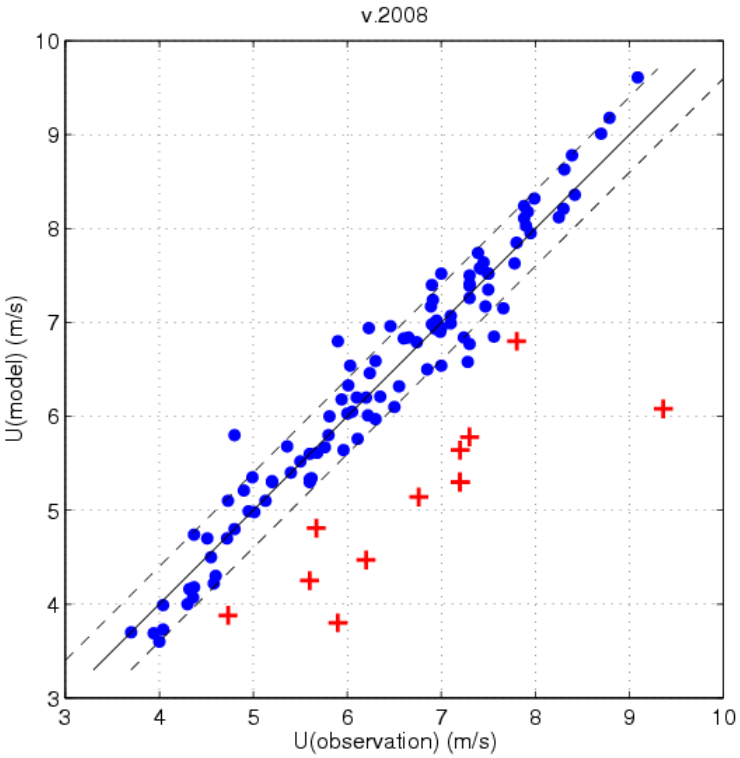

Figure 10: Modelled versus observed annual average wind speed at the sites shown in Figure 8. The sites marked with '+' are located in terrain having a topographical variability on smaller scales than clearly are resolved by the model.

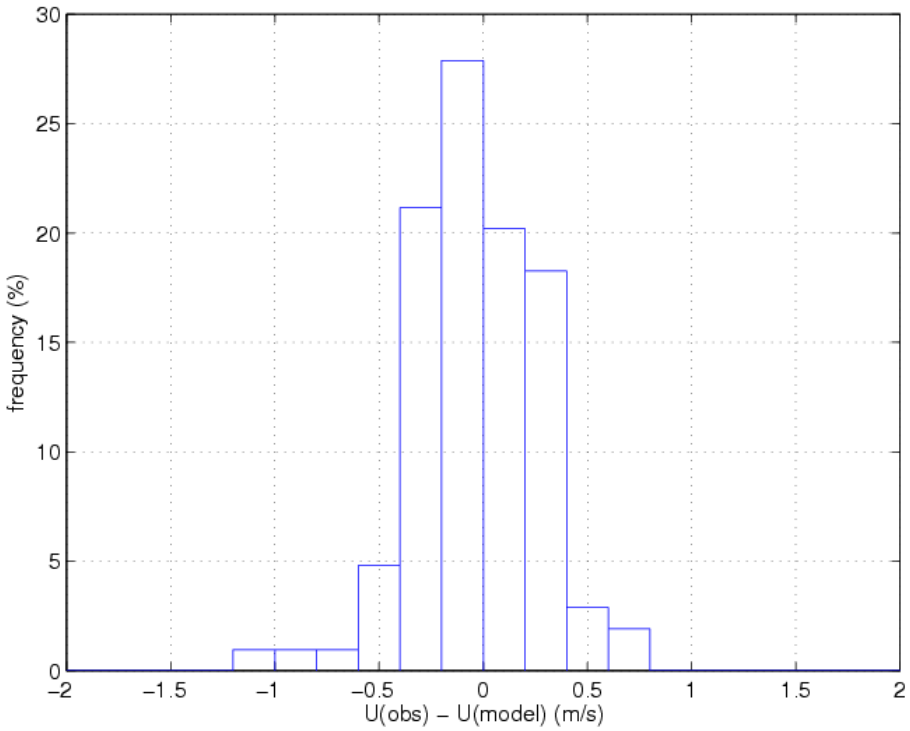

Figure 11: Distribution of difference between observed and modelled annual average wind speed for the 84 observations shown by the dots in Figure 10.

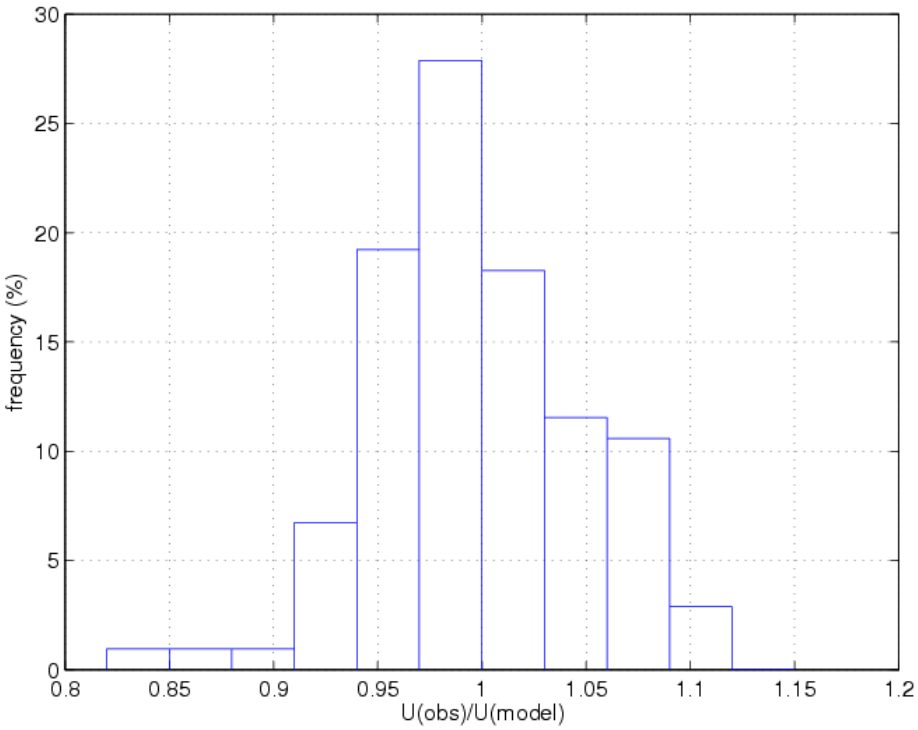

Figure 12: Distribution of ratio between observed and modelled annual average wind speed for the 84 observations shown by the dots in Figure 10.

In Figure 13 the geographical variations in the difference between modelled and observed annual average wind speed are shown. Sites with small differences, less than 0.2 m/s in magnitude (**o**), are found in all parts of Sweden except for the inner parts of northern Sweden. This is probably mostly due to that the measurements sites here often have a small-scale topographical variability, which is not resolved by the model with 1 km horizontal resolution. No systematic geographical variation may otherwise be seen in the results. Sites with both positive and negative differences are found in most areas. This justifies the geographical variation in the average strength of the geostrophic wind used for weighting the geographical variation of the modelled annual average wind speed over the country.

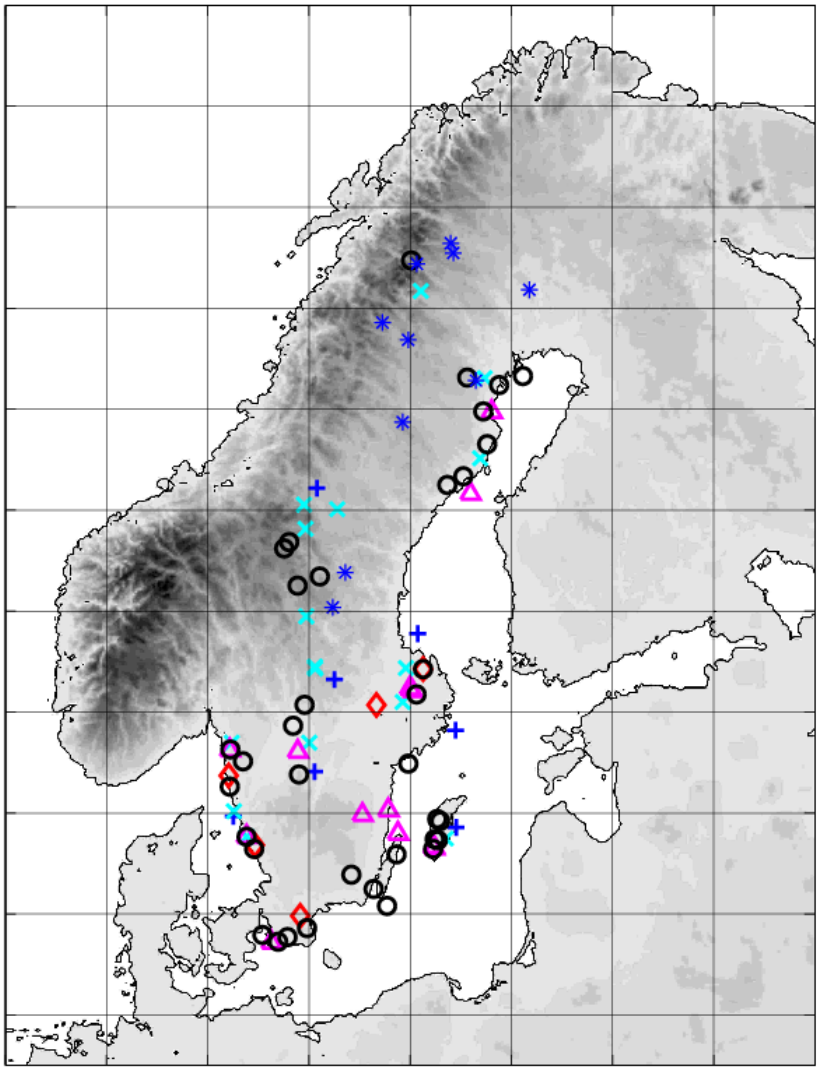

Figure 13: Map showing geographical distribution of the difference between observed and modelled annual average wind speed at the 84 measurement sites. o: Difference within 0.2 m/s. +: Model gives more than 0.4 m/s lower wind. x: Model gives 0.2-0.4 m/s lower wind. Δ: Model gives 0.2-0.4 m/s higher wind. ◊: Model gives more than 0.4 m/s higher wind. *: Sites with small scale topography not resolved by the model.

It is also of interest to verify how well the model catches the shape of the vertical wind profile, i.e. how the wind speed on the average increases with height. Two sites were available with wind profile measurements; Näsudden on Gotland and Maglarp 1.5 km from the southern coast of Skåne. The RT90 coordinates for these sites (cf. Figure 8) are (1646.82, 6329.72) and (1326.154, 6143.264) respectively.

The modelled and observed (1980-1988) average wind profiles at Näsudden and at Maglarp are shown in Figure 14. At Näsudden the modelled vertical wind gradient well describes the observed gradient, but with a slight bias of about 0.3-0 4 m/s. The reason for this bias may be that the small peninsula (about 2 km wide) where the Näsudden tower is located, about 1.5 km from the shoreline, is not fully resolved by the model resolution which is 1 km. The internal boundary layer is, however well caught by the model as the modelled wind gradient on the average agrees with observations at all heights. On the average the observed internal boundary layer height is at the tower between 40 m and 70 m above the ground (Bergström et al., 1988).

At Maglarp the modelled wind gradient is larger than the observed one below about 70 m height, see Figure 14, while higher up the modelled gradient agrees well with observations. The reason for this is again that the model with 1 km resolution does not fully resolve the effects by the local terrain on the wind gradient. The tower is here located on a small hill, about 20 m high and 1-2 km wide. Despite its limited size the hill has been shown to influence the wind profile in accordance with the deviation found here between model results and observations. A speed-up effect could be expected up to 30-40 m height (cf. Smedman and Bergström, 1984) resulting in the smaller wind gradient observed below this height, cf. Figure 14.

Disregarding effects on the wind field caused by terrain variations on scales smaller than a few kilometres, which are not fully resolved by the model results based on a 1 km resolution, the observed and modelled average wind profiles agree well both at Näsudden and Maglarp. The same could in general be expected to be true at other sites, although at sites with very complex topography deviations may be found.

The capability of the model to catch the decrease in average wind speed which we expect to find with increasing distance from a coast is illustrated in Figure 15 where modelled and observed wind speed at four sites in southern Sweden are compared. The locations of the sites are given in Figure 16. Again we include the wind profile at Maglarp, where the tower was located about 1.5 km from the coast. At Bösarp, located 7 km from the coast, the wind speed has decreased about 0.2 m/s as compared to the conditions at Maglarp. The model results are here verified by wind speed observations made at two heights, 54 m and 88 m. At Slimmine about 15 km from the coast the average wind speed has decreased further about 0.4 m/s. Again the observations, made at 77 m height, are in agreement with the modelled wind speed. The final comparison presented in Figure 15 is made at Emmaboda in south-eastern Småland 40-50 km from the coast the modelled average wind speed has decreased almost 2 m/s at 100 m height as compared to the conditions at Maglarp. The modelled wind speed is also at Emmaboda verified by observations made at 100 m height.

When comparing modelled wind speed with observations it is important to remember that the model has been used with a resolution of 1 km^2. The topography and roughness (land use) in the model is thus averages over areas 1 km^2 in size. A comparison between 'true' topography and model topography is shown in Figure 17. In this example the overall shape and size of the mountain is captured in the model topography. But in reality the mountain top is about 40 m higher than as the given by the model topography, which could be expected to affect the modelled local wind climate. Wind measurements have been taken at the mountain top on a 40 m high tower and the observed annual average wind speed (long-time corrected) was found to be 7.2 m/s, while the modelled average wind speed is only 5.6 m/s. This comparison is shown in Figure 10 by one of the 'x'-markers indicating poorly resolved topography.

The wind climate in the area around the site has also been modelled with the same technique as described above, but using a 500 m resolution, which better resolves the terrain. The modelled average wind speed at the mountain site was in this case found to be 6.7 m/s in much better agreement with the observations. But still the real topography could not be expected to be fully resolved even with the 500 m resolution as the dimensions of the mountain top is even less than 500 m.
This example illustrates the importance of keeping in mind the 1 km^2 resolution used when modelling the wind climate. Although graphics of the wind climate gives a nice and seemingly precise location of the different annual average wind speeds, this is not always true and the results must be judged in connection to the variability of the real topography.

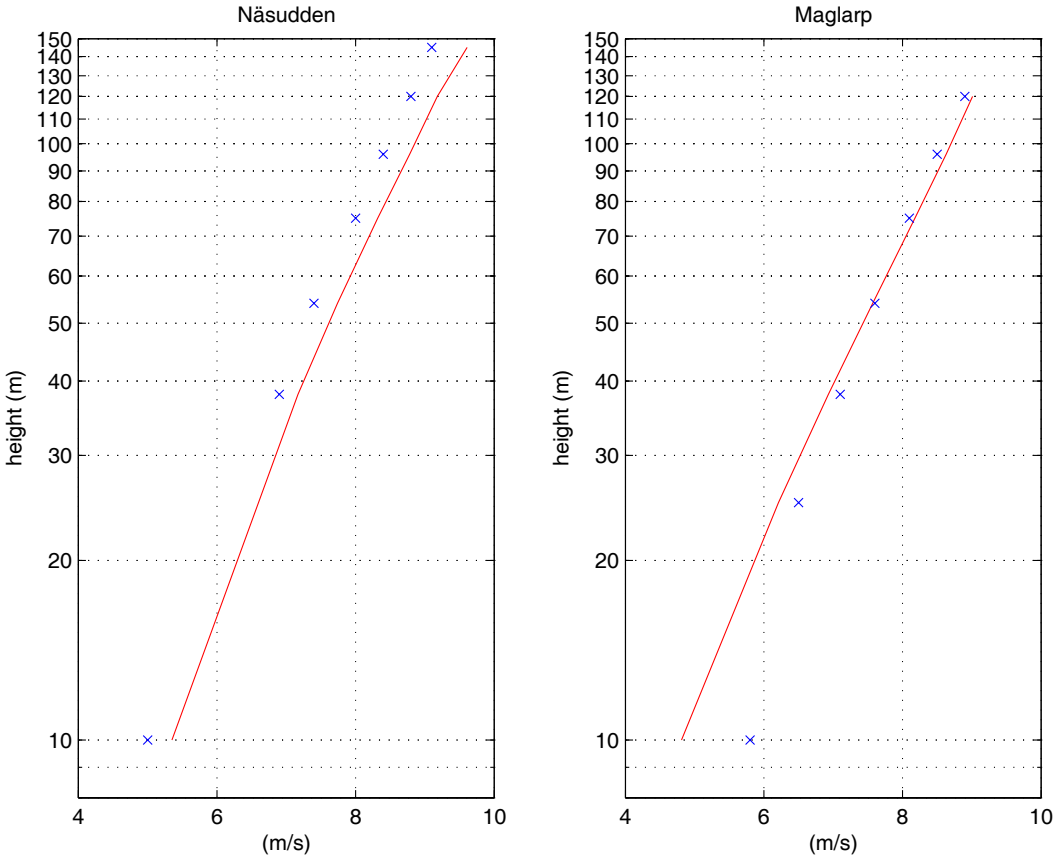

Figure 14: Modelled (full lines) and observed (x) annual mean wind profiles at Näsudden (left) and Maglarp (right). Observations taken 1980-1988.

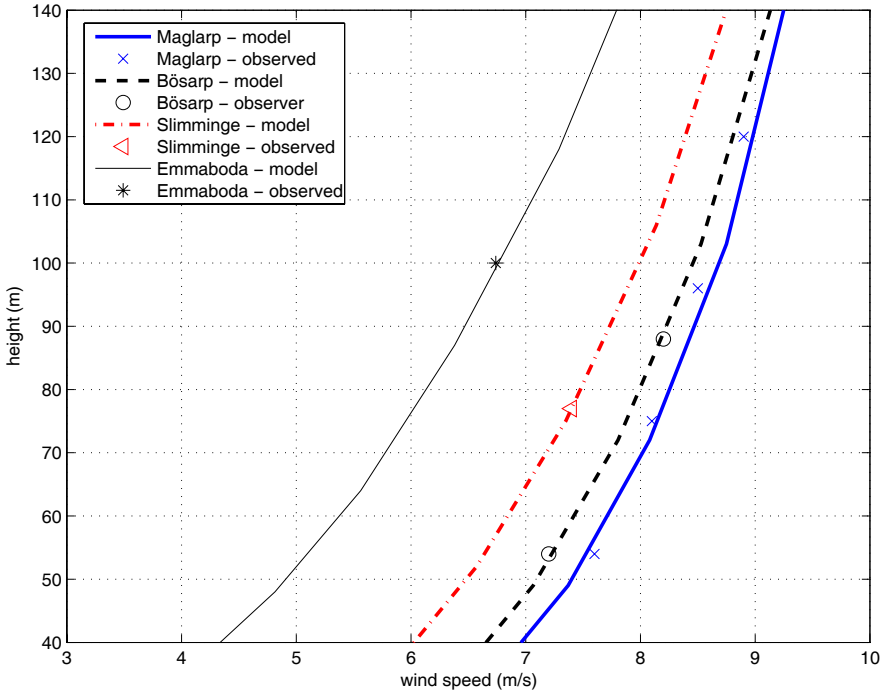

Figure 15: Modelled (lines) and observed (markers) average wind speed at four sites in Southern Sweden at different distance from the coast.

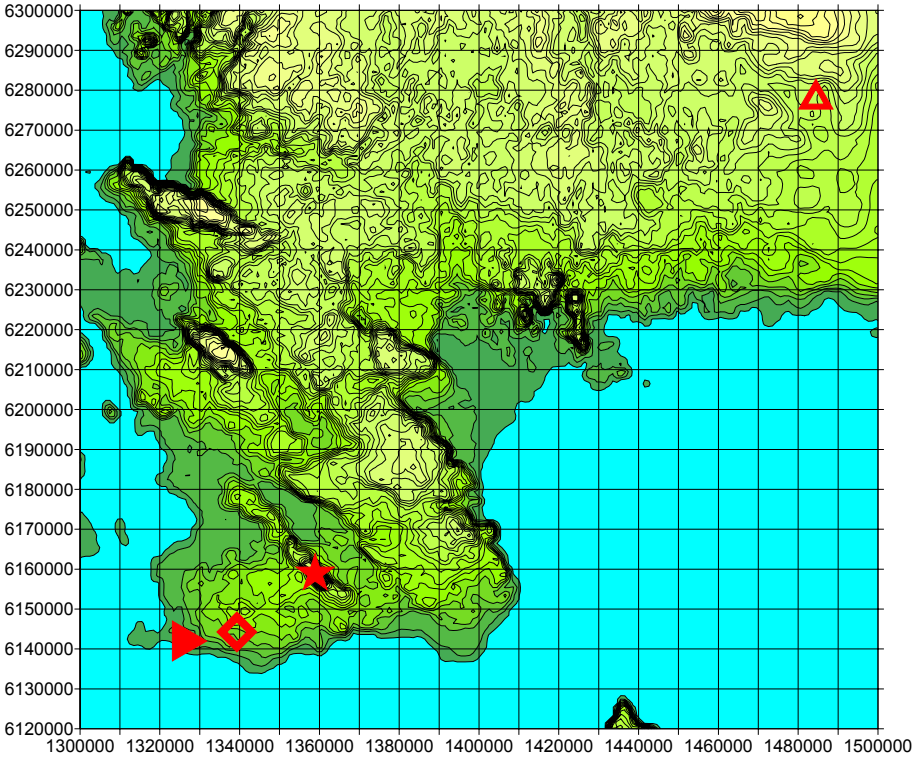

Figure 16: Map of Southern Sweden showing locations of the sites used in Figure 15. ▶: Maglarp. ◇: Bösarp. ★: Slimminge. △: Emmaboda.

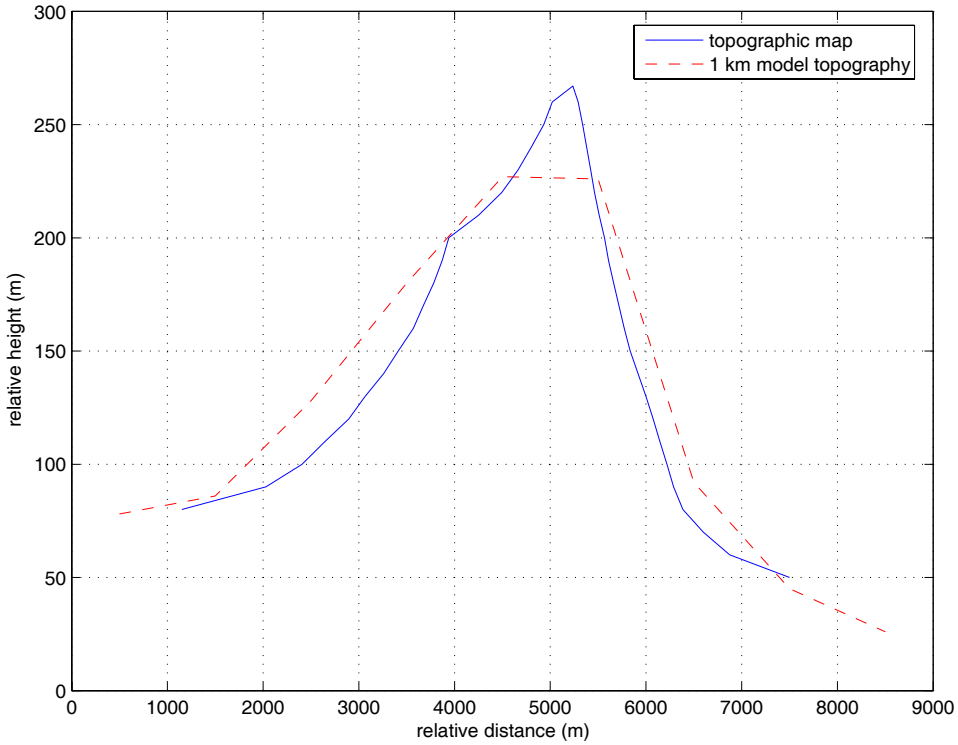

Figure 17: Height contour cross-section showing the relative height of a mountain comparing 'true' topography with the topography used in the model with 1 km horizontal resolution.

8 Additional wind statistics

The modelled wind climate scenarios have produced a large database of meteorological parameters at different heights over the whole of Sweden with 1 km horizontal resolution. This database has been used to extract further statistics of interest for wind energy applications. This will give information on the countrywide variations about the Weibull distribution parameters, the turbulence intensity, extreme winds for 50 years return period, and about the vertical wind shear. All results are available on the Internet at http://www.geo.uu.se/luva/default.aspx?pageid=13152&lan=1.

8.1 Weibull distribution

Observed wind speed distributions are found to be well approximated by the Weibull distribution, which is given by the equation

$$f(U) = \frac{c}{A}\left(\frac{U}{A}\right)^{(c-1)} \cdot e^{-\left(\frac{U}{A}\right)^{c}}, \qquad (8.1)$$

where U is the wind speed, f(U) gives the probability for wind speed U, A is the scale parameter (m/s), and c is the shape parameter. The Weibull distribution is thus an exponential type distribution, which is fully known once, the two parameters A and c are known.

In the previous sections we have only calculated and presented results concerning the average wind speed at different heights, without taking any notice about the wind speed probability distribution. But the database of model results also contains information making it possible to determine the wind speed distribution, together with the wind directions. This makes it possible not only to calculate the total wind speed distribution for all directions, but also the sector wise wind speed distribution together with the probability for different wind directions.

The weighting technique is the same as presented in Equation (3.3), but here the weighting was done for the two horizontal wind components separately. This will give information on the actual wind direction in the modelled winds, making it possible to determine the sector wise wind speed distributions, together with the wind direction distributions at each model grid point representing 1 km^2.

The two Weibull distribution parameters, A and c, were then determined by adapting the theoretical distribution, Eq. (8.1), to the modelled cumulative wind speed distributions by using the method of least squares. This was done both for the complete distribution using all wind direction, and for 12 30° wind directions sectors separately. The variations over Sweden of the scale and the shape parameters for the complete Weibull distribution are shown in Figure 18 to Figure 23. The scale parameter of course closely follows the average wind speed. The shape parameter, giving information about the skewness of the distribution, typically varies between 1.8 and 2.2. In some mountain areas in

northern Sweden values below 1.5 are found, indicating typically low winds but occasionally high winds may occur giving a pronounced tail towards higher wind in the distribution.

This is generally supported by observations where measurements at Suorva 1995-2001 gives c=1.73 in a valley, while measurements at the nearby mountain Juobmotjåkkå 1997-2001 gives c=1.38, both at about 35 m heights. Wind observations at the two SMHI weather station at Ritsem and at Stora Sjöfallet give c=1.52 and c=1.68 respectively.

Measurements in southern Sweden typically give somewhat higher values of the shape parameter, around 2.0 to 2.4, while the model estimates here are typically in the range 1.8-2.0. It should be noted, however, that the uncertainty in the shape parameter is rather large when determined from measurements during just a few years.

8.2 Wind direction distributions

The wind direction distributions were determined together with the sector wise Weibull distributions at all grid points with 1 km^2 resolution. The probabilities for winds from different directions were then determined for 12 30° wide direction sectors. The results are shown in Figure 24 to Figure 26 giving the percentages in these 12 sectors.

An influence from differences between the two geostrophic wind direction distributions used can be seen in these figures. In northern Sweden, see Figure 1, the major peek is at winds from south-southwest with a secondary peek for winds from north. In the southern part of Sweden, see Figure 2, the largest peek is found for winds from west with only a very week secondary maximum for winds from southeast. These differences were of course also transferred to the actual wind direction distributions presented in Figure 24 to Figure 26 when weighting the model results together. The differences can be seen as somewhat too distinct differences between the results in neighbouring model areas (cf. Figure 3) and should not be regarded as true differences. The general differences between southern and northern Sweden are on the other hand as expected, showing the most common winds from southwest in the south and while in the north winds from south to southeast are more common. More local differences are typically results of forcing from the topography and friction, which the model captures well. We can for example see channelling along valleys in the north. Typical is also the locally more common winds from northeast along the west coast of Sweden.

The differences in wind direction distribution over the country are in general agreement with observations. But due to the influences from the differences in geostrophic direction distributions, some caution should be taken regarding the model results especially over southern Norrland in the boundary area between model domains in the south where the wind climate results were weighted together using geostrophic statistics from Visby-Göteborg-Lund, while in the north geostrophic statistics using data from Bodö-Härnösand-Haparanda were used. The difference between the two data sets were regarding the average wind speed handled using a smoothing based on the re-analysis results, see Figure 4. A similar simple technique could not be used regarding wind direction distributions.

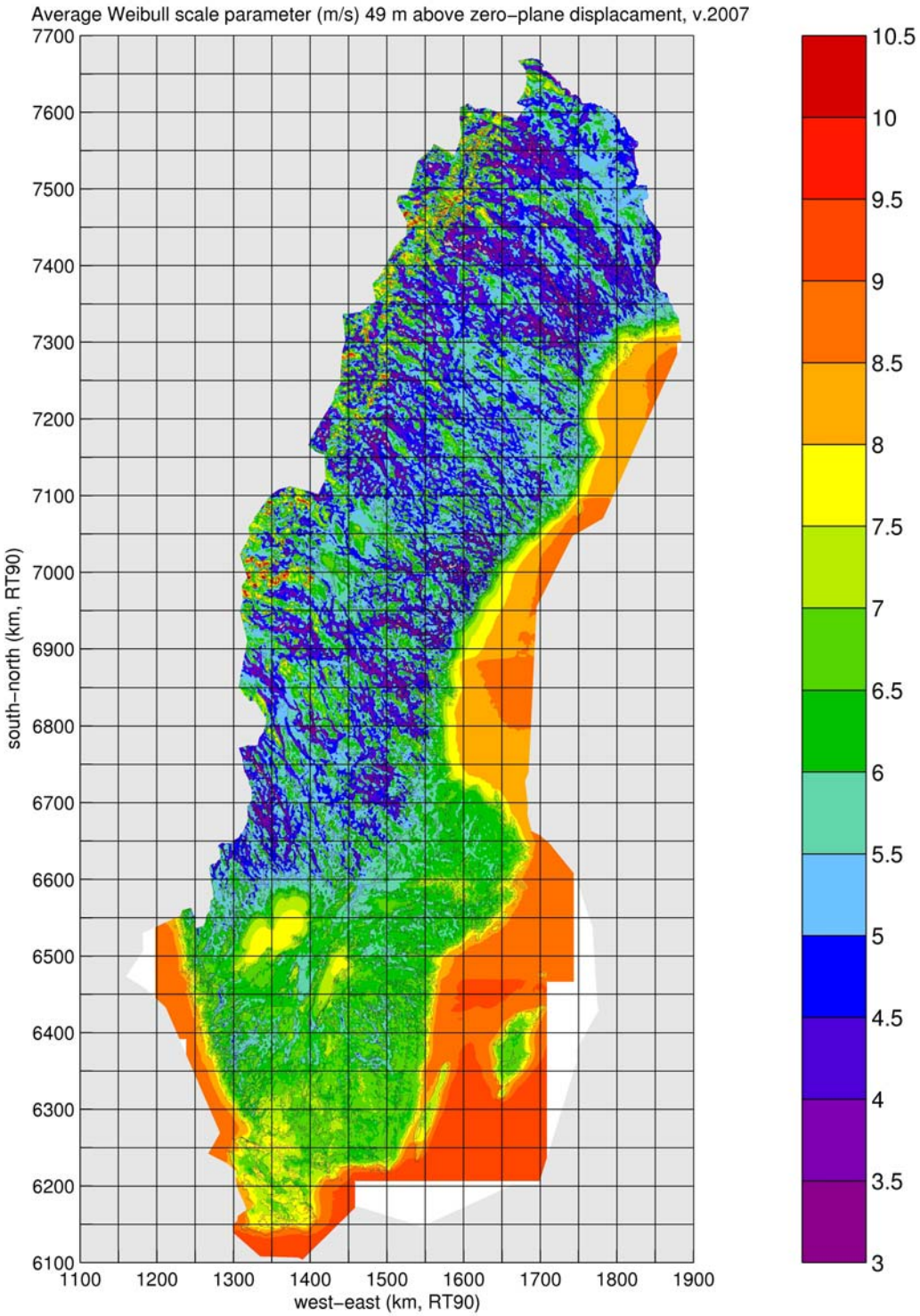

Figure 18: Scale parameter of the Weibull distribution representing the complete wind speed distribution for all wind directions – 49 m above zero-plane displacement.

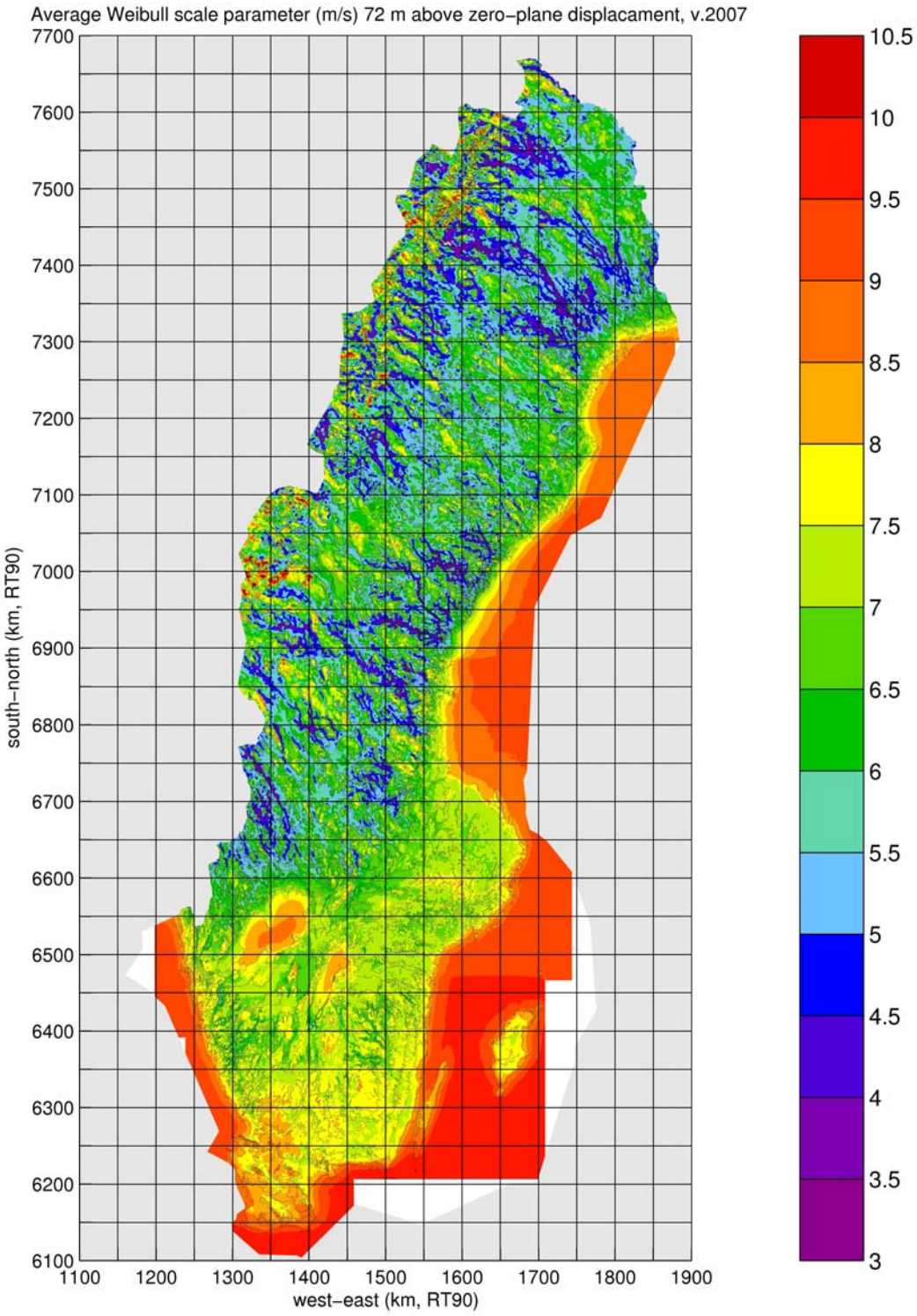

Figure 19: Scale parameter of the Weibull distribution representing the complete wind speed distribution for all wind directions – 72 above zero-plane displacement.

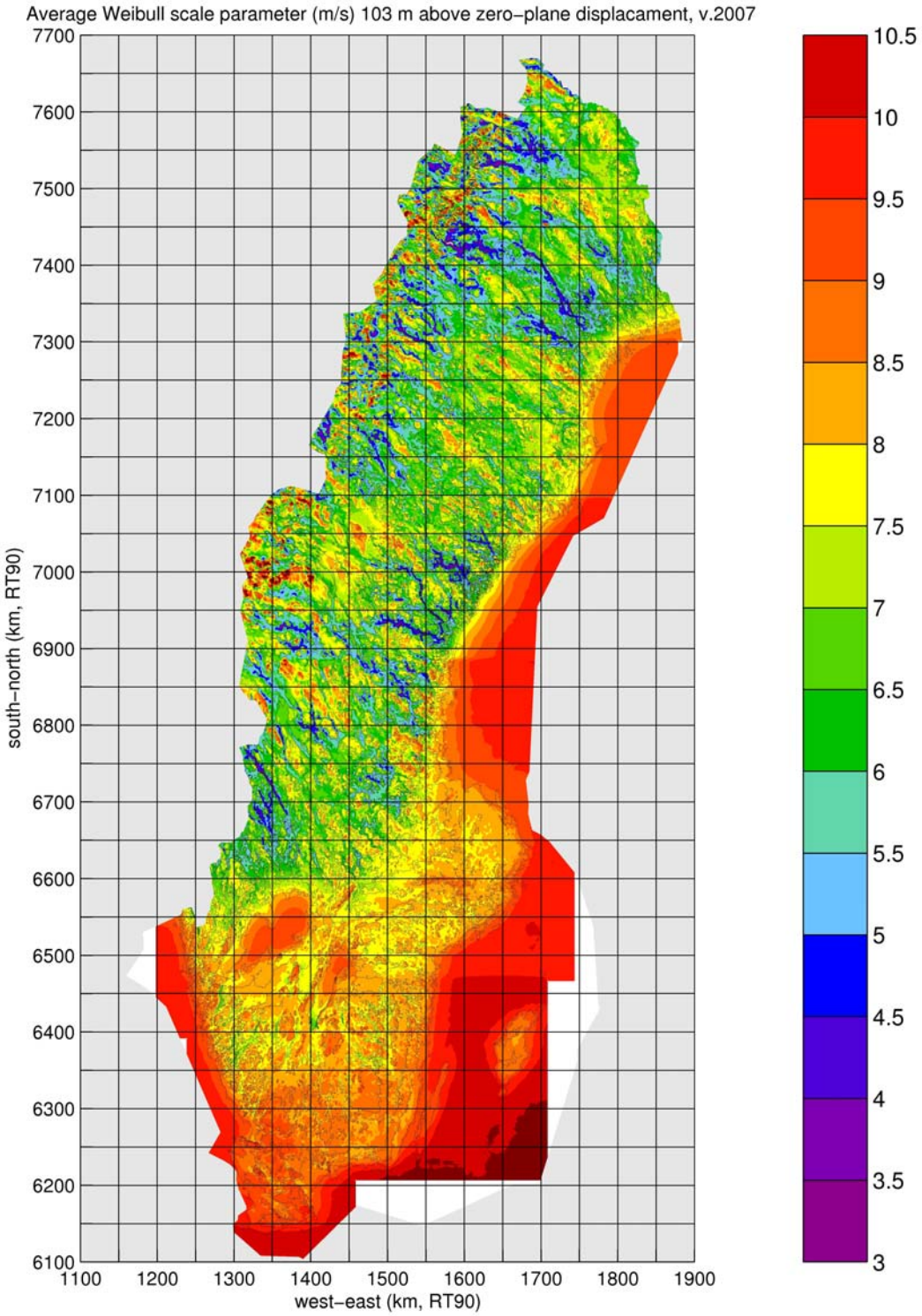

Figure 20: Scale parameter of the Weibull distribution representing the complete wind speed distribution for all wind directions – 103 m above zero-plane displacement.

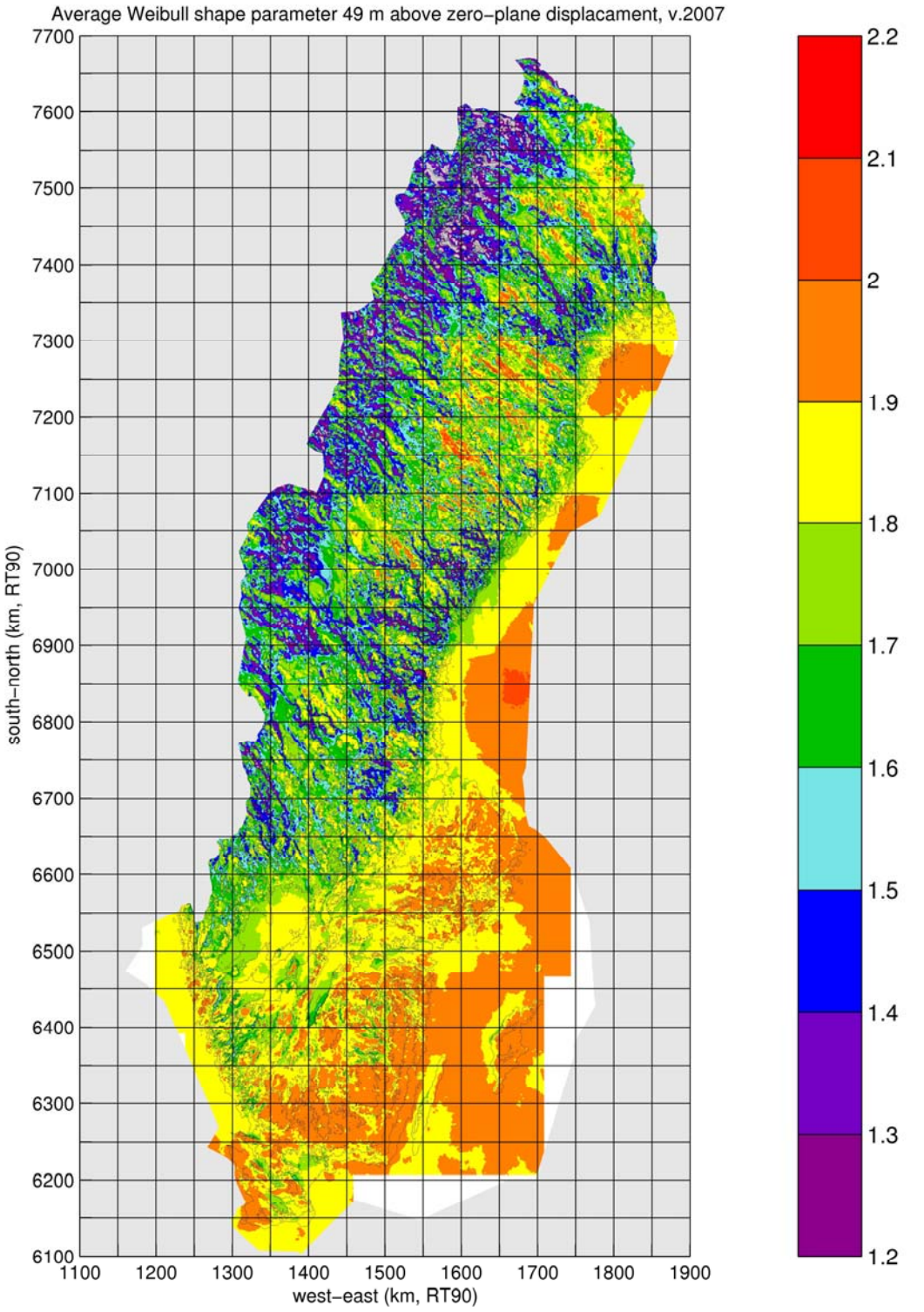

Figure 21: Shape parameter of the Weibull distribution representing the complete wind speed distribution for all wind directions – 49 m above zero-plane displacement.

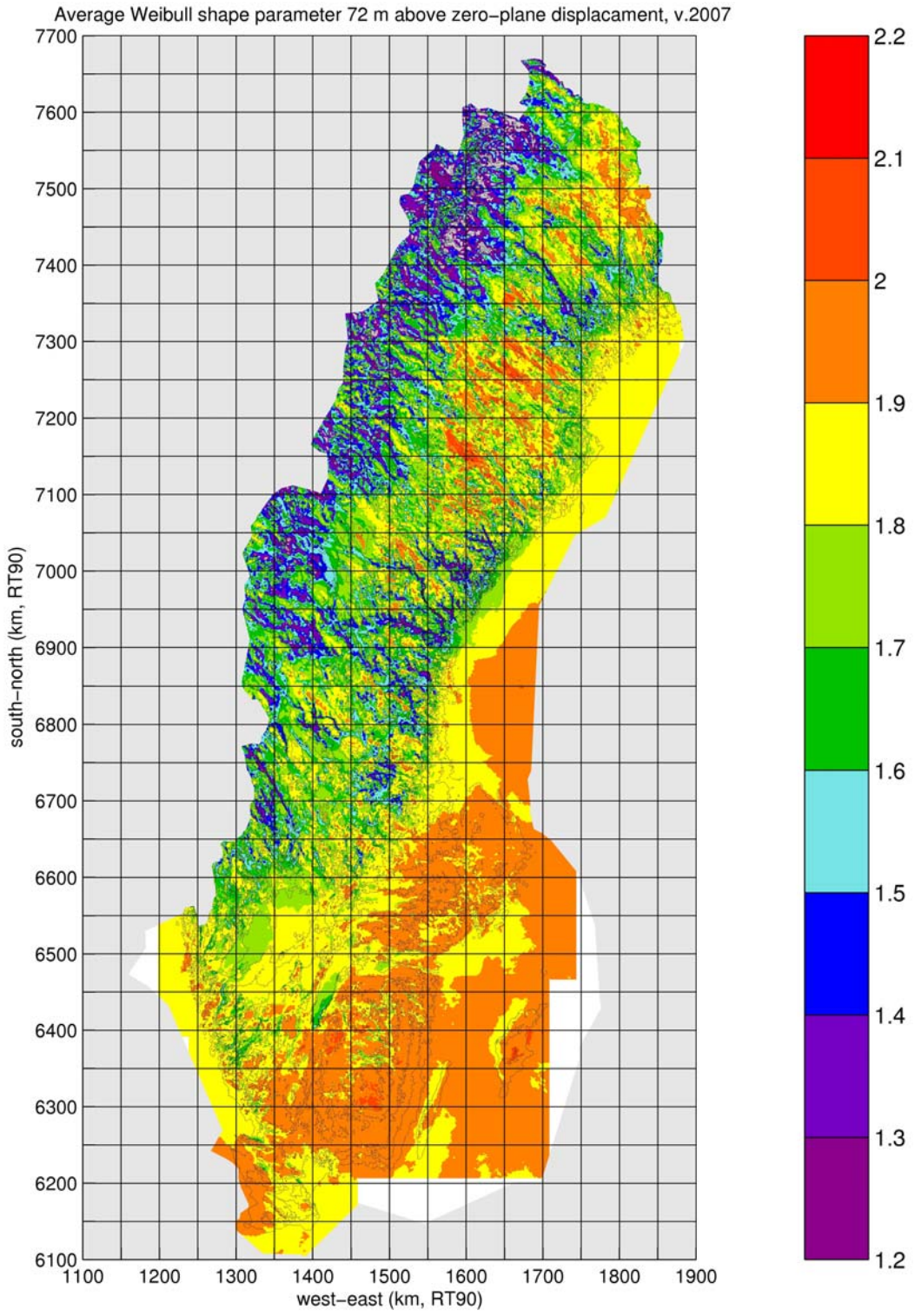

Figure 22: Shape parameter of the Weibull distribution representing the complete wind speed distribution for all wind directions – 72 m above zero-plane displacement.

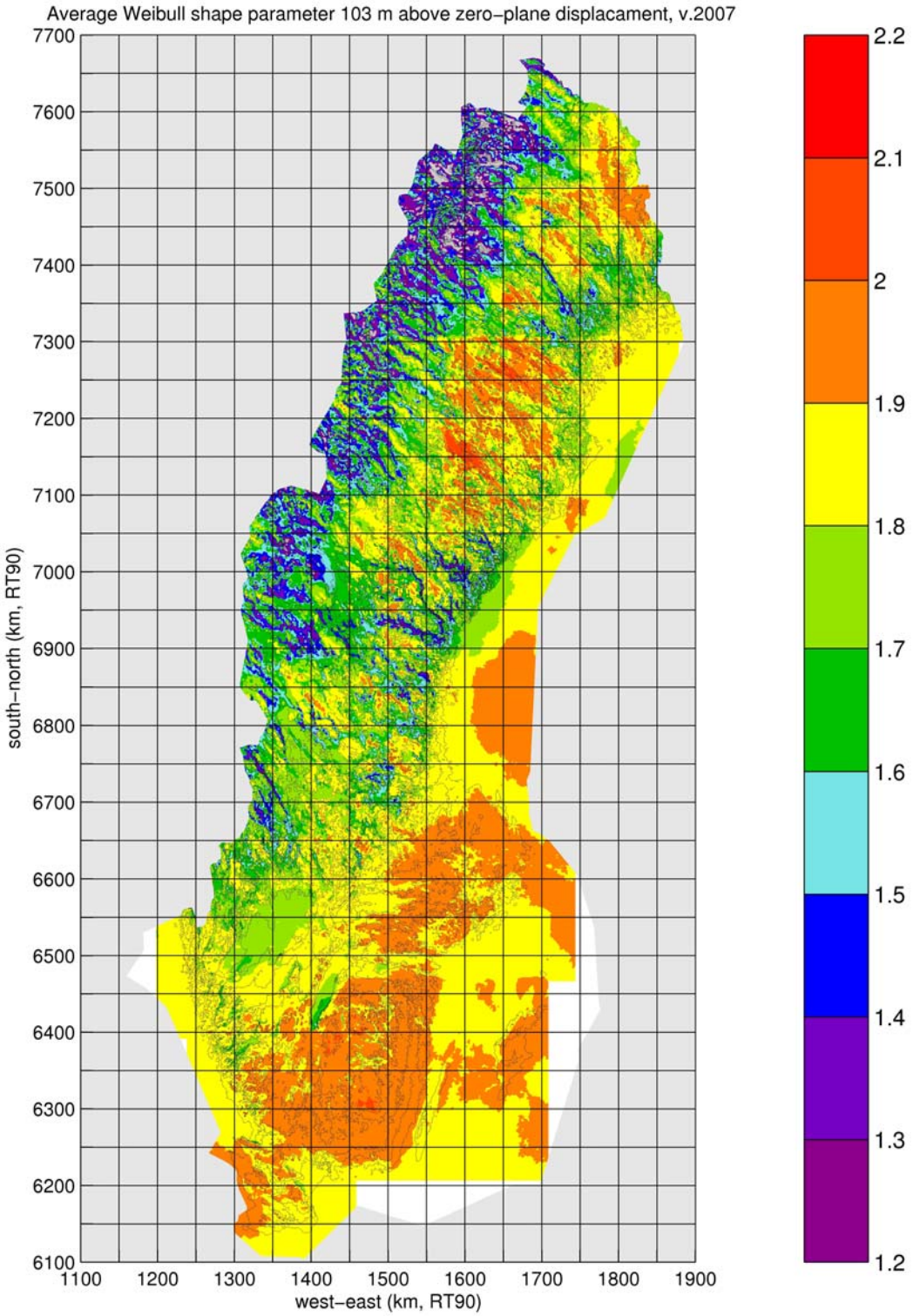

Figure 23: Shape parameter of the Weibull distribution representing the complete wind speed distribution for all wind directions – 103 m above zero-plane displacement.

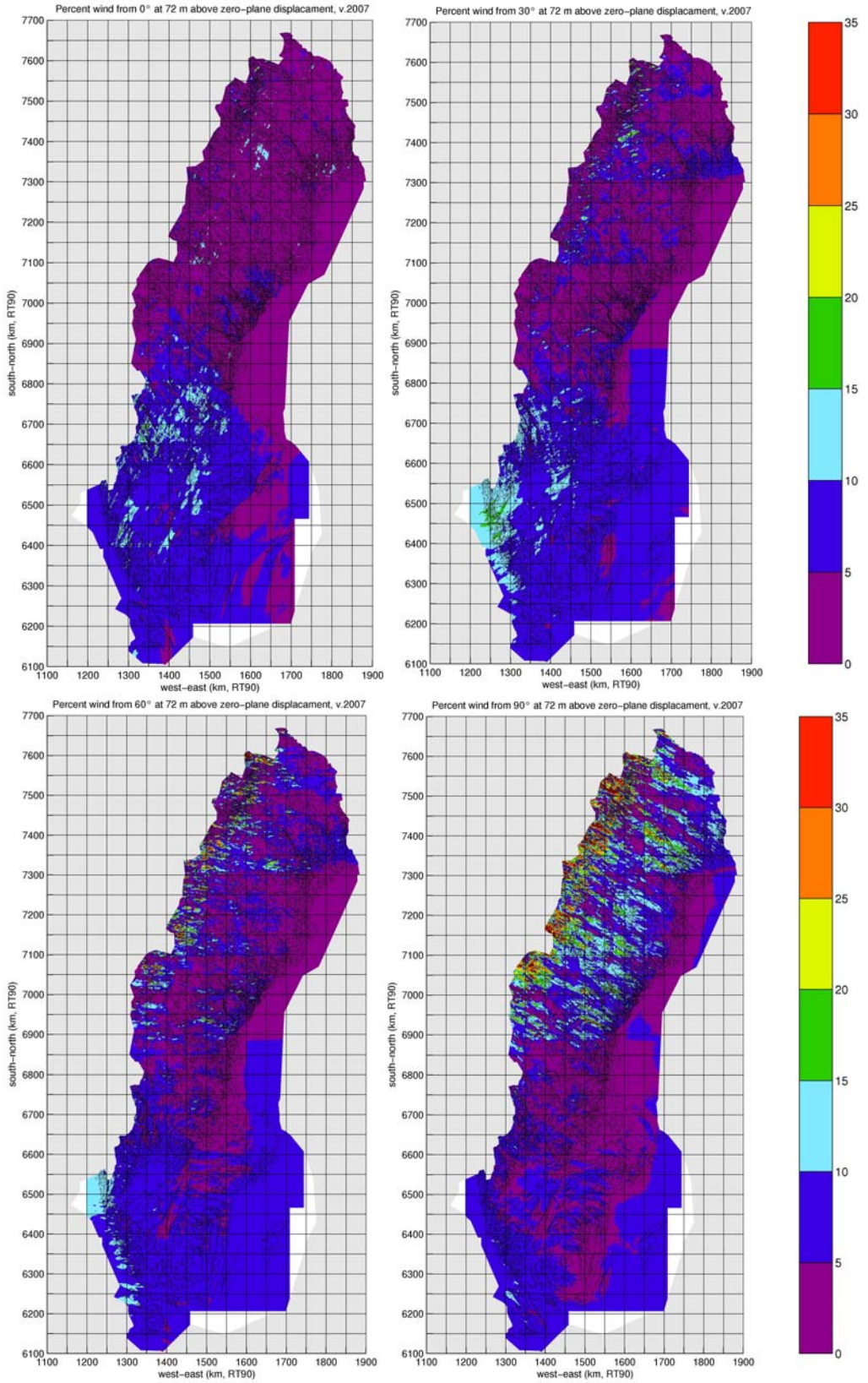

Figure 24. Percentage winds from 0°, 30°, 60°, and 90°.

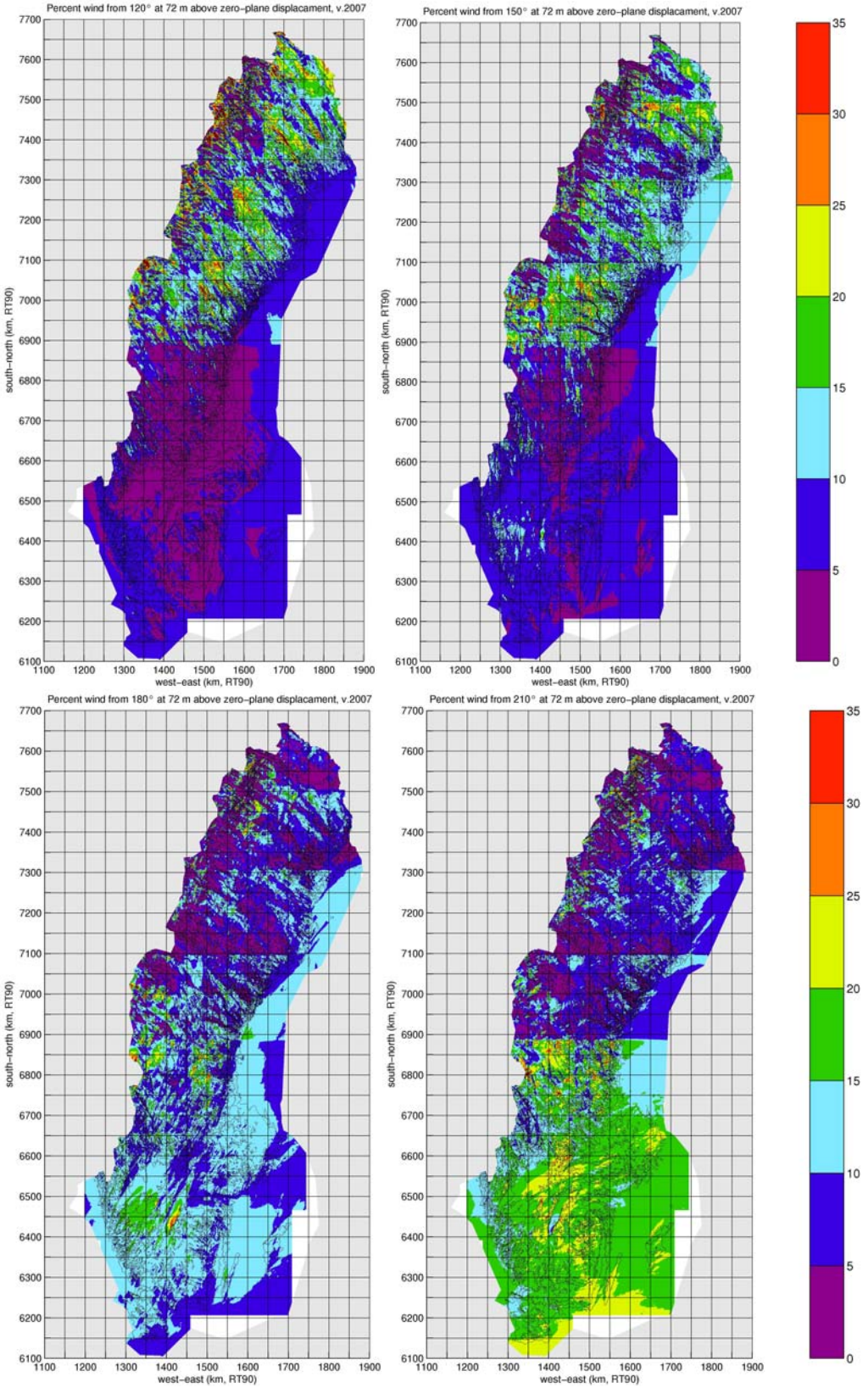

Figure 25: Percentage winds from 120°, 150°, 180°, and 210°.

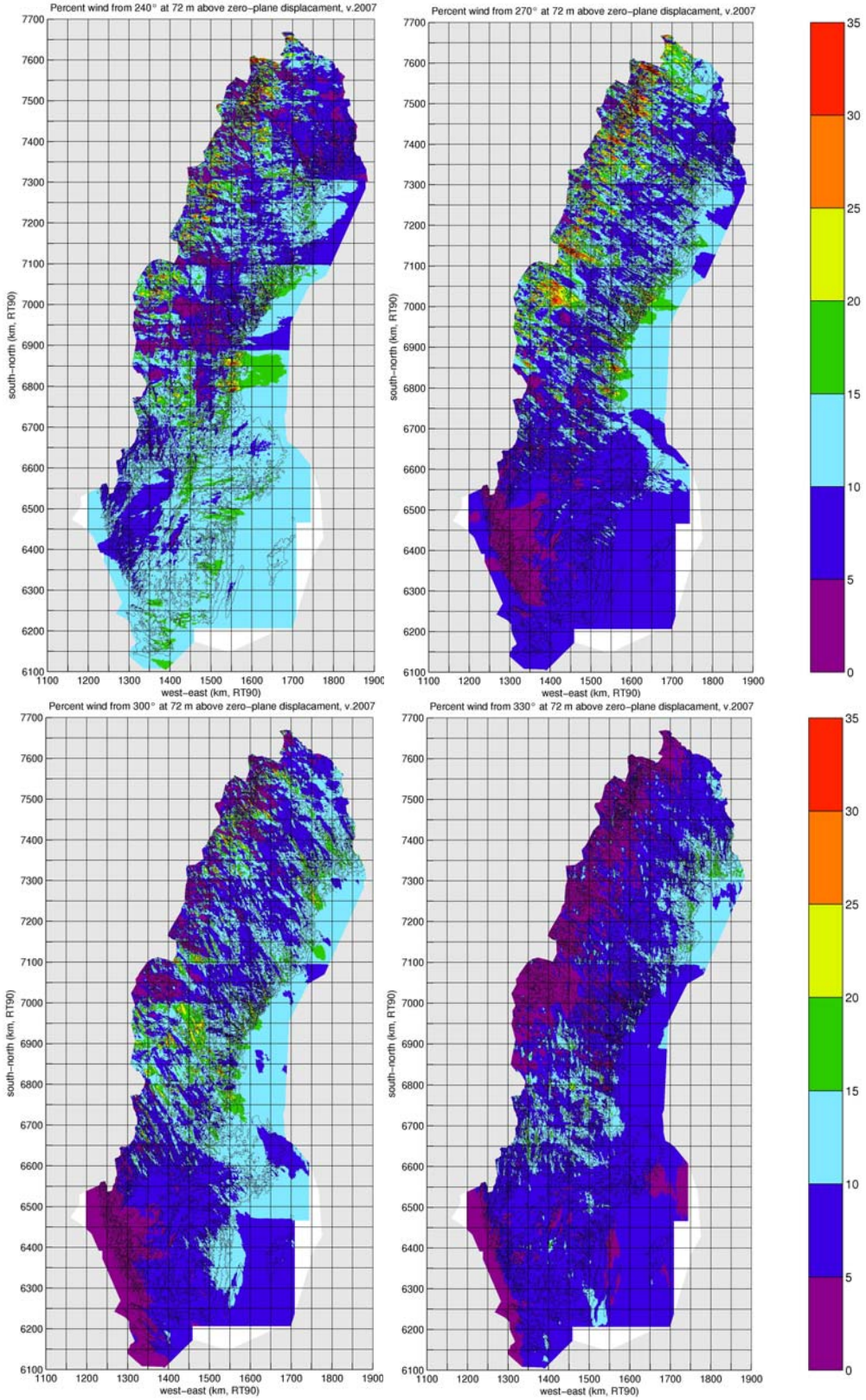

Figure 26: Percentage winds from 240°, 270°, 300°, and 330°.

8.3 Wind shear

The vertical wind gradient in the atmospheric boundary layer is often observed to be close to logarithmic, at least close to the surface. The magnitude of the gradient will then depend on the surface roughness and the influence from friction at the surface. The thermal stability of the boundary layer, that is how the temperature changes with height, will also influence the wind gradient and make it deviate from the logarithmic profile, which is valid only for neutral thermal conditions.

In practice the climatologically averaged vertical wind profile is often approximated by an exponential wind profile, given by

$$U_2 = U_1 \cdot \left(\frac{z_2}{z_1} \right)^{\alpha} \qquad (8.2)$$

where the exponent α will take care of both the influence from surface friction and from thermal stability. Typical values of α are found in the range 0.1 to 0.4. Small values are expected for smooth surfaces and unstable stratification, while large values are found over rough surfaces and also for stable stratification.

The modelled average wind speed at 49 m and 103 m height above the zero-plane displacement were used to determine the exponent α at each modelled grid point representing 1 km^2. The results are shown in Figure 27. Offshore numbers are often around 0.15, while over land α varies between 0.25 and 0.45, except over the mountain tundra where low values are found. Exponents determined from observed wind profiles are of the same magnitude.

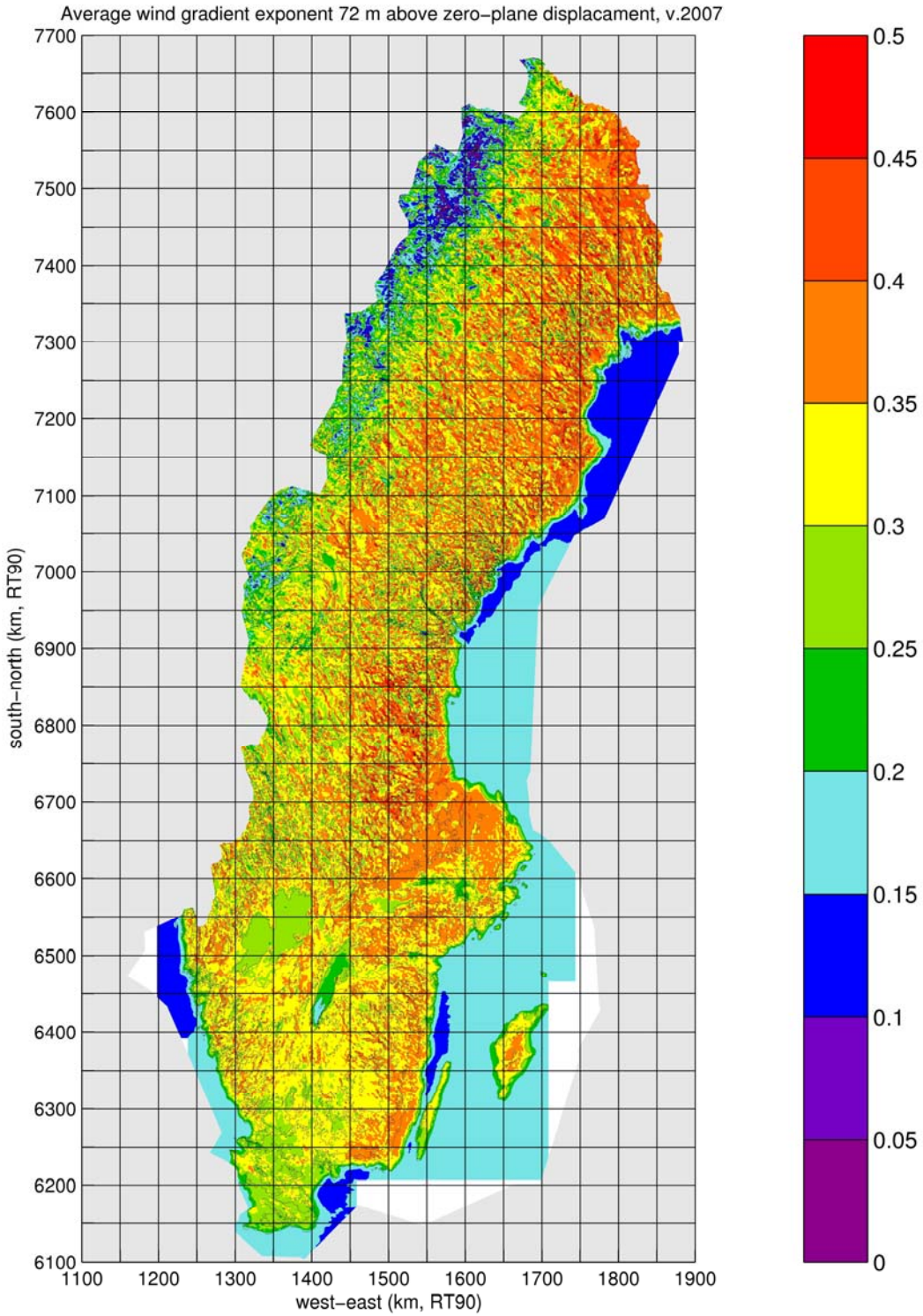

Figure 27: Wind shear exponent α determined from the modelled average wind speed at 49 m and 103 m height above the zero-plane displacement.

8.4 Extreme wind speed

The distribution of the mean wind speed is well approximated by the Weibull distribution, but sometimes it is also of interest to know the highest wind speed, which may be expected to occur during a long period of time, e.g. 50 years. To extend a mean value distribution of the exponential type, such as the Weibull distribution, to an *extreme value distribution* is not too complicated, and will give us the tool to estimate the probability of very high wind speeds. No exact value of the very highest wind speed during e.g. 50 years may thus be determined, but instead probabilities that the extreme wind speed will not exceed certain values are given.

The intention is here to perform such an extreme value analysis. First we will discuss the theory upon which such an analysis is based, cf. Bergström, 1992. After that some general results are presented, giving the extreme wind speed as a function of the Weibull distribution parameters. Finally the 50 year extremes of 10 min average wind speed and 3 s gust speed are estimated using the modelled Weibull distributions as each 1 km^2 grid point at 49 m, 72 m, and 103 m heights above the zero-plane displacement.

8.4.1 Theory

Mean value distribution: The mean wind speed, usually 10 min or 1 hour averages, may be well described by the cumulative Weibull distribution

$$F(U) = e^{-(U/A)^c} = 2^{-(U/U_m)^c} \qquad (8.3)$$

where A = scale parameter (m/s), c = shape parameter, U_m = median wind speed (m/s), U = wind speed (m/s), and F = cumulative frequency [0;1]. The corresponding relative frequency distribution is given by Eq. (8.1).

Usually the Weibull distribution is directly applied to observations of 10 min averages or possibly to 1-hour averages. The Weibull parameters, A and c, are determined by adapting the observed distribution to the theoretical one, as was done in Section 8.1.

Extreme value distribution: To extend the studies to extreme values when the parent distribution (i.e. the Weibull distribution of mean values in this case) is known, is not too complicated and is described in many statistical works (e.g. Gumbel, 1954). We then pass on to study the *extreme value distribution*, which may be determined from the original mean value distribution given above. Thus we do not get an exact value of e.g. the highest wind speed during a 50-year period, but instead the distribution of this maximum wind speed. From this distribution it is possible to judge, from a statistical point of view, the risk that the wind speed will exceed certain values.

The exact distribution of the highest wind speed, u_N, of N *independent* observations from a Weibull distribution is given by the relation

$$F_N(>u_N) = 1 - \left(1 - e^{-\left(\frac{u_N}{A}\right)^c}\right)^N \qquad (8.4)$$

It is important to note that the observations must not depend on each other. In the case of consecutive values in a time series of wind speed, this is by no means true, and must be taken into account when making the extreme value analysis. We will below return to how this may be accounted for.

When the number of independent observations increases, the cumulative extreme value distribution converges towards

$$F_N(>u_N) = 1 - e^{-e^{-\alpha_N(u_N-\beta_N)}} \tag{8.5}$$

and the corresponding relative distribution becomes

$$f_N(u_N) = \alpha_N e^{-\alpha_N(u_N-\beta_N)} e^{-e^{-\alpha_N(u_N-\beta_N)}} \tag{8.6}$$

where $\frac{1}{\alpha_N} = \frac{A}{c}(\ln N)^{(1/c-1)}$ is the dispersion factor and (8.7)

$\beta_N = A(\ln N)^{(1/c)}$ is the modal value (8.8)

The relation for $F_N(>u_N)$, i.e. the probability that the largest among N independent values is greater than u_N, is very general and valid for all initial distributions of the exponential type. The most important characteristics of this extreme value distribution are:

mode: $$\tilde{u}_N = \beta_N \tag{8.9}$$

median: $$\hat{u}_N = \beta_N - \frac{\ln(\ln 2)}{\alpha_N} \tag{8.10}$$

mean: $$\bar{u}_N = \beta_N + \frac{\gamma}{\alpha_N} \tag{8.11}$$

variance: $$\sigma_N^2 = \frac{\pi}{6\alpha_N} \tag{8.12}$$

where γ = 0.5772 = Euler's constant.

Effective frequency: As the observations in a time series depend on each other, we need to determine an "effective frequency" before we can use the relations given above and calculate e.g. the extreme value distribution for a 50 year period. This means that we search for the effective number of observations (number of independent observations) of averaging time T within a sampling time t_m.

A relatively simple and convenient way to make this is to use the auto correlation $\rho(\tau)$, defined as

$$\rho_T(\tau) = \frac{\overline{u_T(t) - u_T(t+\tau)}}{\sigma_T^2} \qquad (8.13)$$

where T is the averaging time (cf. Section 2.4), t is the time, and τ is the time difference over which the auto correlation is calculated. If we put ρ=0.5 and solve for τ, the solution may be interpreted as a measure of the mean time between two 50% correlated values in the time series. Using spectral representation the solution becomes (cf. Rice, 1945)

$$\nu_T = \sqrt{\frac{\int_{n_0}^{0.5/T} n^2 S_u(n)\,dn}{\int_{n_0}^{0.5/T} S_u(n)\,dn}} \qquad (8.14)$$

where $S_u(n)$ is the spectral density function, n is the frequency and $\nu_T = 1/\tau$ is the sought effective frequency valid for the averaging time T. The lower integration limit, n_0, may be chosen to be about 1/(2x3600) Hz to eliminate the synoptical part of the spectrum.

The number of independent intervals of length T within a time period t_m may then be estimated from the relation

$$N = \nu_T t_m \qquad (8.15)$$

Table 2*:* The effective frequency, ν_T [s^{-1}], and the ratio $\sigma_T/\sigma_u = q_T$ for various averaging times, T.

T	ν_T	q_T
1 h	$2.8\ 10^{-5}$	0.00
10 min	$7.3\ 10^{-5}$	0.18
1 min	$1.0\ 10^{-3}$	0.48
10 s	$4.6\ 10^{-3}$	0.78
5 s	$7.9\ 10^{-3}$	0.85
3 s	$1.0\ 10^{-2}$	0.89
1 s	$2.4\ 10^{-2}$	0.95

The effective frequency is rather insensitive to the specific choice of spectral density function, and in Table 2 values calculated from a typical spectrum are given (cf. Alexandersson, 1979). The effective frequency for the one-hour mean values is calculated from a wind speed spectrum containing the low frequency part (van der Hoven, 1957), and shows that we have approximately one independent hourly average every tenth hour.

The error introduced in the extreme value analysis by using an effective frequency has been studied by Davenport (1967). He finds that Equations (7) and (8) should be multiplied by a factor 1.1 to reduce this error and get a better estimate of the 'true' extreme values. Hence we will use:

$$\frac{1}{\alpha_N} = 1.1 \cdot \frac{A}{c}\left(\ln N\right)^{(1/c-1)} \qquad (8.7')$$

$$\beta_N = 1.1 \cdot A\left(\ln N\right)^{(1/c)} \qquad (8.8')$$

Extension to different averaging times: The extreme value distribution we have studied so far is, however, conditional, i.e. it refers to a specific averaging time (1 hour). To get a more general description of the extreme wind speed and how it depends on averaging time T, the mean value distributions for all averaging times of interest must first be determined from the observed distribution of some mean value (e.g. 1 h).

This may be accomplished by assuming that for each hourly mean value of the observed distribution, the wind speed with the shorter averaging time, u_T, is normally distributed around this hourly mean value, $\overline{u}$, with the standard deviation σ_T. The mean value distribution of the wind speed with averaging time T then becomes:

$$f_T(u_T) = \int_0^\infty \frac{1}{\sqrt{2\pi}\ \sigma_T} \cdot e^{\frac{-(u_T-U)^2}{2\sigma_T^2}} \cdot \frac{c}{A}\left(\frac{U}{A}\right)^{(c-1)} \cdot e^{-\left(\frac{U}{A}\right)^c} dU \qquad (8.16)$$

where σ_T is the part of the total turbulent standard deviation, σ_u, which remains after having applied a low pass filter with averaging time T, i.e. the averaging time acts as a filter with the transfer function $(\sin(n\pi T)/(n\pi T))^2$ and we get, using the spectral representation:

$$\sigma_T^2 = \int_{n_o}^\infty \left(\frac{\sin(n\pi T)}{n\pi T}\right)^2 \cdot S_u(n)dn \approx \int_{n_o}^{0.5/T} S_u(n)dn \qquad (8.17)$$

The ratio $q_T = \sigma_T/\sigma_u$ may thus be written

$$q_T \approx \left[\frac{\int_{n_o}^{0.5/T} S_u(n)dn}{\int_{n_o}^{\infty} S_u(n)dn} \right]^{1/2} \qquad (8.18)$$

and is mainly dependent on the averaging time T, and consequently we may determine it once and for all. Assuming neutral stratification we then get:

$$\sigma_T = \sigma_u \cdot q_T \approx \frac{q_T U}{\ln\left(\frac{z}{z_0}\right)} \qquad (8.19)$$

where z is height above ground and z_0 is the roughness length. Some values of q_T are given in Table 2.

The resulting 'new' distributions valid for shorter averaging times are somewhat flatter than the parent distribution of 1 h averages, and with a more pronounced tail to the right towards higher wind speeds. They may also be adapted to the Weibull distribution, and the shape and scale parameters determined as function of averaging time, after which the extreme value distributions are determined as shown above.

Results of the extreme value analysis

An example of a mean wind speed distribution having the Weibull parameters A=8 m/s and c=2.0 is shown in Figure 28, together with the corresponding 50 year extreme value distributions valid for the averaging times 10 min, 1 min, and 3 s. The mean value distribution has its peak around 6 m/s and is rather wide, while the corresponding extreme value distributions are much narrower with peaks at about 30 m/s, 33 m/s and 38 m/s for the 50 year extremes of 10 min, 1 min, and 3 s averages respectively. In Figure 29 the same mean wind speed distribution is shown together with the extreme value distributions of the hourly average valid for the time periods 1, 10, 50, and 100 years.

These extreme value distributions may thus be used to estimate the probability that the wind speed exceeds a certain value during e.g. 50 years or vice versa the wind speed, which will not be exceeded during the 50-year period with a certain confidence level. An illustration of this is given in Figure 30, showing the extreme wind speed in 50 years versus averaging time for the 50%, 75%, 90%, 95%, 99%, and 99.9% percentiles corresponding to the example presented in Figure 28 and Figure 29. Thus e.g. the median of the expected highest 10 min mean wind speed in 50 years is 31 m/s in this case with A=8 m/s and c=2.0, while the 10 min average extreme is not expected to exceed 35 m/s with 95% certainty. If we want to have a higher degree of certainty, say 99%, the expected extreme wind speed will increase to 37 m/s, and at the 99.9% confidence level the corresponding value is 40 m/s. Thus increasing the degree of certainty from 50% to 99.9% will in this example increase the maximum wind speed from 31 m/s to 40 m/s.

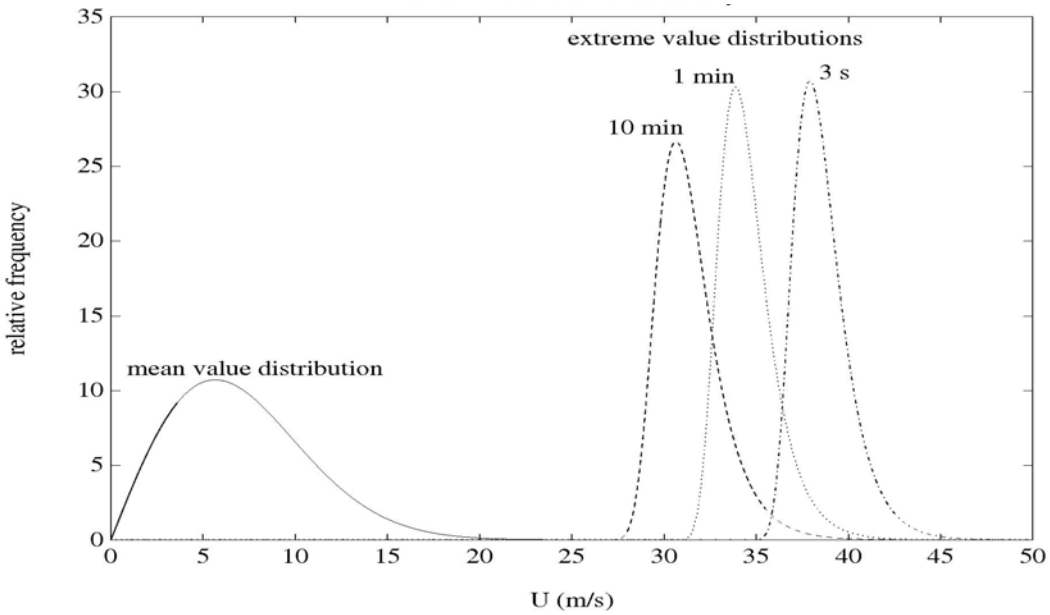

Figure 28: Relative frequency distribution of hourly mean wind speed and the corresponding 50 years extreme value distributions of 10 min, 1 min, and 3 s averages. Estimates made for A=8 m/s, c=2, z=50 m, z0 =0.01 m.

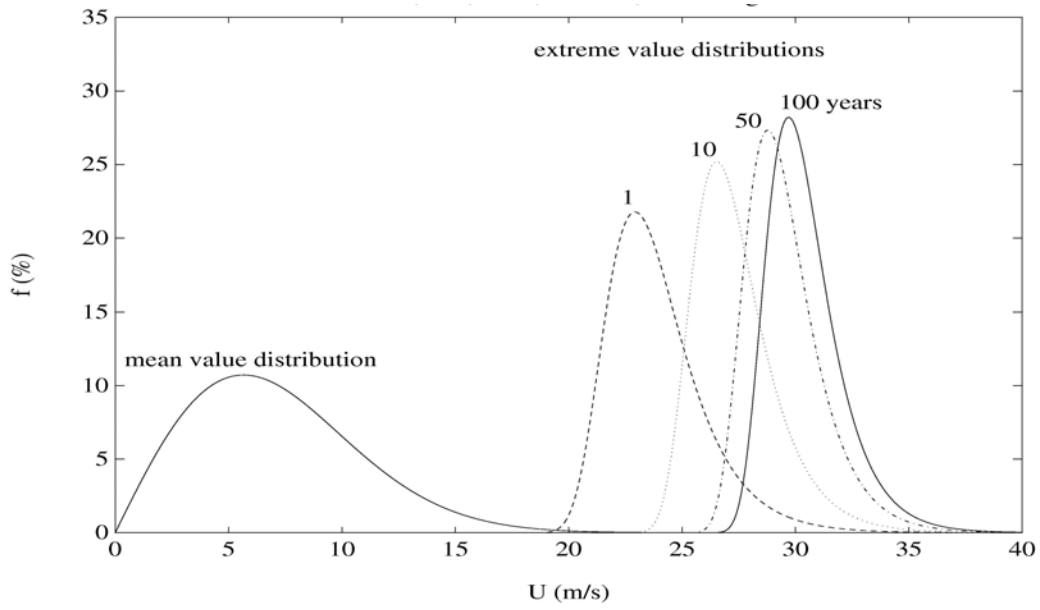

Figure 29: Same as in Figure 28 but the extreme value distributions evaluated for the hourly average during four time periods of various lengths.

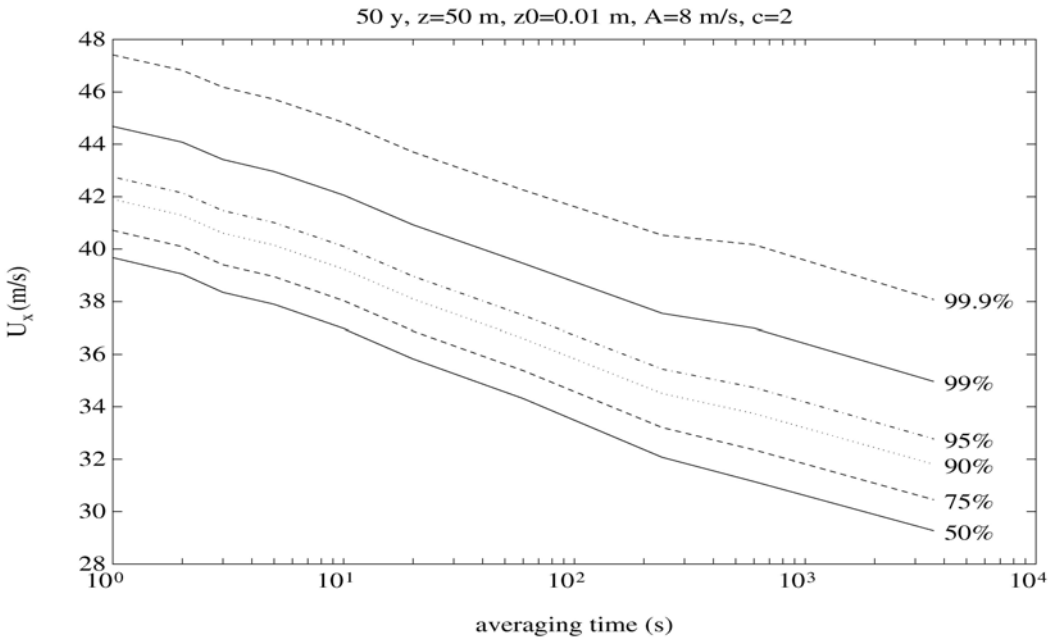

Figure 30: The maximum wind speed versus averaging time for a number of confidence limits. Estimates made for a time period of 50 years and with A=8 m/s, c=2, z=50 m, z0 =0.01 m.

Comparisons with observations: To be able to verify the theoretical extreme value analysis against observations, we need continuous and homogeneous wind measurements for a long period of time. Such data is, however, seldom available. Also measurements have not been taken long enough to make it possible to verify the 50-year extreme values, but as regards the 1-year extremes a few suitable data sets are available.

One such data set is from Marsta 8 km north of Uppsala, where 1 h averages of the wind speed at 10 m height from the period 1959-1991 have been used. The wind speed distribution during those 33 years closely follow the Weibull distribution with the parameters A=4.58 m/s and c=1.86. This can be seen in Figure 31 where we can see the observed mean wind speed distribution together with the corresponding Weibull distribution, having its peak at about 3 m/s. Also shown in Figure 31 is the observed distribution of the annual maximum value of the hourly mean wind speed. This distribution has its peak somewhere between 14 and 15 m/s, and the mean value is 14.8 m/s. This is in very good agreement with the theoretical prediction, which is 14.7 m/s. The agreement between the observed and the theoretical annual extreme value distributions is also quite good.

Two other data sets have also been used to verify the theoretical extreme value estimates. These observations are from the two Swedish wind turbine test sites Näsudden and Maglarp, where wind measurements at 7 heights in two towers (145 m and 120 m high respectively) have been taken. Hourly averages from the period 1980-1990 have been used here.

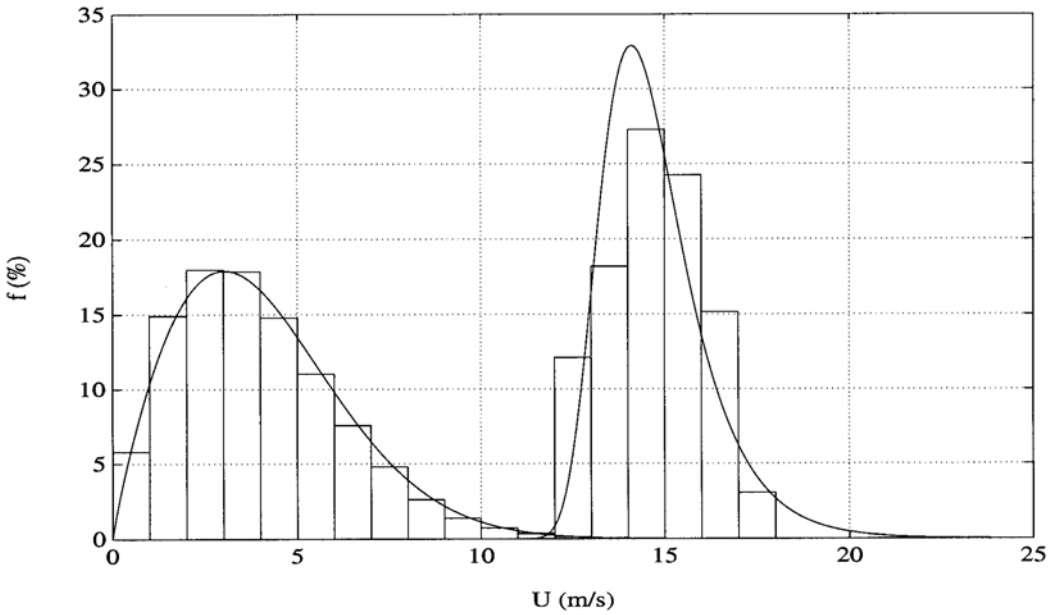

Figure 31: Observed hourly mean wind speed distribution (bars) at 10 m height, Marsta, 1959-1991, and the corresponding Weibull distribution (left part of the figure). To the right is the corresponding observed distribution of annual maximum hourly mean wind speed (bars) together with the corresponding theoretical 1-year extreme value distribution.

Table 3. Observed and estimated mean values of the annual maximum 1 h mean wind speed (m/s) at Maglarp and at Näsudden 1980-90, and at Marsta 1959-91.

Site	Height (m)	Observation	Estimation
Maglarp	10	20.0	19.9
"	25	21.8	21.9
"	38	22.7	22.9
"	54	23.4	23.8
"	75	24.4	24.6
"	96	25.6	26.3
"	120	26.6	27.1
Näsudden	10	16.9	16.9
"	38	22.0	22.4
"	54	23.1	23.3
"	75	24.2	24.6
"	96	25.2	26.0
"	120	25.5	26.3
"	145	26.4	28.0
Marsta	10	14.8	14.7

In Table 3 a comparison is made between the observed and the theoretically estimated mean values of the annual maximum 1 h average wind speed. The differences between theory and observations are small, and vary between -0.1 and 1.6 m/s. The average difference is only 0.4 m/s, which lends support to the theoretical calculations.

Result from the wind resource mapping data: Knowing the mean wind distribution at a site, i.e. knowing the scale and shape parameters, the theory of extreme value distributions may thus be used to estimate the extreme wind speed. This has been applied at the heights 49 m, 72 m, and 103 m above the zero-plane displacement for each 1 km^2 grid point using the model estimates scale and shape parameters. In doing this account has also been taken of the local roughness lengths used by the model.

Extreme values have been estimated for a 50-year return period. The results for 10 min average wind speed are presented in Figure 32 to Figure 34 and for 3 s gust wind speed in Figure 35 to Figure 37, in both cases as 95 % percentiles. The highest extremes are found in the mountain areas, with 10 min average extremes reaching above 65 m/s at 100 m height. Over sea areas the extremes at 100 m are typically 45-50 m/s, but reaches above 50 m/s in some offshore areas around southern Sweden. Over land in southern Sweden the 50 year 10 min extreme wind speed is typically around 35-40 m/s at 100 m height, while in northern Sweden the maxima varies between 30 and 40 m/s. All numbers refer to the 95 % confidence limit. The median extremes are typically 5 m/s lower.

The 50 year extreme 3 s gust wind speed at 100 m reaches above 75 m/s in the mountain areas. Offshore typical values are between 50 and 60 m/s. Over land in southern Sweden the 3 s gust extremes are estimated to be 45-50 m/s, while over northern Sweden the typical range is 40-50 m/s at 100 m height above zero-plane displacement.

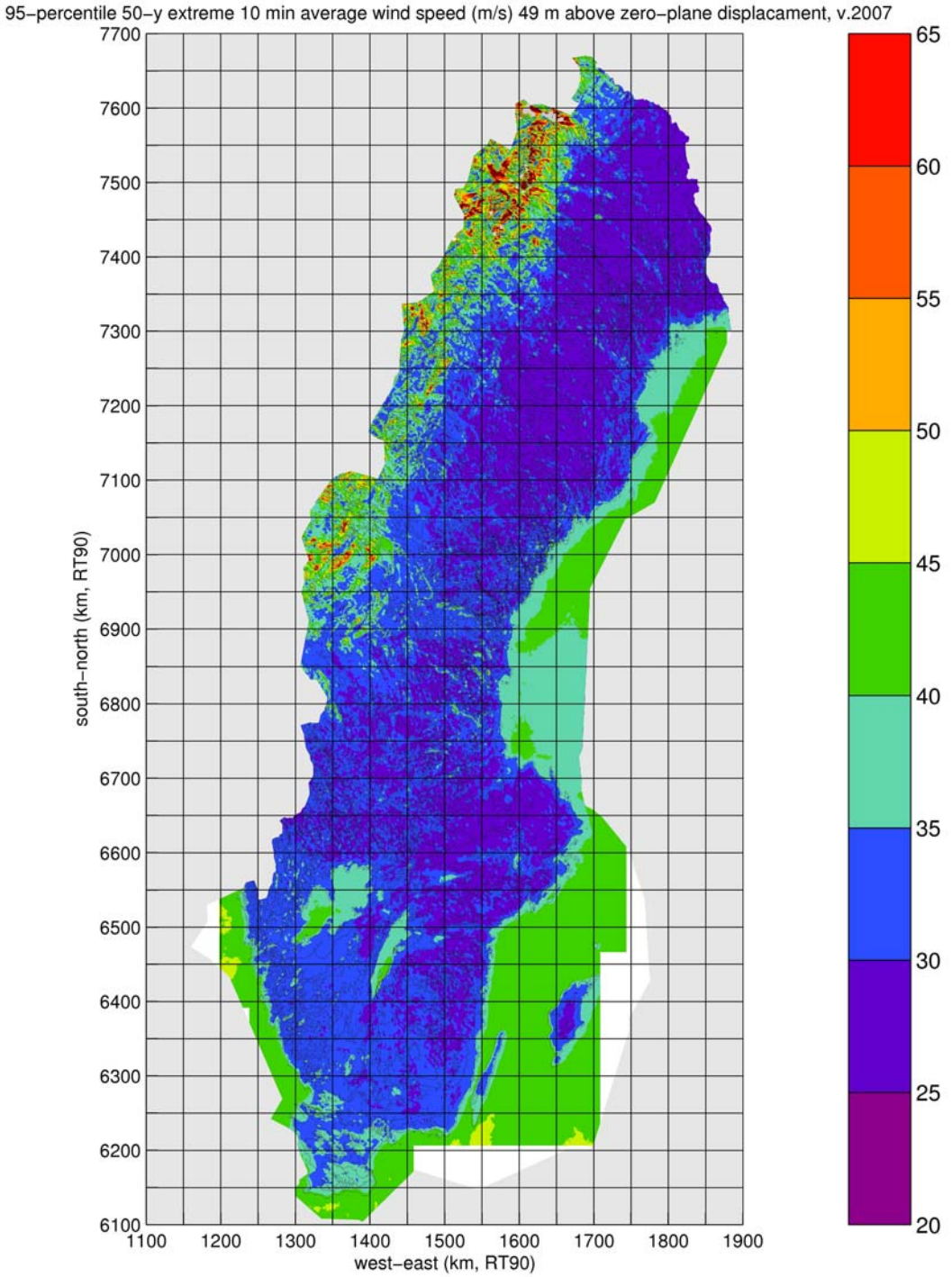

Figure 32: 95 % percentile of the 50 years extreme 10 min average wind speed at 49 m height above zero-plane displacement.

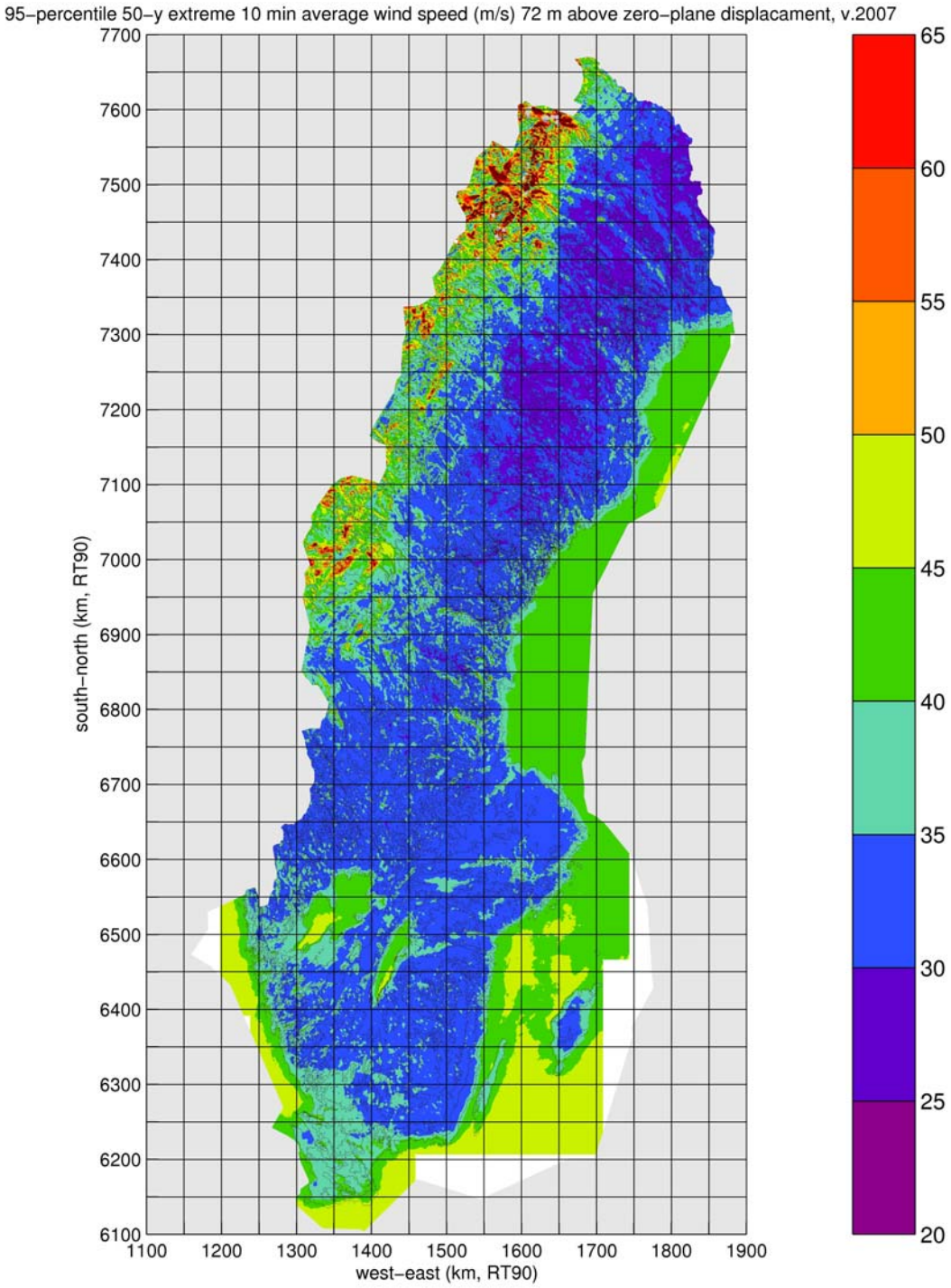

Figure 33: 95 % percentile of the 50 years extreme 10 min average wind speed at 72 m height above zero-plane displacement.

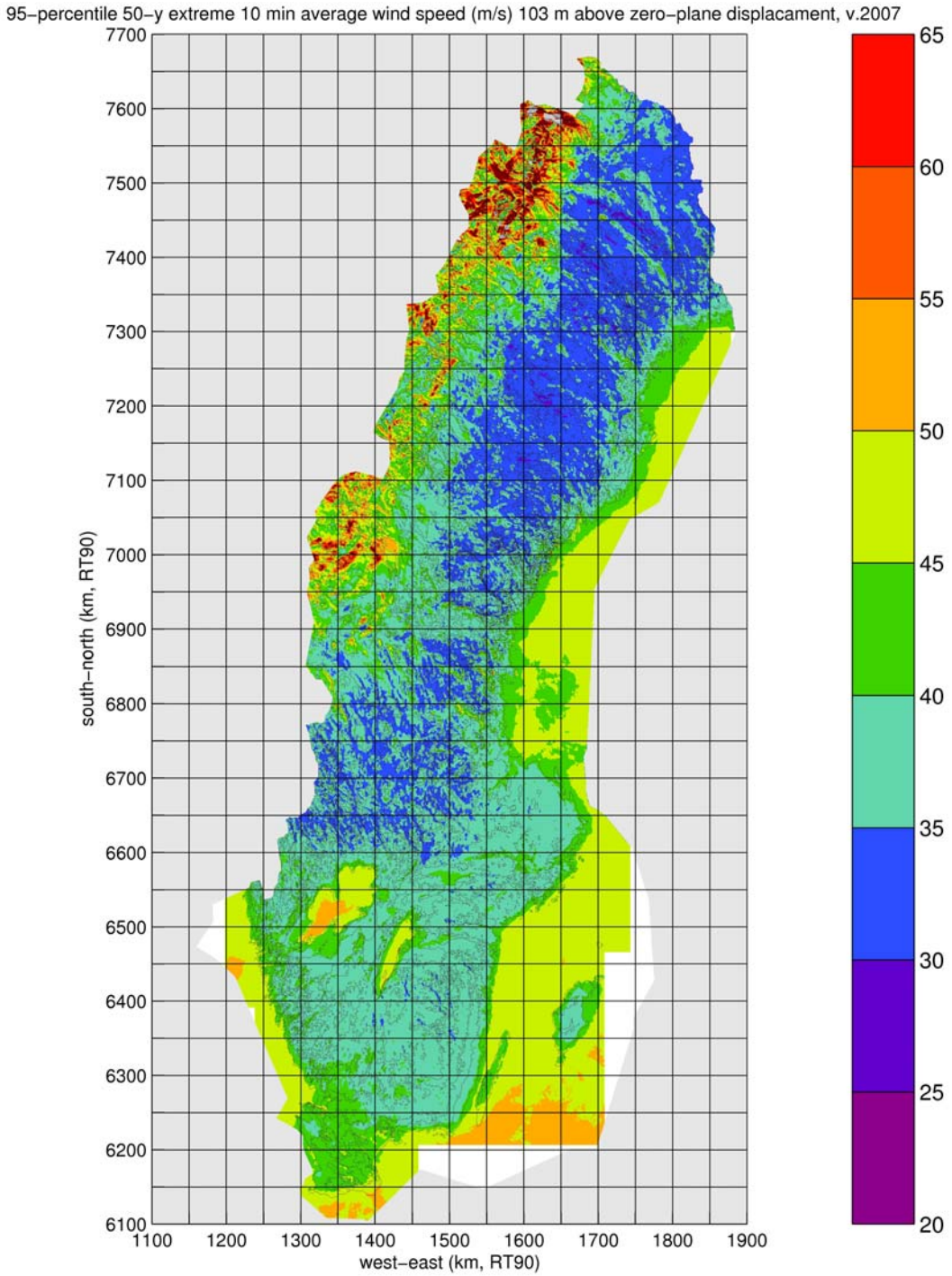

Figure 34: 95 % percentile of the 50 years extreme 10 min average wind speed at 103 m height above zero-plane displacement.

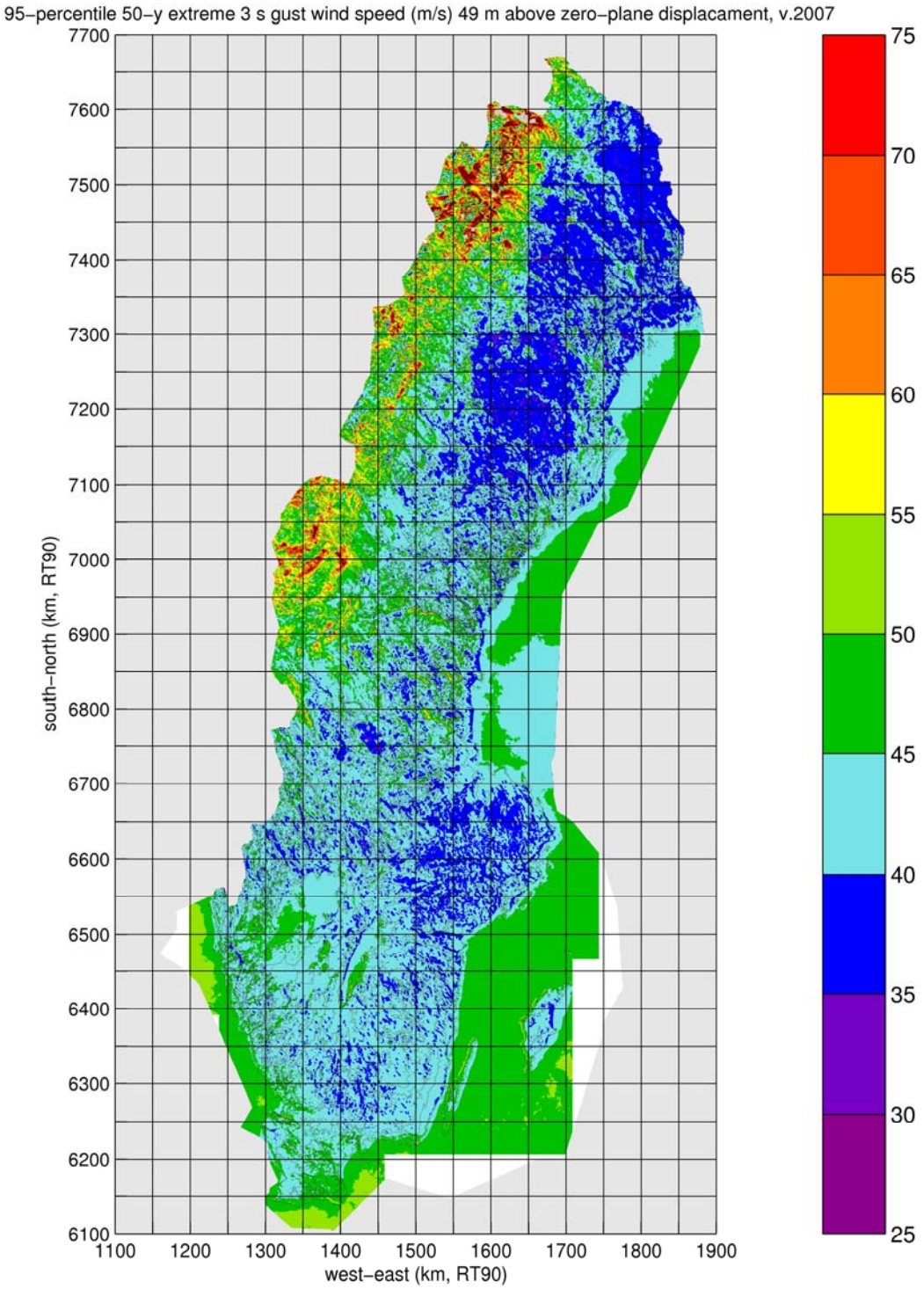

Figure 35: 95 % percentile of the 50 years extreme 3 s gust wind speed at 49 m height above zero-plane displacement.

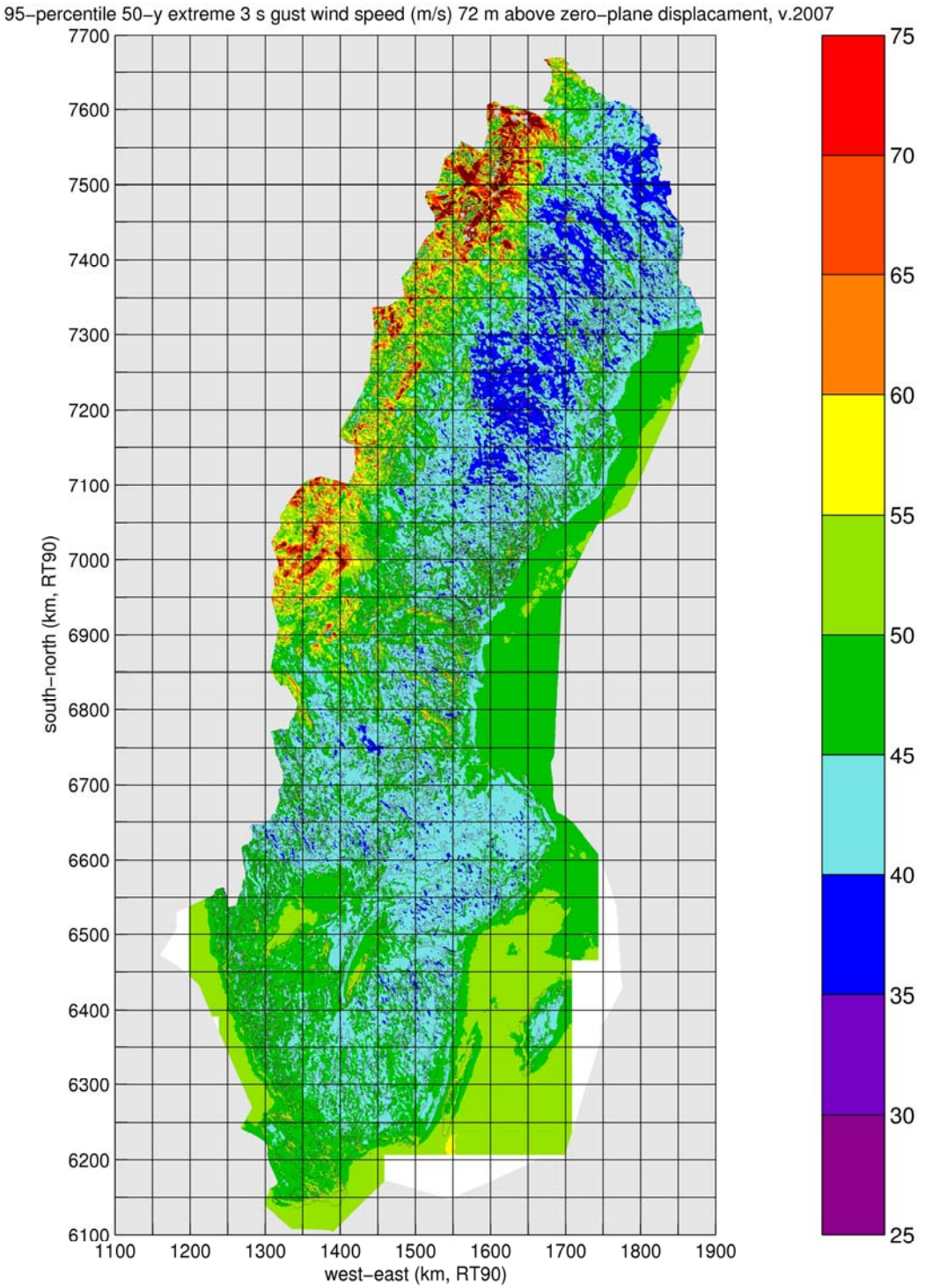

Figure 36: 95 % percentile of the 50 years extreme 3 s gust wind speed at 72 m height above zero-plane displacement.

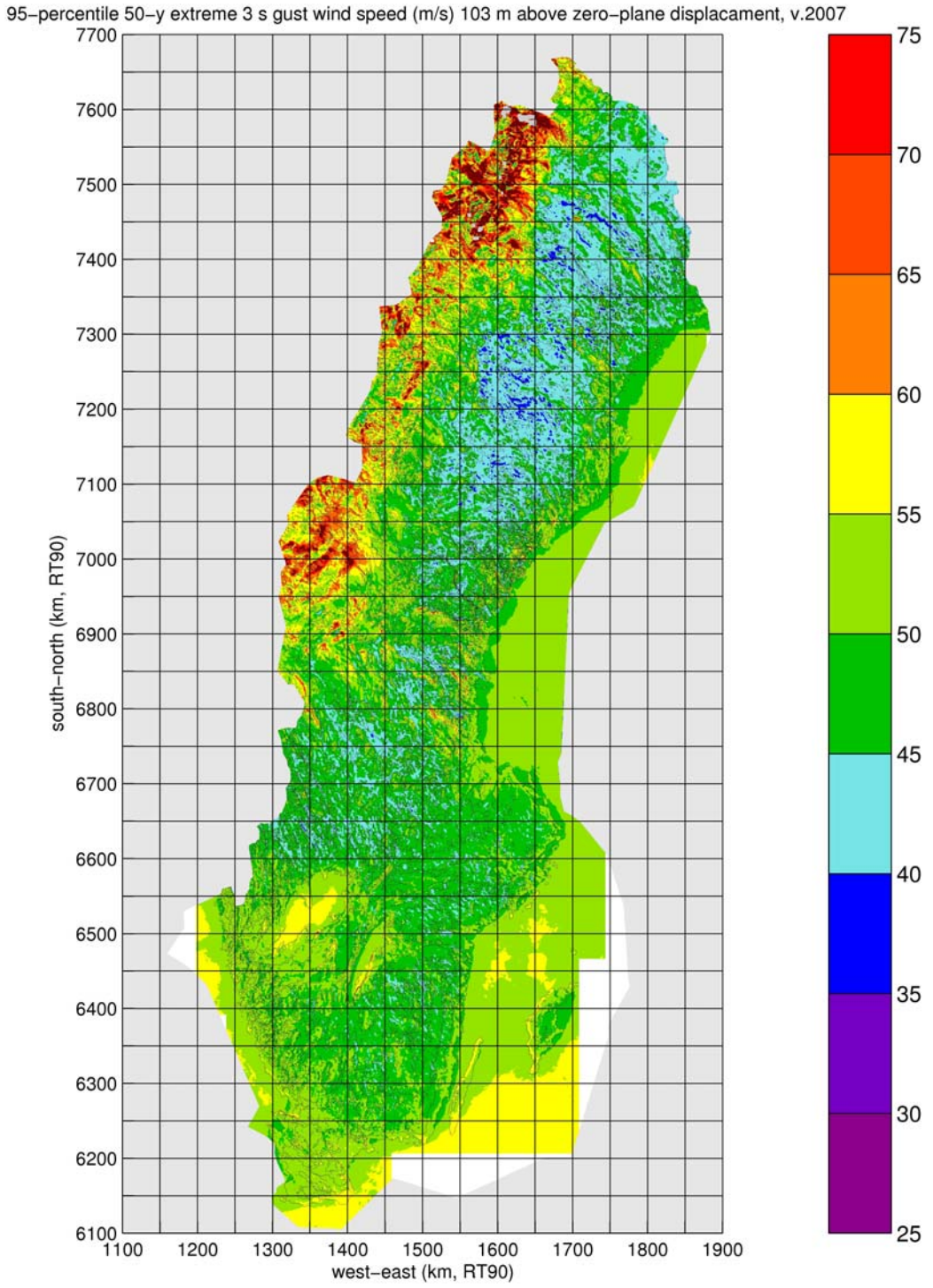

Figure 37: 95 % percentile of the 50 years extreme 3 s gust wind speed at 103 m height above zero-plane displacement.

8.5 Turbulence intensity of wind speed

The model, being a higher-order closure model, includes an equation describing the turbulent kinetic energy of the wind (Eq. 2.12). Following this it is quite straightforward to estimate the turbulence intensity of the wind speed, given by the ratio between the standard deviation of the wind speed and the average wind speed. Using a similar weighting technique as in Eq. (3.3) but instead of using the wind speed applying the weighting equation on the ratio between the square root of the turbulent kinetic energy (~the standard deviation of the wind speed) and the average wind speed.

The resulting annual average turbulence intensities at 49 m, 72 m, and 103 m above the zero-plane displacement area shown in Figure 38 to Figure 40. The values over land typically vary between 0.15 and 0.24 at 49 m height, and decreases with height to 0.09 to 0.18 at 103 m height. Over sea the numbers are 0.12-0.15 at 49 m and decreases to 0.09 to 0.12 at 103 m. Over lakes the model estimates are even below 0.09 already at the 49 m level, but this may be due to that the lake water temperatures were kept constant in the model, giving too stable stratification at certain times.

Comparisons with observations at some sites show turbulence intensities of the same order as estimated from the modelled turbulent kinetic energies. In agricultural areas observed values are 0.10-0.15, while above forests observations give 0.15-0.20 at 100 m height.

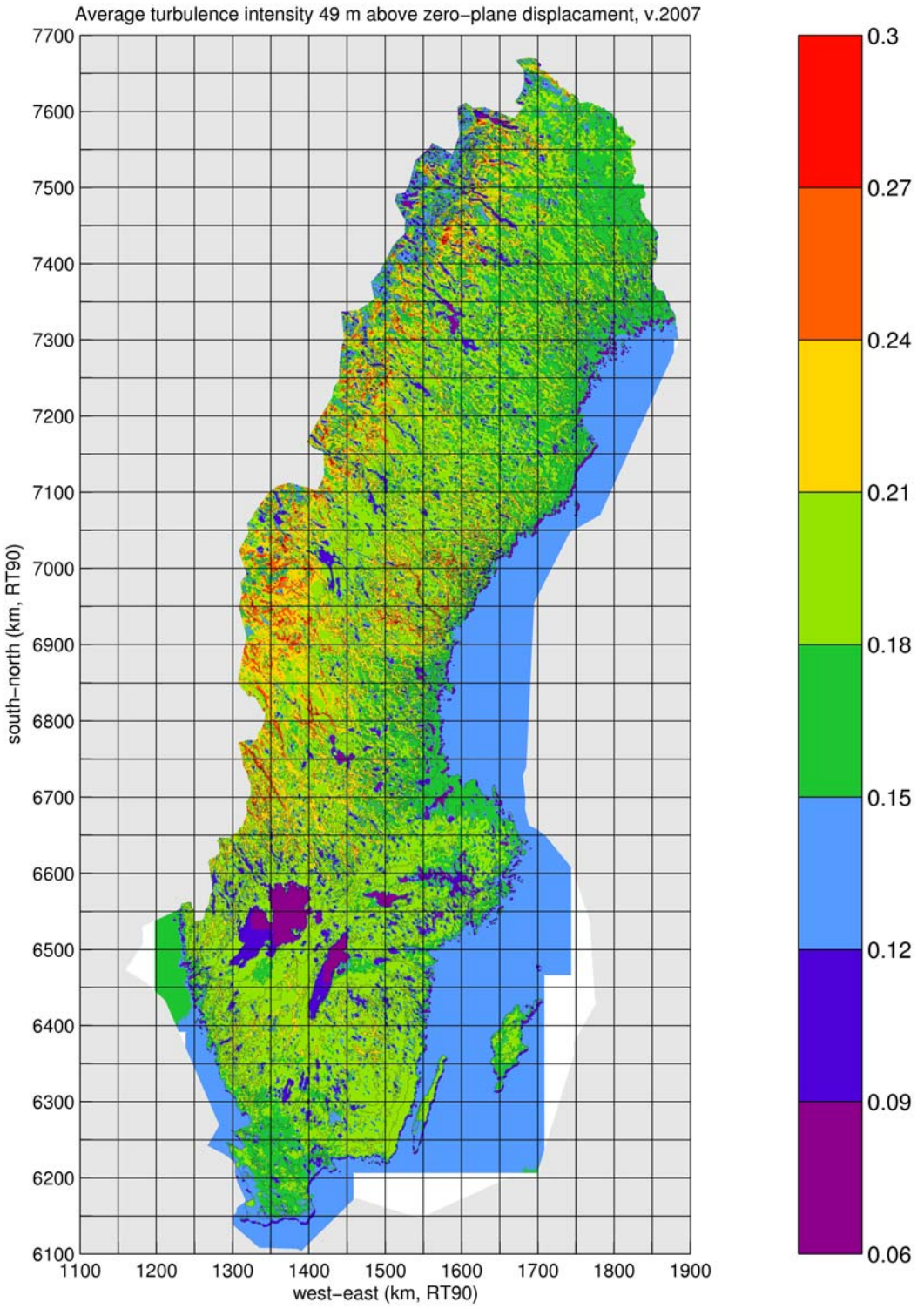

Figure 38: Annual average turbulence intensity of the wind speed at 49 m height above zero-plane displacement.

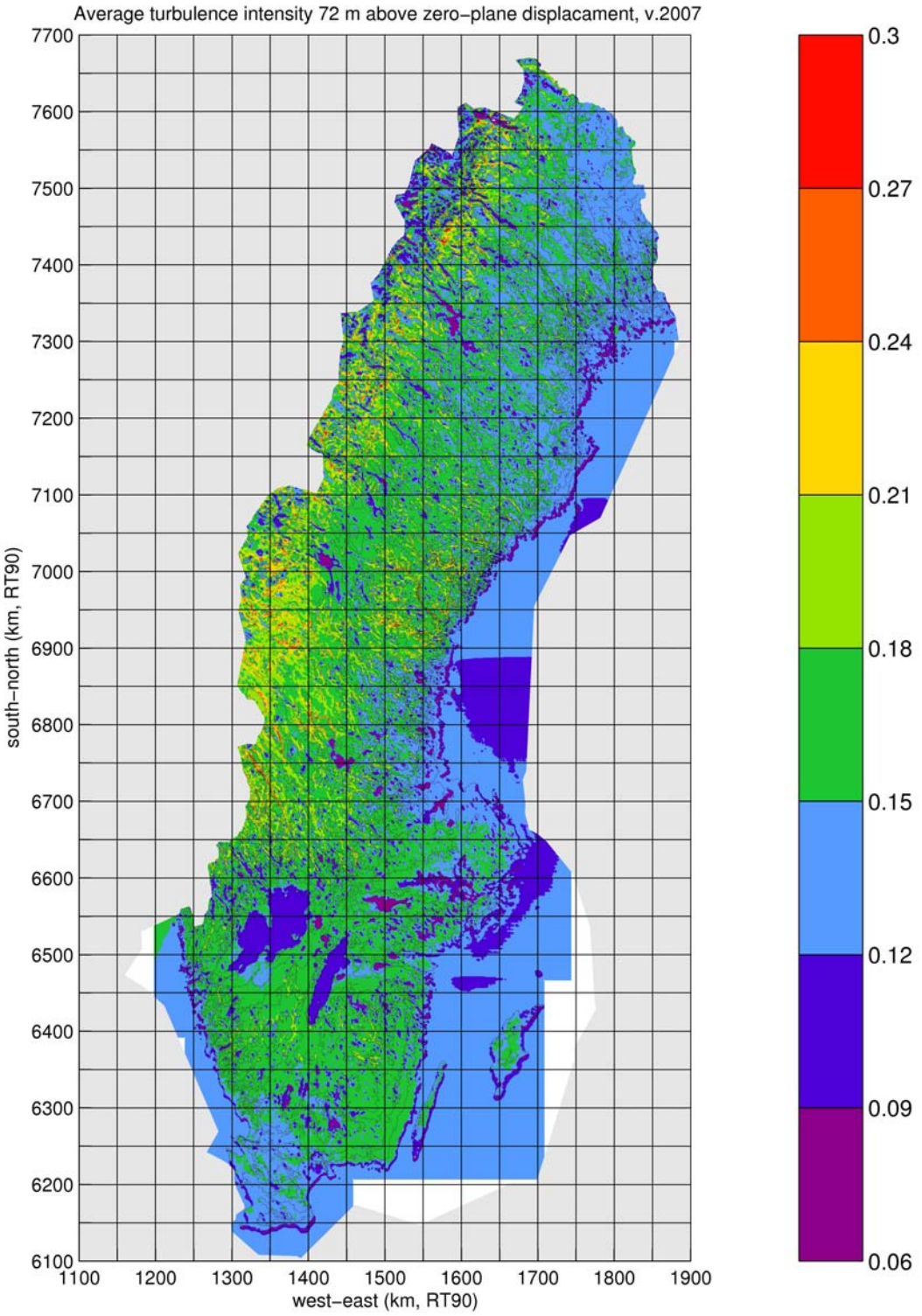

Figure 39: Annual average turbulence intensity of the wind speed at 72 m height above zero-plane displacement.

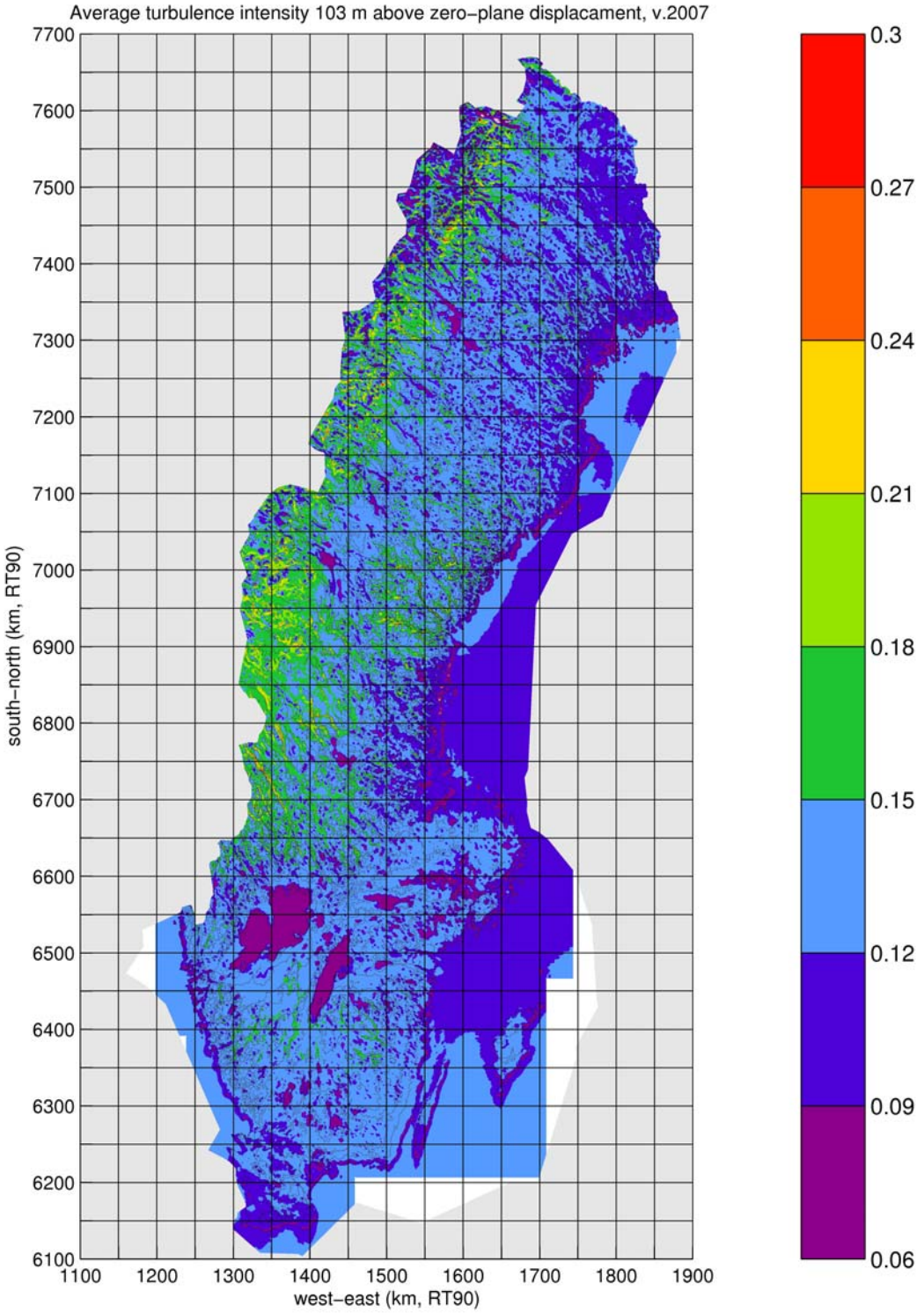

Figure 40: Annual average turbulence intensity of the wind speed at 103 m height above zero-plane displacement.

8.6 Wind turbine class

Following the IEC 61400 document on International Standards for Wind Turbines, part 1, 2005, describing design requirements, wind turbines could be divided into different classes. Two basic parameters are used for this. The reference wind speed average over 10 min, V_{ref}, and the expected value of the turbulence intensity at 15 m/s, I_{ref}. In Table 4 the criteria to define the different turbine classes are specified.

Table 4: Basic parameters at hub height for wind turbine classes.

Wind turbine class		**I**	**II**	**III**	**S**
		V_{ref} (m/s)			Values specified by the designer
		50	42.5	37.5	
A	I_{ref}	0.16			
B		0.14			
C		0.12			

The reference wind speed, V_{ref}, is related to the average wind speed at hub height, V_{ave}, by the equation

$$V_{ave} = 0.2 \cdot V_{ref} \qquad (8.20)$$

Thus V_{ref} may easily be determined from the modelled average wind speed.

To determine I_{ref} an assumption must be made about the relationship between average turbulence intensity and its value at 15 m/s wind speed. From observations we know that the turbulence intensity typically decreases from rather high values at low wind speed to a minimum somewhere between 5 and 10 m/s, and then increases somewhat again for wind speed above 10 m/s. The magnitude of this increase for higher winds varies, but is typically around 0.02 over sea and increases to around 0.04-0.06 over forests.

No information about how the turbulence intensity varies with wind speed has been determined from the model results. Only the annual averages are available. Due to the typical variability of turbulence intensity with wind speed it is reasonable to assume that the turbulence intensity at 15 m/s should be slightly larger than the average value. I_{ref} is thus estimated from the modelled average turbulence intensity by adding 0.02.

The wind turbine classes were then finally defined using $46.25 \leq V_{ref} < 55$ m/s for class I, $40 \leq V_{ref} < 46.25$ m/s for class II, and $V_{ref} < 40$ m/s for class III. For the turbulence classes, class A was used for $0.15 \leq I_{ref} < 0.18$, class B for $0.13 \leq I_{ref} < 0.15$, and class C for $I_{ref} < 0.13$. The resulting wind turbine classes following the modelled average wind speed and turbulence intensity at 49 m, 72 m, and 103 m above zero-plane displacement are shown in Figure 41 to Figure 43. At 49 m most land areas fall outside the defined turbine classes, while over sea turbine class IIA dominate in the south and class IIIA in the north. At 72 m still large areas in central and northern Sweden are outside the pre-defined classes. Also forested areas in the southern highlands are outside pre-classes, while other areas in southern Sweden are mostly in class IIIA. At 103 m only smaller areas are still outside the pre-defined classes. Typical classes in the forested southern Swedish highland are now IIIA, while in the north classes IIIA and IIIB are common. Offshore classes IIA and IIB are typical, in the southern Baltic Sea also IA and IB.

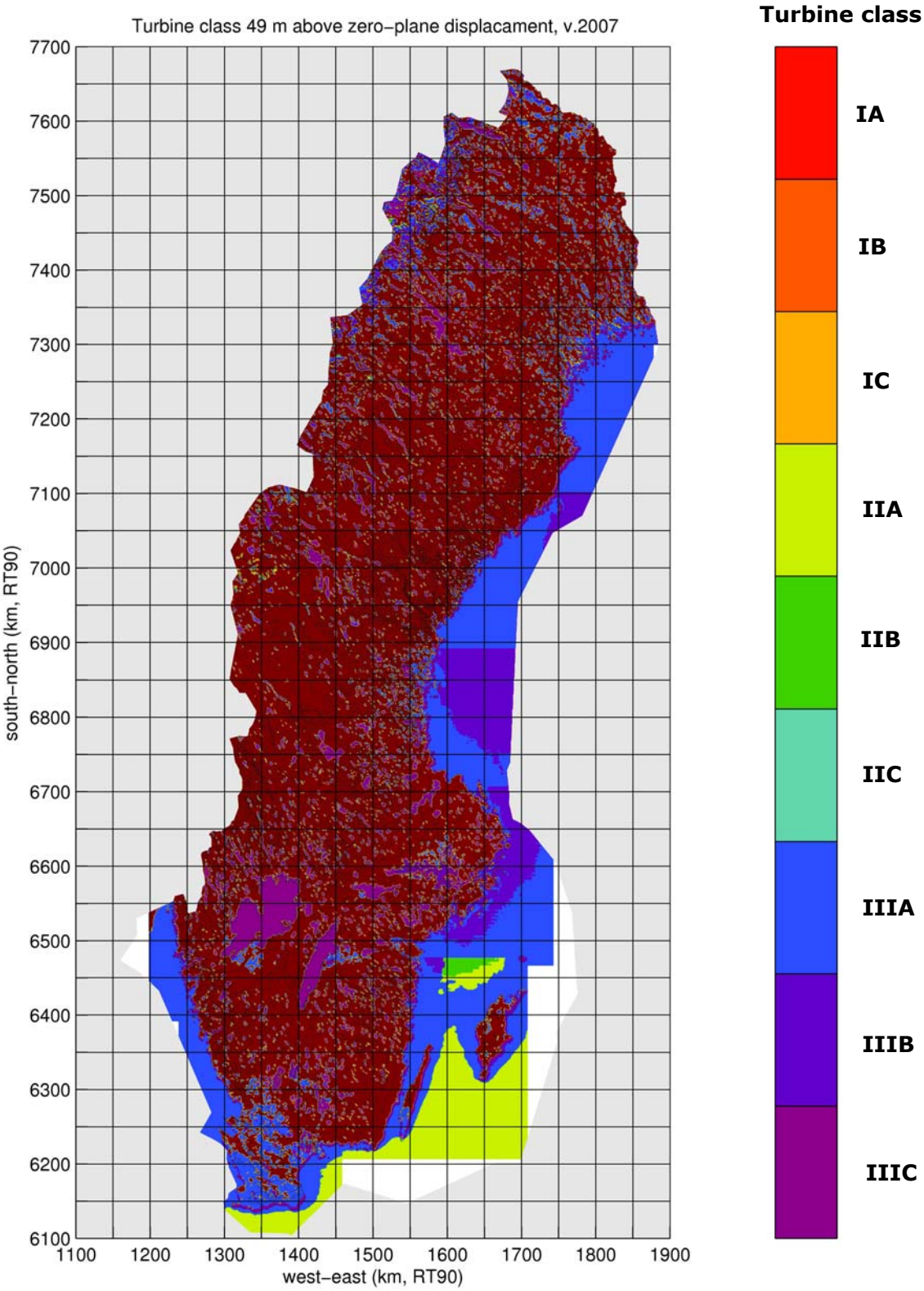

Figure 41: Wind turbine class at 49 m height above zero-plane displacement. The brownish areas fall outside defined turbine classes.

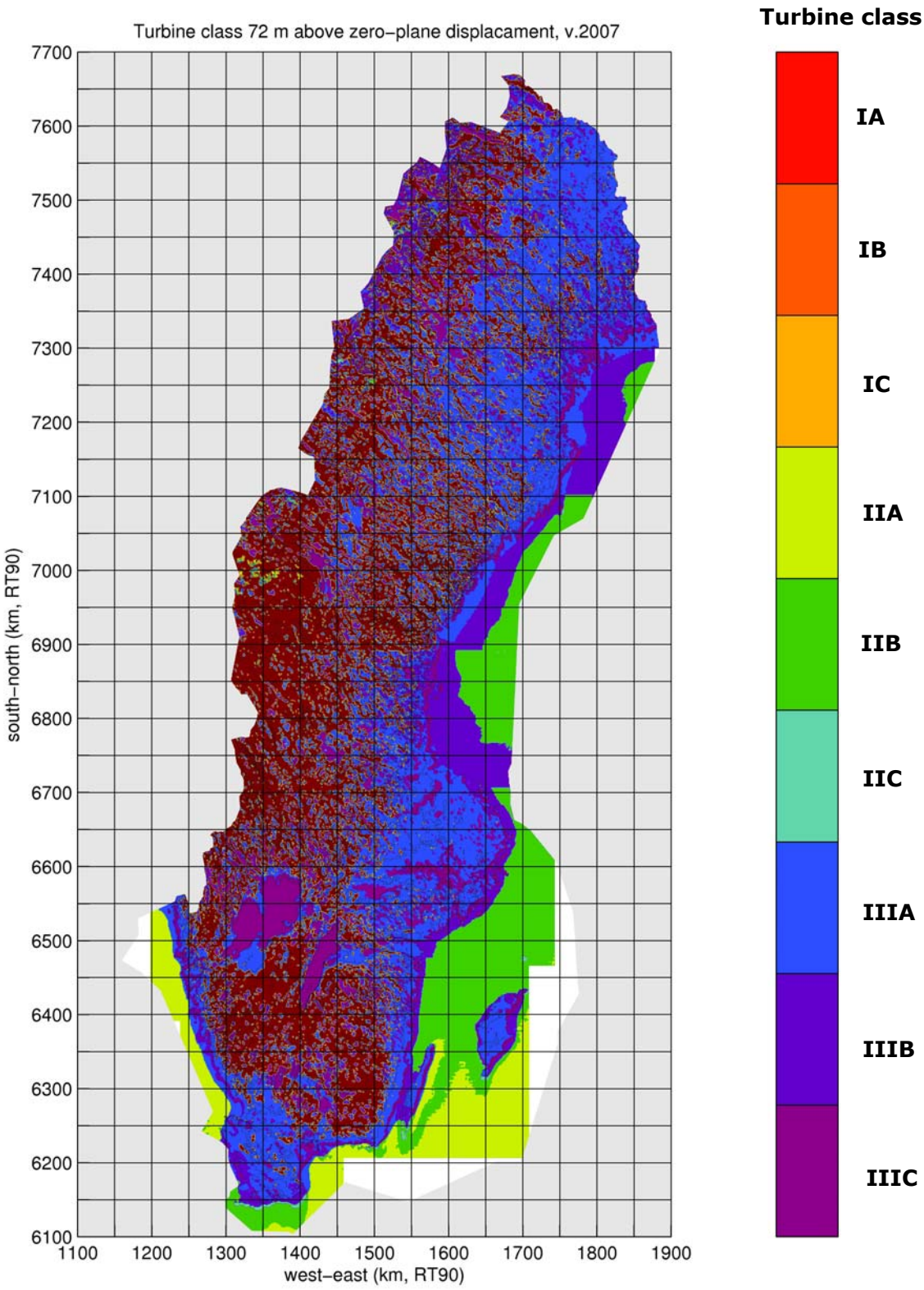

Figure 42: Wind turbine class at 72 m height above zero-plane displacement. The brownish areas fall outside defined turbine classes.

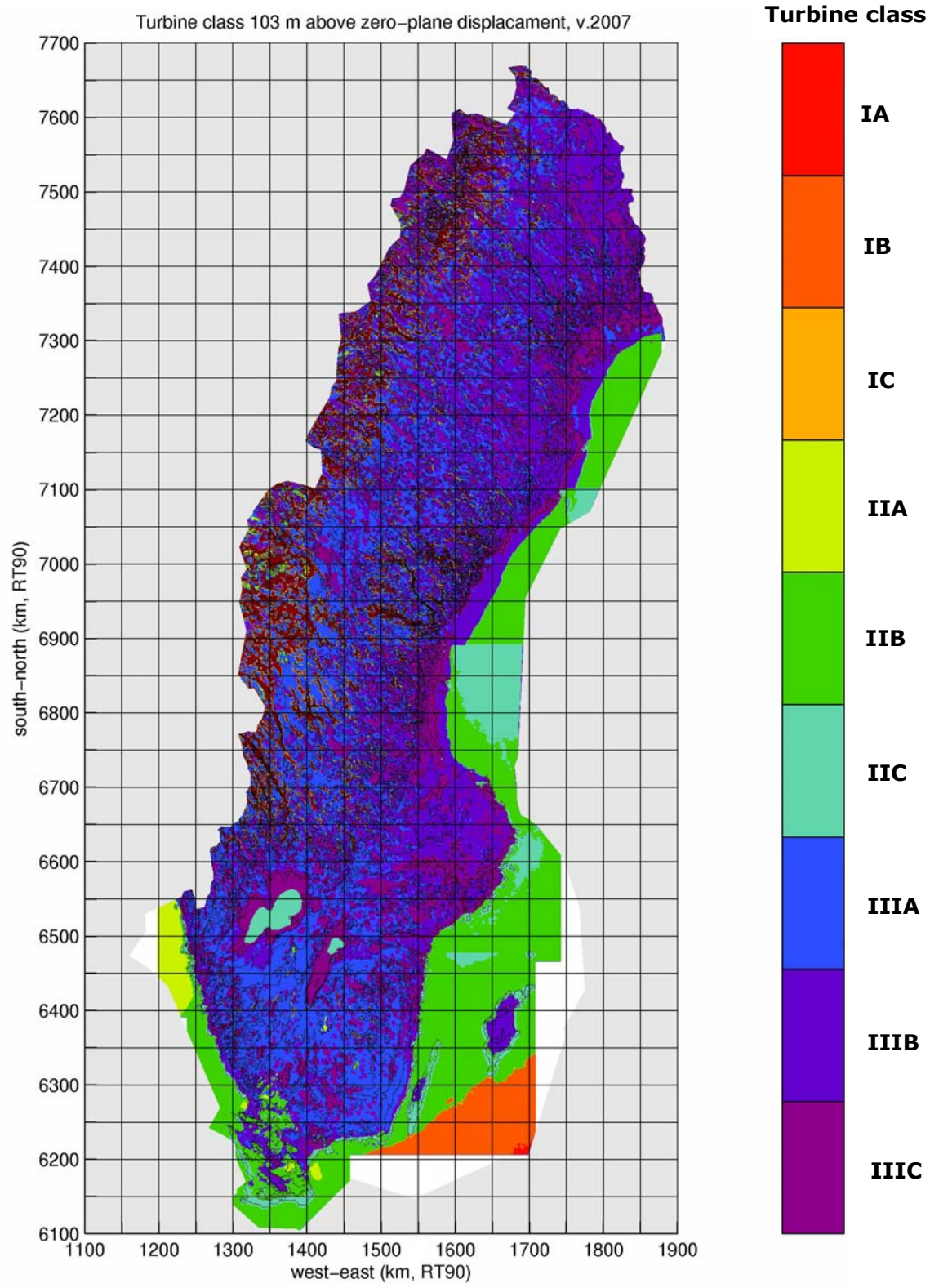

Figure 43: Wind turbine class at 103 m height above zero-plane displacement. The brownish areas fall outside defined turbine classes.

9 Downscaling of the wind resource mapping

With 1000 m-grid resolution, which was used in the national wind resource mapping with the MIUU-model, the main characteristics of the variability of the wind climate is captured. However, with a 1000-m grid resolution, the variability of the real topography is partly smoothened out. Numerical simulations at a higher grid resolution is needed in order to get a better understanding of the small scale variability in the wind climate in areas with topographical variations less than 1000 m.

Experience from previous case studies with 500 m-grid resolutions have shown that the wind climate is captured with reasonable accuracy in most areas with space for smaller wind farms. For wind farm planning purposes, this is too coarse. To increase the resolution in wind resource mapping models such as WA^{S}P, have in many cases been used. Due to the simplified physical description of the atmosphere in for example WA^{S}P, a fair amount of uncertainties are introduced in the wind resource estimate in complex terrain. Lately it has become increasingly popular using so-called CFD-models (Computational Fluid Dynamics-models). One of the main weaknesses using this type of models is that the models seek for steady state solutions and thus not an ideal tool for describing the atmospheric flow, which by its nature is not in steady state.

In this study the resolution in the national wind resource mapping is increased to 100 m using *meteorological CFD-models*, i.e., numerical models developed to describe the atmosphere and its interactions with varying surface properties etc. Increasing the resolution to 100 m the results also have a potential to serve as a basis for planning of wind farm layouts and production calculation from individual turbines or wind farms.

In the following sections, results from a wind resource mapping covering Fjällberget/Saxberget in central Sweden are presented. Two mesoscale models with grid resolutions down to 100-m are used and the model results are compared to measurements.

For comparison, the measurements have also been used to estimate wind resources using WA^{S}P at 100-m resolution, even though many factors which control the variability of the wind in space and time is missing in WA^{S}P.

9.1 Model description

Two similar mesoscale numerical models were used in the downscaling experiment, the MIUU-model and the Coupled Ocean/Atmosphere Mesoscale Prediction System (COAMPS®, a registered trademark of the Naval Research Laboratory). The main difference between the two models is that the MIUU-model is hydrostatic while COAMPS® is non-hydrostatic.

In complex topography, the influence of vertical acceleration, which is not included in hydrostatic models, may be important to the atmospheric structure. However, the models are here used to study the wind climate and not to forecast individual events; while being important on a day-to-day basis, non-hydrostatic motions in the atmosphere have little influence on the general wind climate. Moreover, in this study terrain steepness does not violate the hydrostatic assumption.

In the next section, a brief description of COAMPS® is given. A description of the MIUU-model is found above in Section 2 and not repeated here.

9.1.1 COAMPS®

COAMPS®, developed at the US Naval Research Lab, Monterey, CA (Hodur, 1997), is a non-hydrostatic compressible model with a terrain-following sigma-z vertical coordinate similar to that used in the MIUU-model. The model has prognostic equations for the mean variables u (wind in the east-west direction), v (wind in the north-south direction), w (vertical wind), Θ (potential temperature), and π (the Exner function/pressure perturbation). Turbulence is parameterised with a level-2.5 turbulence closure (Mellor and Yamada, 1982); hence, TKE (turbulent kinetic energy) is a prognostic variable. In this study, version 2.0 of COAMPS® was used.

Moist physics is parameterised using a mixing ratio scheme (Rutledge and Hobbs, 1983). Predictions of mixing ratios are given for the microphysical variables water vapour, pristine ice, snow, rain, and cloud water. Other physical parameterisation schemes included in COAMPS® are long- and shortwave radiation (Harshvardan et al., 1987) and cumulus convection (Kain and Fritsch, 1990). Ground surface temperature is computed using a surface energy balance scheme. High resolution for a given area of interest can be achieved by using nested grids in idealised and real-case simulations. A more complete model description is found in Hodur (1997).

COAMPS® is used operationally by the US Navy to produce forecasts. Examples of areas in which COAMPS® is used on a daily basis are along the US west coast and in the Mediterranean Sea. In Sweden, COAMPS® is used as a research tool at Uppsala University and Stockholm University, and operationally by WeatherTech Scandinavia AB to produce wind forecasts. The model has also been used in numerous research studies, e.g. on coastal jets (Burk and Thompson 1996, Burk et al. 1999) and katabatic flow (Söderberg and Parmhed 2005).

Typically, terrain height, roughness, soil temperature, and soil wetness is taken from a database compiled to suite COAMPS®. However, in this study we used the same terrain height, roughness, and soil temperature as in the simulations with the MIUU-model. Moreover, COAMPS® was modified allowing the model to be initialised in the same way as the MIUU-model with vertical profiles of wind speed and direction, temperature, and specific humidity describing the mean state of the atmosphere.

9.2 Experiment setup

In order to increase the horizontal resolution, both the MIUU-model and COAMPS® were nested in the 5-km model runs made with the MIUU-model in the initial phase of the wind resource mapping (cf. Section 4). The increase in horizontal resolution with the MIUU-model was done in three separate steps: a 1000-m grid forced by the 5-km model runs, a 300-m grid forced by the 1000-m model runs, and finally a 100-m grid forced by the 300-m model runs. With COAMPS®, the increase in horizontal resolution was achieved by nesting a 900-m grid in the MIUU 5-km model runs. In each time step of the model integration, the 900-m grid feeds an inner nest with 300-m grid, which in turn feeds the innermost model nest with 100-m grid. The model grids and topography are shown in Figure 44 and Figure 45.

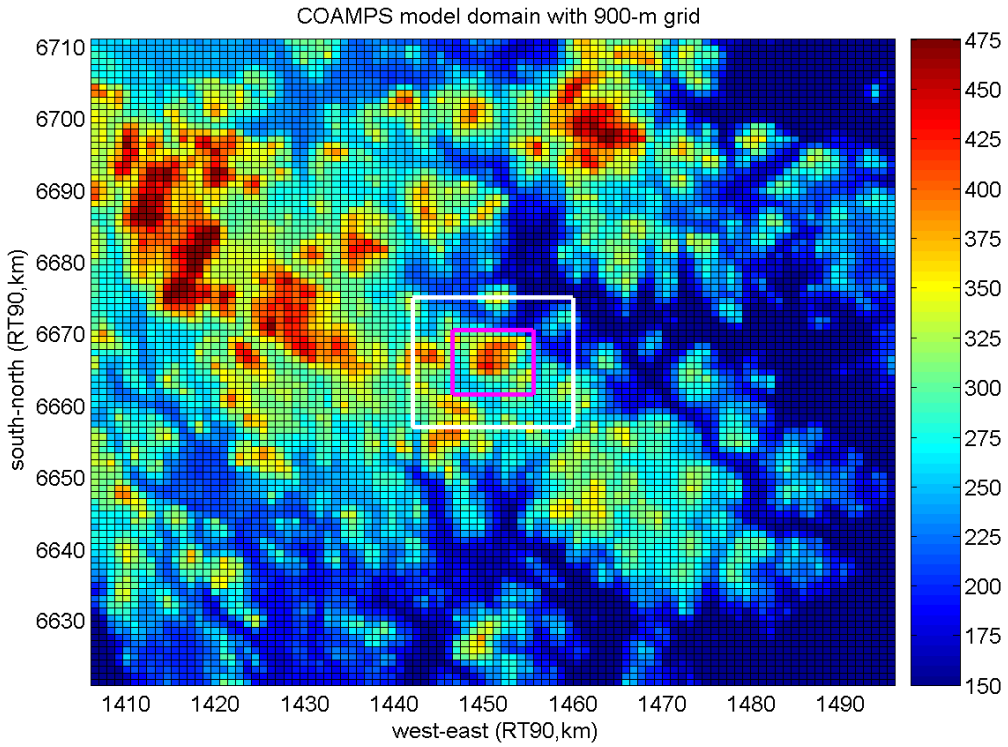

Figure 44: 900-m model domain showing also the 300 m and 100 m domains (inner rectangles). Colours show topography in m above sea level.

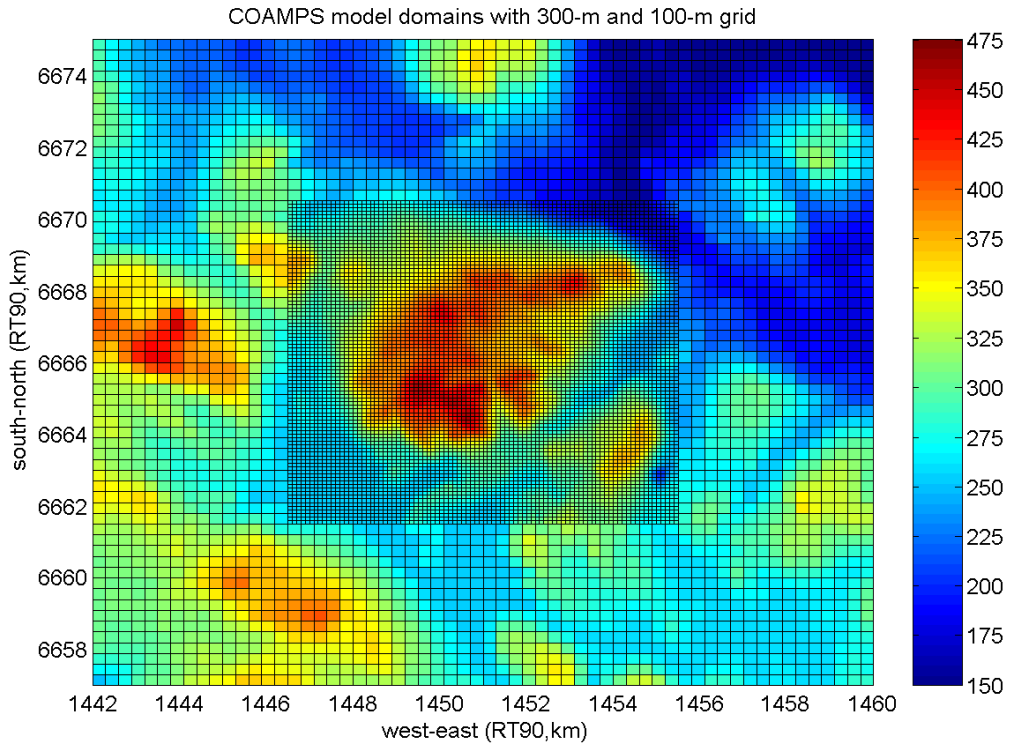

Figure 45: 300 m and 100 m model grids over Fjällberget/Saxberget. Colours show topography in m above sea level.

For the areas of interest, the same terrain height, roughness length, and initial soil temperature were used in the 300-m and 100-m grid runs with the MIUU-model and COAMPS®. The MIUU-model uses a stretched grid in the outer ends of the domain (see Section 2). The 1000-m MIUU and 900-m COAMPS®-grids were derived from the same database sources. Since there is a difference in the horizontal grid, grid-point to grid-point comparisons may not represent the same surface characteristics while the results in a more general sense are comparable. Both models were initialised with the same background atmospheric vertical profile.

In the experiment, the MIUU-model and COAMPS® used the same vertical distribution of model levels. The model top was set at 10000 m; 8 levels were used up to 100 m height at 2.0, 6.4, 12.4, 20.9, 32.6, 48.9, 71.3, and 103.0 m.

Note that no local observations are included or needed in the simulations. Hence, the model output is totally independent of the observations with which a comparison is made.

9.3 Results

Annual average wind speed was determined using the same technique as described in Section 3 and which was used in the Swedish wind resource mapping. The results in the area around Fjällberget/Saxberget are shown in Figure 46 to Figure 48.

Calculations with both the MIUU-model and COAMPS® down to 100 m grid resolution seems to give reasonable results. The main differences found are that at low grid resolution the MIUU-model in general gives higher annual mean wind speeds than COAMPS®. At 300 m resolution the results from COAMPS® also show high wind speed over the high elevation terrain. At 100 m grid resolution, COAMPS® gives higher local increase in wind speed over local mountain tops.

Comparisons between model results and observations from Saxberget and Fjällberget are shown in Figure 49 and Figure 50. It can be seen that the MIUU-model captures the highest mean wind speed already at relatively low resolutions while COAMPS® underestimates the wind speed at low resolutions. With increased resolution, COAMPS® performs better and at Saxberget, both the MIUU-model and COAMPS® with 100 m-grid resolutions show an excellent agreement with observations. Also at Fjällberget the MIUU-model with 100 m-grid resolution show a good agreement with observations while COAMPS® here overestimates the wind speed.

WA^{S}P in general gives smaller differences in mean wind speed between high and low elevation terrain as may be seen in Figure 51. WA^{S}P was here driven by the observations at Fjällberget, 61 m level and results are presented at 80 m height approximately corresponding to the 72 m level above zero-plane displacement presented in the results from the MIUU-model and COAMPS® as the forest on the mountain is relatively low. It should be noted that the same colour scale has been used presenting the results from all three models. WA^{S}P also gives different wind climates when observations from Fjällberget or Saxberget are used (not shown).

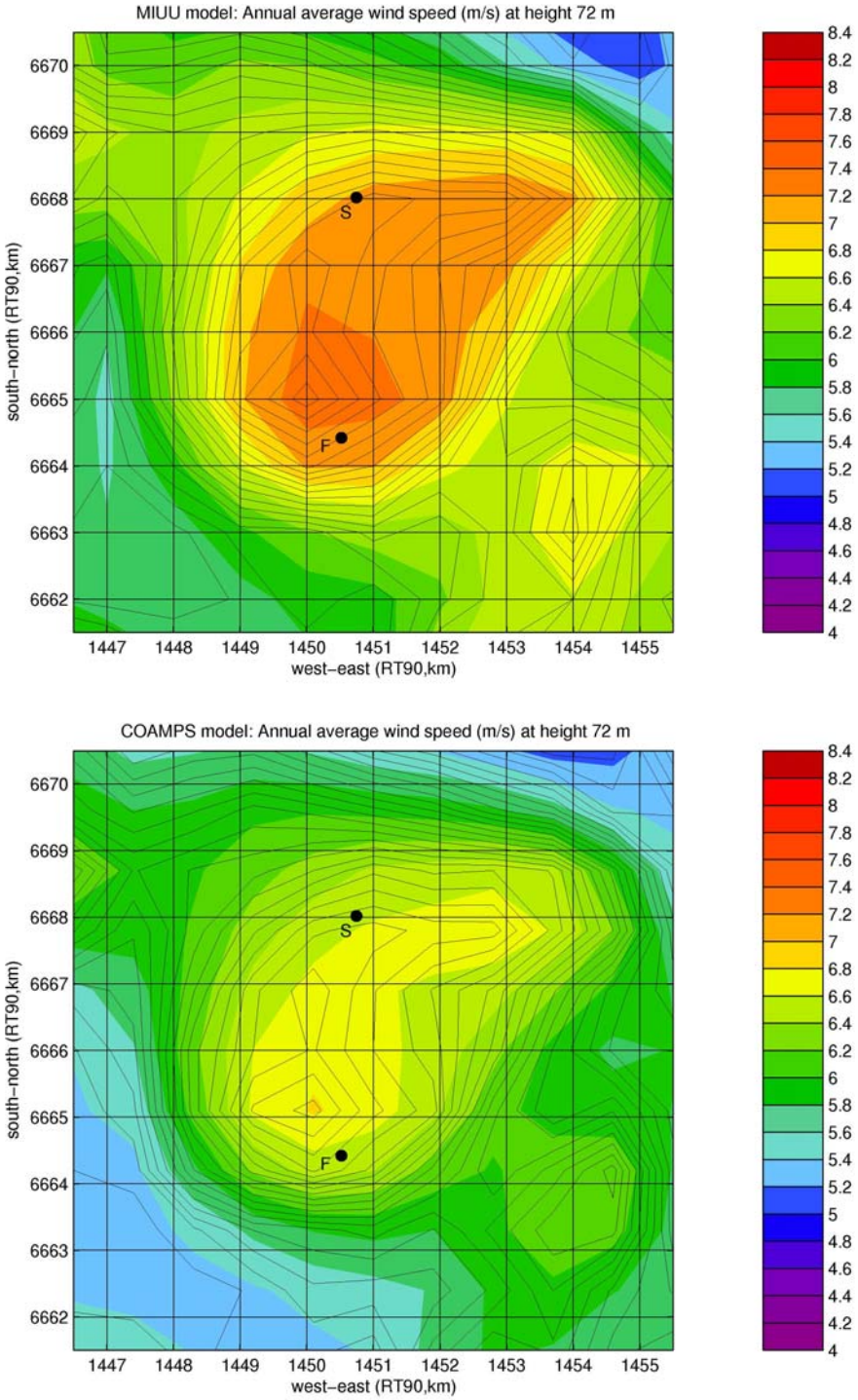

Figure 46: Annual average wind speed in the Fjällberget/Saxberget area as estimated by the MIUU-model (top) and by COAMPS® at 72 m height above zero-plane displacement using 1000 m and 900 m grids respectively. F and S indicate locations of two measurement masts at Fjällberget and Saxberget.

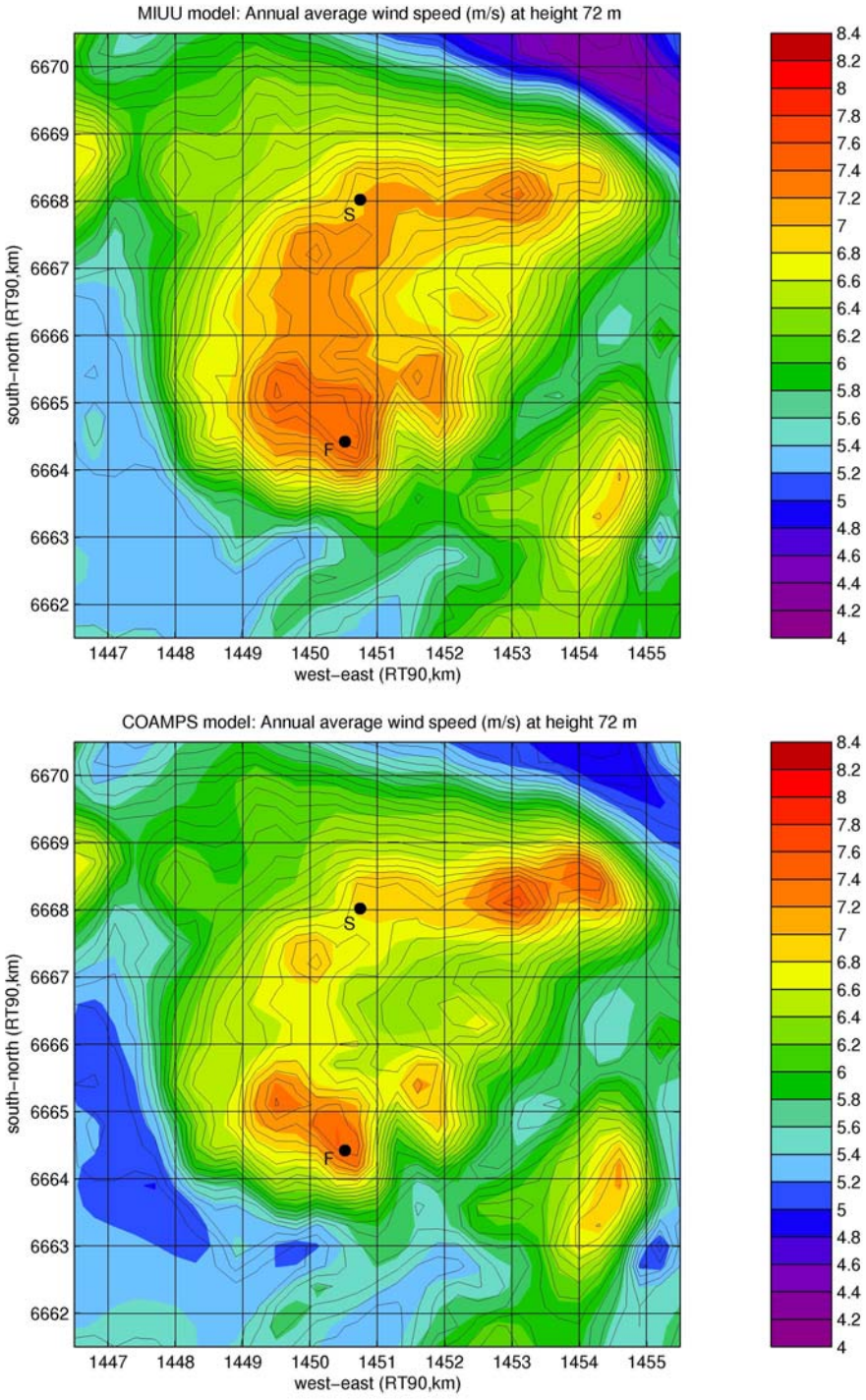

Figure 47: Annual average wind speed in the Fjällberget/Saxberget area as estimated by the MIUU-model (top) and by COAMPS® at 72 m height above zero-plane displacement using 300 m grids. F and S indicate locations of two measurement masts at Fjällberget and Saxberget.

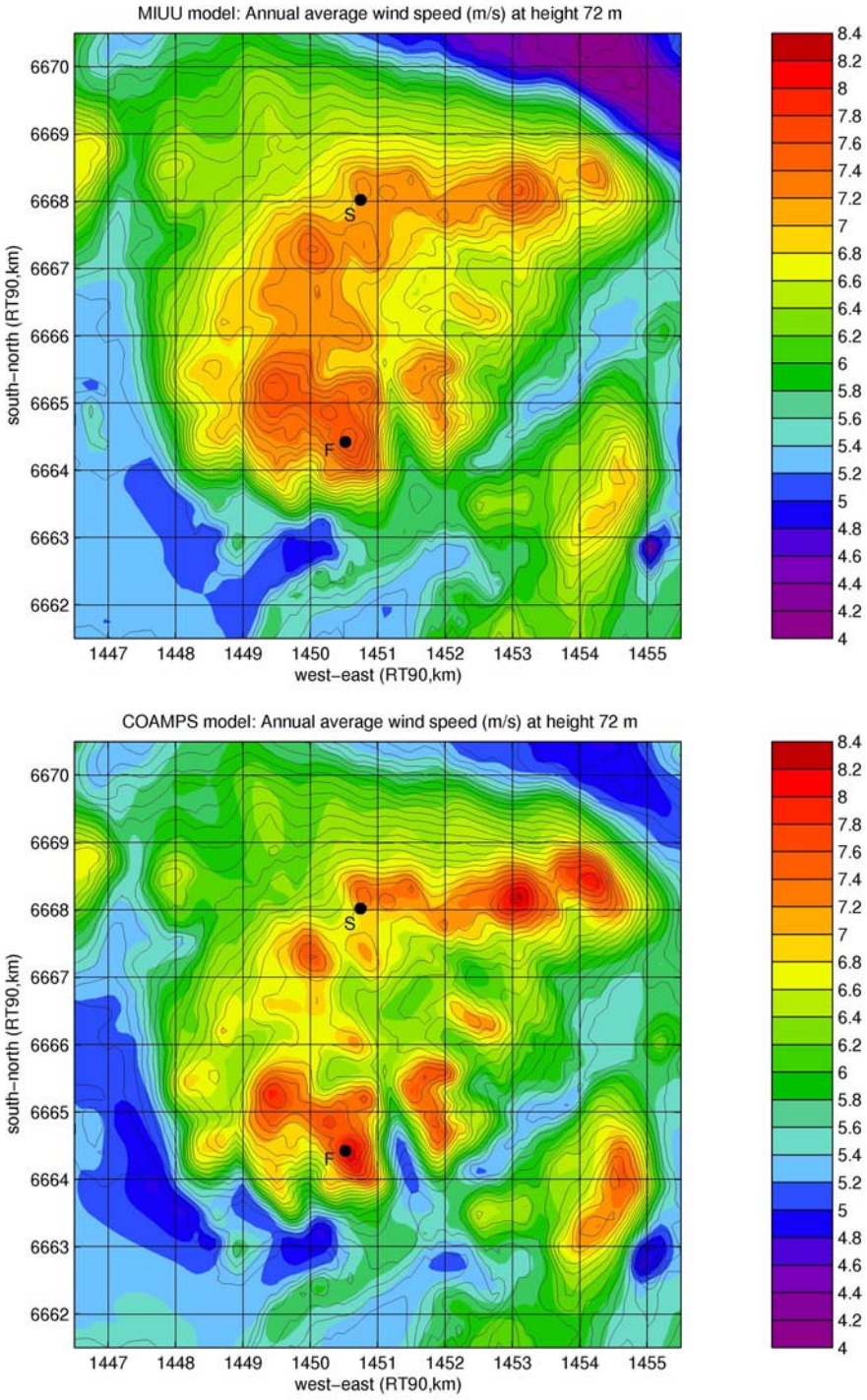

Figure 48: Annual average wind speed in the Fjällberget/Saxberget area as estimated by the MIUU-model (top) and by COAMPS® at 72 m height above zero-plane displacement using 100 m grids. F and S indicate locations of two measurement masts at Fjällberget and Saxberget.

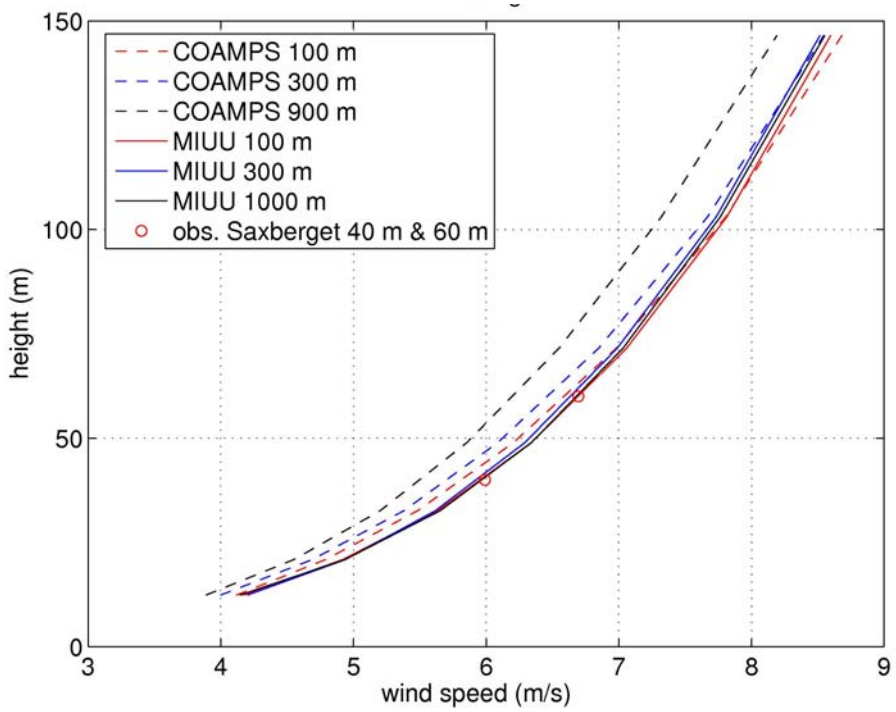

Figure 49: Modelled and observed annual average wind speed profile at Saxberget.

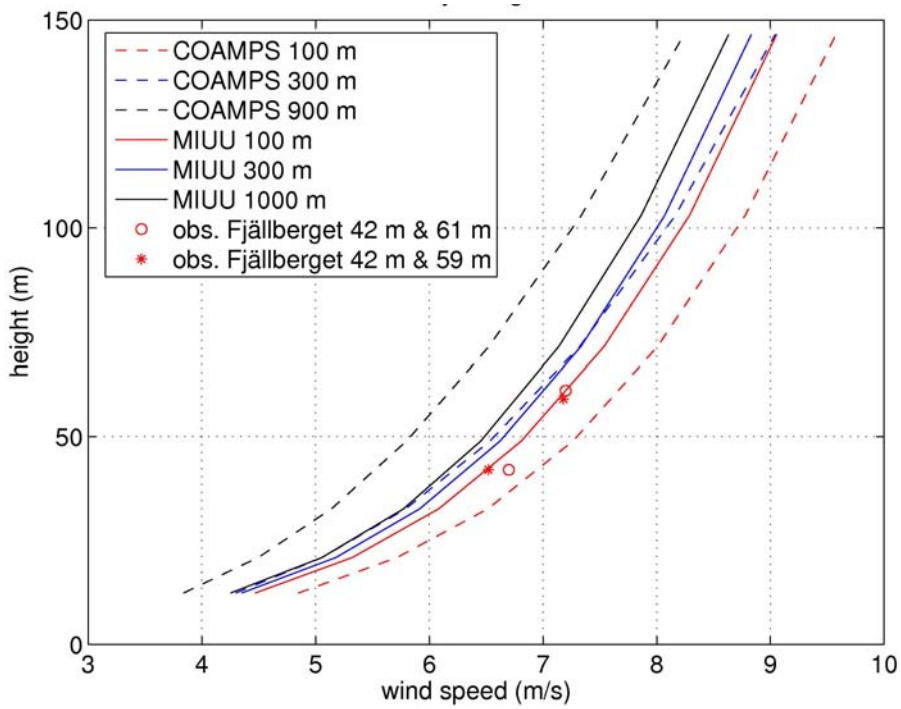

Figure 50: Modelled and observed annual average wind speed profile at Fjällberget.

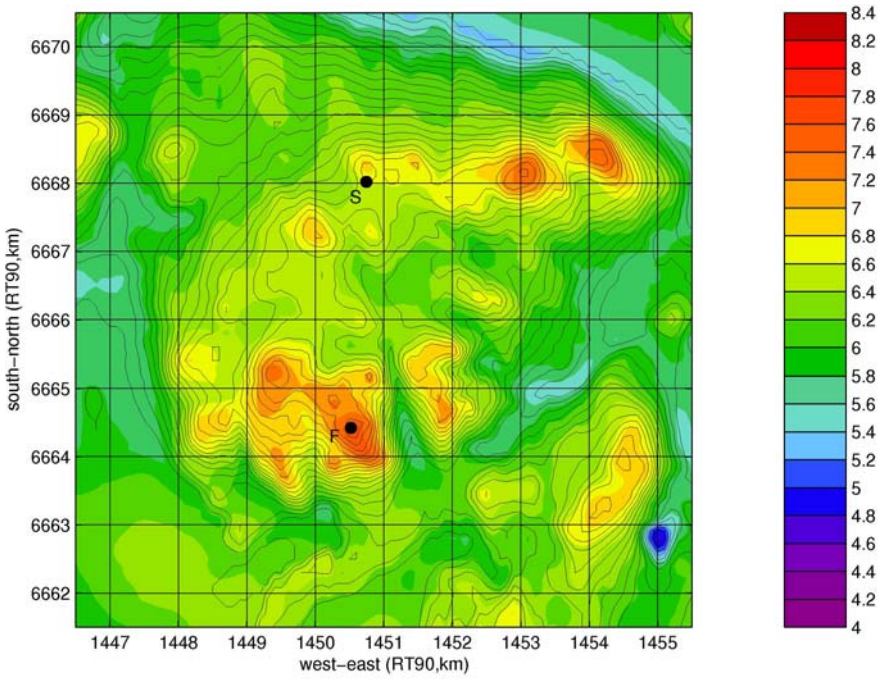

Figure 51: Annual average wind speed in the Fjällberget/Saxberget area as estimated by the WA^{S}P-model at 80 m height above ground using 100 m grid and input data from 61 m level observations at Fjällberget. F and S indicate locations of two measurement masts at Fjällberget and Saxberget.

10 Summary and conclusions

To get a high resolution mapping of wind resources, a model has to be used since there are too few wind-measuring stations to get any details otherwise. Another aspect making some kind of model necessary is that most wind measurements are at 10 m height while the wind turbine hub heights are commonly between 50 and 100 m.

Here the MIUU-model has been used to investigate the wind climate in Sweden. This model is a three-dimensional meso-scale numerical higher-order closure model that takes special notice of the atmospheric boundary layer. The model is rather computer time consuming and some choices regarding the most important flow forcing parameters have to be made, as it is difficult to model all meteorological conditions. The main idea is to minimize the number of needed model runs and to evaluate which flow forcing parameters that can be put aside or simplified while still keeping a good credibility of the results.

The influence on the modelled wind climate from using a larger or smaller number of model runs as regards the magnitude and direction of the geostrophic wind was studied in Bergström and Lindholm (2003). The result showed that at least two strengths and 8 directions must be used in order not to reduce the accuracy of the modelled wind climate, although it was recommended to use three strengths and 16 directions, and to include model runs from at least two seasons, but preferably four.

The technique to just model some samples of the meteorological conditions governing the wind climate at heights of interest to wind energy, has the potential to give accurate results in good agreement with observations, making it unnecessary to model a long period of 'true weather' cases. By choosing the 'relevant' samples, the number of model runs could be limited to 96 (192) which corresponds to 2304 (4608) simulated hours (4 months x 3 speeds x 8 (16) directions x 24 hours).

Statistics on the horizontal air pressure gradient (geostrophic wind), the major driving force of the actual wind, are used to weight the model output together into the final wind climate estimates. Surface pressure data from 3 pressure observing sites in Southern Scandinavia and 3 sites in Northern Scandinavia were then primarily used.

As the geostrophic wind may vary quite a lot over an area as large as Sweden, it was also needed to take this into account. For this purpose 850 hPa geopotential heights from the NCEP/NCAR reanalysis data were used to calculate the geostrophic wind. These 850 hPa geostrophic winds were found to be in good agreement with geostrophic winds estimated from surface pressure data observations, both in Southern and Northern Scandinavia, and both as regards annual averages and geostrophic wind speed distributions. Thus the geostrophic winds estimated from the 850 hPa geopotential heights were used to weight the influence of the geographical variation in geostrophic wind into the results regarding the modelled wind climate.

Results from a wind resource mapping for Sweden with 1 km horizontal resolution have been presented here. The model was run for 192 meteorological conditions taken to be good representatives of the wind climate. Comparisons with wind observations show that the modelled annual average wind speed is in good agreement with measured values. The average difference between model results and observations were found to be -0.03 m/s, and for 87 % of the comparisons the differences were within ±0.4 m/s. The wind profile was verified at two coastal sites, with good agreement between observations and model results. Also the decrease in wind speed with increasing distance inland from the coast was verified against observations in Southern Sweden.

Additional wind statistics, besides the annual average wind speed, have also been determined using the database of modelled atmospheric conditions. These results include:

- Distributions of wind speed and wind directions, giving the sector wise Weibull parameters for 12 wind direction sectors.
- Extreme wind speed for 10 min average wind speed and 3 s gust wind speed with an expected 50-year return period.
- The wind gradient presented as the exponent of the exponential wind profile.
- Turbulence intensity determined from the modelled turbulent kinetic energy.
- Wind turbine classes estimated from the modelled average wind speed and turbulence intensity being translated to reference wind speed and reference turbulence intensity at 15 m/s.

All these additional wind statistics will be available through internet at http://www.geo.uu.se/luva/default.aspx?pageid=13152&lan=0.

It is important to remember that the model does not adequately resolve terrain features smaller than a few times the model grid spacing. One should always be aware of, and keep in mind, the resolution with which a wind resource investigation has been made, and judge the results and variability on a smaller, local, scale from this. It is easy to misinterpret results overlaid on a 'real' topographical map, as being the 'truth', while the scale upon which the investigation was done may limit the usefulness on a local scale.

The 1 km resolution will in most cases be too coarse when planning the details of a wind farm and exact wind turbine locations within the farm. For that case higher resolution wind resource mapping is needed. This has commonly been done using models such as WA^{S}P, either directly or as a tool within WindPro. However, due to the simplified physical description of the atmosphere results from such a model may sometimes be questioned, in particular when estimating wind resources in complex terrain.

Using a higher-order closure meteorological CFD-model such as the MIUU-model has previously been unrealistic with the high resolution needed for local microscale planning due to the short time-steps needed. But the steadily increasing capacity of modern PCs using the very fastest CPUs has altered this. There are, however, also limitations in meteorological CFD-models, which

may question their results when used with very small grid spacing. One such limitation is the hydrostatic approximation used in the MIUU-model, which do not allow small-scale vertical accelerations, which may influence the winds from time to time, although this is probably not important when only the wind climate is investigated. Due to the hydrostatic approximation in the MIUU-model it was decided also to use another meteorological CDF-model of the same type, but with a non-hydrostatic closure. The decision fell on COAMPS®, Coupled Ocean/Atmosphere Mesoscale Prediction System (COAMPS®, a registered trademark of the Naval Research Laboratory).

A comparison between modelled annual average wind speeds in the Fjällberget/Saxberget area in Sweden show that both CFD-models give realistic results. Differences are found, but comparisons with observation at the site show that the MIUU-model seems to perform better in spite of its hydrostatic approximations. The reasons for this is not presently clear, but may also have to do with differences regarding the turbulence closure and also regarding the surface energy balance which may in turn result in differences in thermal stratification.

The conclusion of the comparisons is that downscaling of the national wind resource mapping using higher-order meteorological CFD-models give realistic and promising results in good agreement with observations. Observations with high horizontal resolution are needed to fully evaluate the differences found between the two models and to evaluate the small-scale gradients in the estimated wind resources. We may also conclude that the results are probably more realistic than results using models with more simplified physics, especially when input data to the simplified models are not available from the site or even only at a specific location with an altitude not representative for the whole area of interest. This is so because the differences between high and low altitude terrain are much smaller using a simplified model than using a CFD-model.

Finally, it is once again pointed out that no local observations are included or needed in the simulations when calculating the wind resources using the MIUU-technique together with a meteorological CFD-model. Hence, the model output is independent of the observations with which comparison may be made.

Acknowledgements: The work has been sponsored by the Swedish Energy Agency, project nr. 20484-1, and Vindforsk projects nr. 05-586 and V-115. Many thanks also to all who have contributed in making the wind measurements, which have been used. The Naval Research Laboratory is acknowledged for the use of COAMPS®.

11 References

Alexandersson, H., 1979: A statistical analysis of wind, wind profiles and gust ratios at Gränby, Uppsala. Report No. 55, Department of Meteorology, Uppsala University, 71 pp.

Andrén, A., 1990: Evaluation of a turbulence closure scheme suitable for air pollution applications. *J. Appl. Meteor., 29, 224-239.*

Belward, A.S., Estes, J.E., and Kline, K.D., 1999: The IGBP-DIS 1-Km Land-Cover Data Set DISCover: A Project Overview: *Photogrammetric Engineering and Remote Sensing*, v. 65, no. 9, p. 1013-1020.

Bergström, 2004: Higher-order closure meso-scale modelling for wind resource estimates in Sweden. Proceedings from EWEC2004, London, 22-25 Nov. 2004, 10 pp.

Bergström, H., and Lindholm, M., 2003: Higher-order closure meso-scale modelling for wind climate estimates. Proceedings from World Wind Energy Conference, WWEC2003, 23-26 November 2003, Cape Town, South Africa.

Bergström, H., 2002: 'Boundary-layer modelling for wind climate estimates'. *Wind Engineering*, vol. 25, No. 5, 289-299.

Bergström, H. and Källstrand, B., 2001: Estimating Wind Potential in a Complex Terrain Arctic Mountain Valley. Proceedings EWEC2001, Copenhagen 3-7 July 2001, 842-845. WIP-Renewable Energies, München.

Bergström H. and Källstrand K., 2000: Measuring and modelling the wind climate in a mountain valley in northern Sweden. Proceedings, Boreas V, 29 Nov.-1 Dec. 2000, Levi, Finland.

Bergström, H., 1996: A climatological study of boundary layer wind speed using a meso-γ-scale higher-order closure model. *J. Appl. Meteor., 35, 1291-1306.*

Bergström, H., 1992: Distribution of extreme wind speed. Wind Energy Report WE92:3, Department of Meteorology, Uppsala University, 26 pp.

Bergström H., Johansson P. and Smedman A., 1988: A study of wind speed modification and internal boundary-layer heights in a coastal region. Boundary-Layer Meteorol., 42, 313-335.

Brooks, I. M., Söderberg S. and Tjernström M., 2003: The Turbulence Structure of the Atmospheric Boundary Layer around a Coastal Headland. Boundary-Layer Meteorol., 106, 531-559.

Burk, S. D., and W. T. Thompson, 1996: The summertime low-level jet and marine boundary-layer structure along the California coast. *Mon.Wea. Rev.,* 124, 668-686.

Burk, S. D., T. Haack, and R. M. Samelson, 1999: Mesoscale simulation of supercritical, subcritical and transcritical flow along coastal topography. J. Atmos. Sci., 56, 2780-2795.

Davenport, A. G., 1967: The dependence of wind loads on meteorological parameters. Proc. Int. Res. Seminar, Wind effects on buildings and structures. Ottawa, University of Toronto Press, pp 19-82.

Enger L., 1990: Simulation of dispersion in a moderately complex terrain. Part A. The fluid dynamic model. *Atmos Environ., 24A, 2431-2446.*

Enger, L., and Grisogono, B.: 1998, 'The response of Bora-type flow to sea surface temperature', *Q. J. R. Meteorol. Soc.,* 124, 1227-1244.

Enger, L., Koracin, D. and Yang, X.: 1993, 'A numerical study of boundary-layer dynamics in a mountain valley. Part 1: Model validation and Sensitivity Experiments', Boundary-Layer Meteorology, 66, 357-394.

Gumbel, E. J., 1954: Statistical theory of extreme values and some practical applications. Applied Mathematics, Series #33, Washington.

Harshvardhan, R. Davies, D. Randall, and T. Corsetti, 1987: A fast radiation parameterization for atmospheric circulation models. *J. Geophys. Res.,* 92, 1009-1016.

Hasager, C.B., Nielsen, M., Astrup, P, Barthelmie, R., Dellwik, E., Jensen, N.O., Jørgensen, B.H., Pryor, S.C., Rathmann, O., Furevik, B.R. 2005 Offshore wind resource estimation from satellite SAR wind field maps. *Wind Energy,* v. 8, no. 4, 403-419.

Hodur, R. M., 1997: The Naval Research Laboratory's Coupled Ocean/Atmosphere Mesoscale Prediction System (COAMPS). *Mon. Wea. Rev.,* 125, 1414-1430.

IEC 61400-1 Ed.3, 2005. International Standards. Wind Turbines – Part 1: Design requirement. International Electrotechnical Commission, 99 pp.

Johansson, C., and Bergström, H., 2004: Variability in the energy content of the wind over Scandinavia, a 101-year perspective. Proceedings EWEC2004, London, 21-25 Novermber 2004.

Kain, J.S. and Fritsch J. M., 1990: A one-dimensional entraining/detraining plume model and its application in convective parameterization. *J. Atmos. Sci.,* 47, 2784-2802.

Kalnay, E. et al.: 1996: The NCEP/NCAR 40-year reanalysis project, Bull. Amer. Meteor. Soc., 77, 437-470.

Koracin, D. and Enger, L.: 1994, 'A numerical study of boundary-layer dynamics in a mountain valley. Part 2: Observed and simulated

characteristics of atmospheric stability and local flows', *Boundary-Layer Meteorology*, 69, 249-283.

Krieg, R., Kvick, T., and Andersson, H., 1987: Vindmätningar i höga master – Utvärdering av 7 års mätningar (in Swedish). SMHI Meteorologi Klimatsektionen, rapport nr. 42, 56 pp.

Källstrand B., Bergström H., Højstrup J., and Smedman A.-S., 2000: Mesoscale wind field modifications over the Baltic Sea. *Boundary-Layer Meteorol.*, 95, 161-188.

Källstrand B. 1998. Low level jets in a marine boundary layer during spring. *Contr. Atmos. Phys*. 71: 359--373.

Källstrand B. and Smedman A., 1997: A case study of the near-neutral coastal internal boundary-layer growth: Aircraft measurements compared with different model estimates. *Boundary-Layer Meteorol.*, 85, 1-33.

Mellor, G. L., and T. Yamada, 1982: Development of a closure model of geophysical flows. *Reviews of Geophysics and Space Physics,* **20,** 851-875.

Mellor, G. L., and Yamada, T., 1974: A hierarchy of turbulence closure models for planetary boundary layers, *J. Atmos. Sci., 31, 1791-1806.*

Pielke, R. A., 1984: *Mesoscale Meteorological Modeling*. Academic Press, 612 pp.

Rice, S. O., 1945: Mathematical analysis of random noise. Bell System Technical J., 24, 45-156.

Rutledge, S. A. and P. V. Hobbs, 1983: The mesoscale and microscale structure and organization of clouds and precipitation in midlatitude cyclones. Part VIII: A model for the "Seeder-Feeder" process in warm-frontal rainbands. *J. Atmos. Sci.*, 40, 1185-1206.

Sandström, S., 1997: Simulations of the Climatological Wind Field in the Baltic Sea Area using a Mesoscale Higher-Order Closure Model, *J. Appl. Meteor., 36, 1541-1552.*

Söderberg, S., and O. Parmhed, 2006: Numerical modelling of katabatick flow over a melting outflow glacier. *Bound.-Layer Meteor.,* 120, 509-534.

Törnblom K., Bergström H. and Johansson C., 2007: Thermally driven mesoscale flows – simulations and measurements. *Boreal Environment* Research, 12: 623–641.

van der Hoven, I., 1957: Power spectrum of horizontal wind speed in the frequency range from 0.0007 to 900 cycles per hour. J. of Meteorol., 14, 160-164.